Significance of Active Site Residues in the N-Domain Selectivity of Angiotensin-Converting Enzyme

Ross Gavin Douglas

Thesis Presented for the Degree of

DOCTOR OF PHILOSOPHY

in the Division of Medical Biochemistry

University of Cape Town

February 2011

Supervisor: Prof E.D. Sturrock

Declaration

I, Ross Douglas, declare that this thesis is my own, unaided work (except where acknowledgements indicate otherwise). Neither the whole work nor part thereof has been, is being, or is to be submitted for any degree or examination at any other university.

I empower the University of Cape Town to reproduce for the purposes of research either the whole or any part of the contents of this thesis, in any manner whatsoever.

Signature of candidate: _____

Signed on the ____ day of _____, 2011

Abstract

Angiotensin-converting enzyme (ACE) is a zinc metallopeptidase that plays an important role in vascular function; with ACE inhibitors being clinically utilised in the treatment of cardiovascular disease and diabetic nephropathy. Somatic ACE consists of two homologous catalytically active domains (designated N- and C-domains) that share high overall sequence identity and structural topology. Despite the high degree of similarity between domains, each domain displays differences in substrate processing and inhibitor binding abilities. This suggests that active site residues differing between the two domains could provide unique interactions within the N-domain that allow for N-selective binding and processing. Literature reports of ACE crystal structures and studies with substrate and inhibitor analogues have implicated unique residues present in the S_2 and S_2' subsites in providing important interactions for N-selectivity.

In order to assess the contribution of residues to N-selectivity, implicated N-domain amino acids were converted to their corresponding C-domain counterparts by site-directed mutagenesis. Mutant derivatives were expressed in a heterologous mammalian protein expression system and purified to homogeneity by lisinopril-sepharose affinity chromatography. Analysis of binding and hydrolysis of non-domain specific substrate Abz-FRK(Dnp)P indicated that activities of mutated enzymes were comparable to controls with the exception of S_2' mutant ST/VV (which showed a 10-fold decrease in catalytic efficiency). S_2 mutant Y369F showed improved catalysis of C-domain specific substrate hippuryl-His-Leu and reduced catalytic ability of N-selective substrate Abz-SDK(Dnp)P implicating the terminal phenolic hydroxyl group in providing important contacts for substrate positioning. Other S_2 subsite mutations (R381E and YR/FE) also showed decreased catalytic efficiency of Abz-SDK(Dnp)P and a C-domain enzyme with an N-domain S_2' subsite had 10-fold improved catalysis of this substrate, suggesting interplay between subsites in selective substrate processing. A high-throughput AcSDKP assay using fluorescamine was also developed and achieved N-domain kinetic characteristics comparable to previous reports.

Binding affinity of RXP407 to mutant active sites served to address the extent of contribution of residues to N-selective inhibitor binding. Single S_2 and S_2' mutations had little effect on

RXP407 binding, as did double S_2' mutant ST/VV. However, double S_2 mutant YR/FE resulted in a 122-fold increase in K_i, suggesting important contact of both Tyr369 and Arg381 with RXP407. The importance of the S_2 subsite was further emphasised with the addition of a P_2 Asp and aliphatic *N*-protecting group improving the N-selectivity of a keto-ACE inhibitor backbone, as determined from inhibition assays and molecular docking experiments. This work gives an understanding of active site residue contribution to N-selective substrate processing and inhibitor binding and has shown consistent involvement of the S_2 subsite, particularly residues Tyr369 and Arg381, in these events. Further, this study provides important information in the design of N-selective ACE inhibitors.

Acknowledgements

I would like to extend sincere thanks to the following people, without whom this study would neither have been possible nor enjoyable:

My supervisor, Prof Ed Sturrock: thank you for your supervision in this work. Your insights, guidance and sense of humour have greatly assisted me in my development as a researcher. Thank you for taking an interest in a curious undergraduate student and for providing me with fantastic opportunities in both training and teaching during the past five years.

Ms Sylva Schwager: thank you for technical assistance and bench-side guidance during the course of this project. I would like to particularly acknowledge your helpful advice regarding tissue culture techniques and protein purification. Your enthusiasm and practical management has inspired us all.

Other members of the Zinc Metalloprotease Group, both past and present: Colin Anthony, Dr Tony Chang, Itai Chitapi, Nailah Conrad, Riyad Domingo, Kerry Gordon, Henry Kambafwile, Dr Wendy Kröger, Kate Larmuth, Raymond Moholisa, Dr Trudi O'Neill, Tanya Paquet, Dr Ayesha Parker, Mrs Sia Samuels, Dr Adele Thomas, Dr Jean Watermeyer and Christopher Yates. I can't think of a more supportive and fun laboratory team!

Dr Sheriff Salisu and Dr Rajni Sharma for the synthesis of captopril and keto-ACE analogues respectively.

Dr Wendy Kröger for helpful assistance in setting up this project (particularly her help with enzyme kinetics) and for the kind donation of the C-domain S_2' mutant.

Dr Aloysius Nchinda and Simon Broadley for helpful instruction and advice regarding molecular docking studies.

Prof Vincent Dive for the kind donation of phosphinic inhibitor RXP407 and Prof Adriana Carmona for the generous gifts of internally quenched fluorogenic substrates used in this study.

The National Research Foundation, Deutscher Akademischer Austausch Dienst, Ernest & Ethel Eriksen Trust and the University of Cape Town for financial support throughout this project.

All my friends who have supported me in this study: Dr Warren Gatcke, Peter Waller, JP and Sharon Kloppers, Andrew and Fiona Thomson, Michael Rapson, and Dr Chris Warton. Your thoughts, prayers and encouragements have been incredible!

My parents (Gavin and Ann), my brother and new sister-in-law (Brett and Antoinette): thank you for your love, support and generosity not only in this study, but all the days of my life. I love you guys dearly.

My beautiful bride, Catherine: thinking of all the support you have given me in this venture brings me close to tears. I have loved every minute of being your husband. I know that this is just the start and look forward to walking out this journey with you by my side.

My Lord and Saviour, Jesus Christ: thank you for the honour and privilege of being part of this study. I trust that this thesis displays my love for you and my love for people.

Abbreviations and acronyms

°C	degree Celsius
γ-irradiation	gamma-irradiation
µl	microlitre
µM	micromolar
Å	angstrom
Aβ	amyloid β-peptide
Abz	*o*-aminobezoic acid
Abz-FRK(Dnp)P	Abz-Phe-Arg-Lys(Dnp)-Pro
Abz-Gly	*o*-aminobenzoic acid-glycine
Abz-SDK(Dnp)P	Abz-Ser-Asp-Lys(Dnp)-Pro
ACE	Angiotensin-converting enzyme
ACE2	Angiotensin-converting enzyme 2
ACEi	Angiotensin-converting enzyme inhibitor
AcSDKP	*N*-acetyl-Ser-Asp-Lys-Pro
ADEs	adverse drug effects
Ala	alanine
AngI	angiotensin I
AngII	angiotensin II
Ang(1-7)	angiotensin (1-7)
Arg	arginine
Asp	aspartic acid
BK	bradykinin
BK(1-7)	bradykinin (1-7)
BK(1-5)	bradykinin (1-5)
CDOCKER	CHARMm-based docker
CHARMm	Chemistry at Harvard Molecular Mechanics
CHO	Chinese hamster ovary
CPA	carboxypeptidase A
D629	soluble N-domain construct coding residues 1-629
dH_2O	distilled H_2O
DMSO	dimethyl sulfoxide
DNA	deoxyribonucleic acid
Dnp	2,4-dinitrophenyl
DS	Discovery Studio
E. coli	*Escherichia coli*
EDTA	ethylenediaminetetraacetic acid
ERK	extracellular signal-regulated kinase
FRET	fluorescence resonance energy transfer
G418	Geneticin
Gln	glutamine
Glu	glutamic acid
GnRH	gonadotropin-releasing hormaone
HEMGH	zinc binding motif (His-Glu-Met-Gly-His)
HEPES	4-(2-hydroxyethyl)-1-piperazineethanesulfonic acid

HHL	hippuryl-His-Leu
His	histidine
HL	His(L)-Leu(L)
HPLC	high pressure liquid chromatography
IC_{50}	the amount of inhibitor required for 50% residual activity
k_{cat}	enzymatic turnover rate of substrate
K_i	inhibition constant
K_m	Michaelis constant
Lys	lysine
Met	methionine
ml	millilitre
mM	millimolar
nM	nanomolar
PAGE	polyacrylamide gel electrophoresis
PCR	polymerase chain reaction
PDB	Protein Data Bank (http://www.rcsb.org/pdb)
Phe	phenylalanine
pmol	picomole
POP	prolyl oligopeptidase
Pro	proline
RAS	renin-angiotensin system
RMSD	root mean square deviation
sACE	somatic angiotensin-converting enzyme
SD	standard deviation
SDS	sodium dodecyl sulphate
SEM	standard error of the mean
Ser	serine
Smad	small-mothers-against-decapentaplegic
tACE	testis angiotensin-converting enzyme
tACEΔ36NJ	modified tACE construct lacking the transmembrane region and 36 amino acid N-terminus
TBE	Tris-borate-EDTA buffer
t-Boc	*t*-butoxycarbonyl group
TEMED	tetramethylethylenediamine
TGFβ	transforming growth factor β
Thr	threonine
Tris	tris-(hydroxymethyl)-aminomethane
Tyr	tyrosine
ZBG	zinc binding group
Z-FHL	Cbz-Phe-His-Leu

Table of Contents

List of Figures

List of tables

Chapter 1

Review of the Literature

1.1 Introduction to angiotensin-converting enzyme related pathologies

The development and advancement of proteomic techniques has emphasised the vital role of proteolytic enzymes in overall cell functioning, with aberrant protease expression and activity playing a major role in the progression of numerous disease states (Drag and Salvesen, 2010). Thus, appropriate understanding of the structure-function relationships of these enzymes is an integral part in the design of therapeutic strategies for many human diseases. Angiotensin-converting enzyme (ACE, EC 3.4.15.1) is a protease key in the regulation of blood pressure and electrolyte homeostasis and has been implicated in a number of disease states particularly relating to vascular function (Turner and Hooper, 2002; Acharya *et al*., 2003).

The role of ACE in the production of the potent vasopeptide angiotensin II (AngII) is well established and the association of ACE and cardiovascular disease is well documented in the literature (Lazartigues *et al*., 2007; Probstfield and O'Brien, 2010). Inhibition of ACE remains a frontline treatment in the management of hypertension, a major risk factor in the development of cardiovascular disease, and the success of specific ACE inhibitors in the treatment of cardiovascular disease stresses the centrality of this enzyme in vascular function (Acharya *et al*., 2003; Bicket, 2002; Ondetti *et al*., 1977). ACE is pivotal in cardiac remodelling (Schartl *et al*., 1994) and in the pathogenesis of cardiac hypertrophy, with overexpression of ACE resulting in increased thickness of cardiomyocytes and collagen deposition (Higaki *et al*., 2000).

ACE related pathogenesis does occur outside of its classic cardiovascular role. High ACE expression has been found in granulomas associated with sarcoidosis (Silverstein *et al*., 1979), elevated ACE activity has been correlated in patients with later stages of this disease and thus ACE activity is utilised as a diagnostic tool in this condition (DeRemee and Rohrbach, 1980; Friedland and Silverstein, 1976; Danilov *et al*., 2010). Elevated ACE levels have also been noted with type 2 diabetes mellitus and higher activities correlated to more severely scored retinopathy (Lieberman and Sastre, 1980). ACE is implicated in influencing

glucose absorption (Henriksen and Jacob, 2003) and ACE inhibitors have been clinically used in reduction of severity of diabetic nephropathy (Burnier and Zanchi, 2006).

The influence of ACE activity in a variety of states and systems, and the success of ACE inhibitors, underpin the importance of this enzyme as a therapeutic target. Thus, appropriate studies improving the understanding of the structure-function relationship of ACE are likely to allow for better treatment of several disease states.

1.2 Angiotensin-converting enzyme

1.2.1 General properties

As with proteases thermolysin and neutral endopeptidase; ACE belongs to the gluzincin family (MA clan) of metallopeptidases and contains a characteristic HEXXH zinc binding motif critical to the metalloenzyme substrate hydrolysis mechanism (Rawlings *et al*., 2010). ACE is a zinc dipeptidyl carboxypeptidase and is best known for its conversion of angiotensin I (AngI) to potent vasoconstrictor AngII and the inactivation of vasodilator bradykinin (BK); highlighting its important role in blood pressure regulation (Acharya *et al*., 2003). The major role in ACE mediated blood pressure regulation is illustrated in hypotensive ACE specific knockout mice (Krege *et al*., 1995; Esther *et al*., 1996). While this is important, it must be stressed that ACE is able to cleave a diverse set of substrates and can also exhibit endopeptidase activity *in vitro* (discussed below) (Skidgel *et al*., 1984; Skidgel and Erdos, 1985; Hu *et al*., 2001; Sun *et al*., 2008).

The *Ace* gene is located on the 17q23 locus and is 21 kilobases in length consisting of 26 exons of variable sizes (Figure 1.1) (Hubert *et al*., 1991). The promoter region consists of a classic TATA box upstream of the transcription start site and is regulated by glucocorticoid responsive elements (Hubert *et al*., 1991). In addition, the *Ace* gene contains an insertion/deletion polymorphism of 287 base pair length in intron 16, with the group homozygous for the deletion (D/D) generally displaying higher serum ACE activity than the insertion (I/I) group (Rigat *et al*., 1990; Rieder *et al*., 1999).

ACE requires the presence of chloride for activity, with several amino acids implicated in chloride binding (Shapiro and Riordan, 1983; Tzakos *et al*., 2003; Rushworth *et al*., 2008). ACE is also heavily glycosylated and this plays an important role in correct intracellular folding prior to export, thermal stability (O'Neill *et al*., 2008; Anthony *et al*., 2010) and possibly dimerisation (Kost *et al*., 2003). The extent of glycosylation is variable and accounts for up to approximately 37% of the total enzyme mass and such glycan heterogeneity previously hampered efforts in the determination of ACE crystal structures (Ripka *et al*., 1993; Deddish *et al*., 1994; Yu *et al*., 1997). The use of expensive glycosidase inhibitors or site-directed mutagenesis studies to determine the minimum glycosylation requirements for proper folding were employed to circumvent this problem (Natesh *et al*., 2003; Gordon *et al*., 2003; Anthony *et al*., 2010).

Two isoforms, products of the same *Ace* gene, are detected in tissues as the result of a tissue specific promoter within intron 12 (Soubrier *et al*., 1988; Ehlers *et al*., 1989; Howard *et al*., 1990; Hubert *et al*., 1991). Somatic ACE (sACE) is expressed as a 1 277 amino acid mature protein and is widely expressed in many human tissues, especially on vascular endothelial cells (Soubrier *et al*., 1988). Molecular cloning of the sACE gene revealed the uncommon feature of two homologous domains (designated N- and C-domains based on their location on the polypeptide chain) each containing a putative active site of which both are catalytically active (Soubrier *et al*., 1988; Wei *et al*., 1991). In contrast, testis ACE (tACE) is expressed exclusively in male germinal cells and is essentially a truncated form of sACE containing 701 amino acids as a mature protein (Ehlers *et al*., 1989). With the exception of the first 36 residues arising from the translation of codons in exon 13; tACE is identical to the C-domain region of sACE (Ehlers *et al*., 1989).

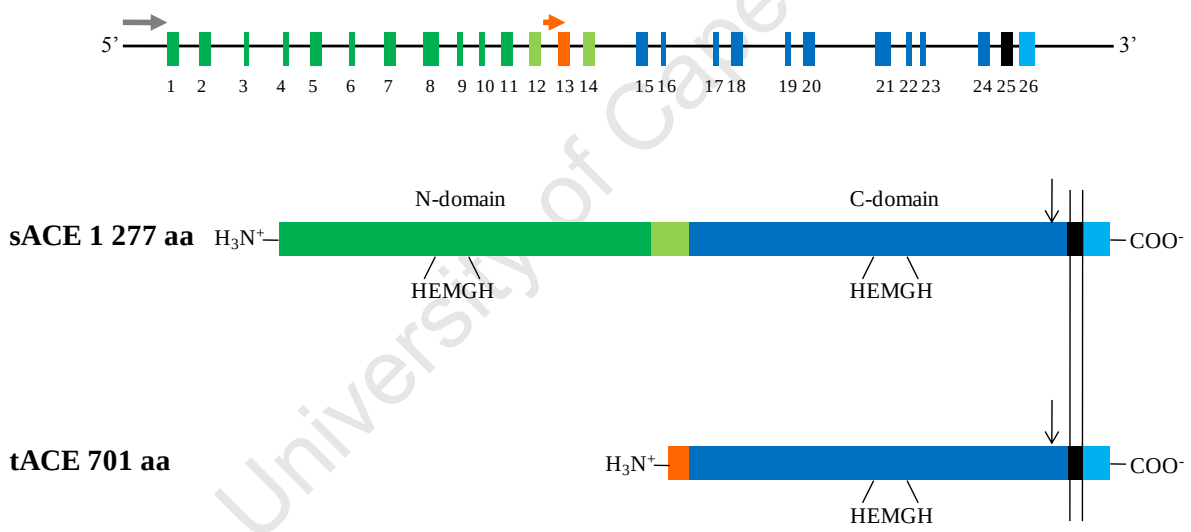

Figure 1.1: Schematic representation of the Ace gene and the two isoform products. The *Ace* gene consists of 26 exons all of which are transcribed for sACE with the exception of exon 13. The promoter for sACE expression is indicated as a grey arrow, sACE N- and C-domains with catalytic HEMGH motifs are shown in green and blue respectively, the inter-domain linker region in light green, transmembrane region in black and cytoplasmic C-terminus in light blue. tACE arises from the presence of a germinal cell specific promoter in intron 12 (orange arrow) and translation of exon 13 results in a unique 36 amino acid N-terminus of tACE; whereas the remainder of the protein is identical to the C-domain of sACE. The black arrow indicates the approximate cleavage site of ACE to be solubilised into the surrounding medium.

The structural elements of the enzyme emphasise its functional role and outline the structural similarities between the two isoforms (Figure 1.1). Each isoform contains a 17-amino acid hydrophobic sequence that allows for insertion into the plasma membrane as a type I integral membrane protein, with catalytic domains in contact with pertinent substrates in the extracellular milieu (Soubrier *et al*., 1988). Despite being anchored in the plasma membrane, both isoforms are able to undergo proteolytic cleavage near the transmembrane region by a currently unknown protease (termed the "ACE sheddase") and thus released into the surrounding environment in soluble form (Ehlers *et al*., 1996; Woodman *et al*., 2000).

1.2.2 The N- and C-domains of ACE

1.2.2.1 Comparison of the two domains

Alignment of the N- and C-domains of sACE reveals 60% overall sequence identity and the active site regions between the domains are even more conserved with approximately 90% similarity (Soubrier *et al*., 1988). Such high identity between domains is further seen in the overall conserved topology of the individual domains (Figure 1.2).

The overall structure of both the N- and C-domains represents an ellipsoid shape divided into two sub-domains by a deep central cleft (Natesh *et al*., 2003; Corradi *et al*., 2006). The active site containing the catalytic zinc ion of the domains is buried within this cleft and recent work has shown that substrates could possibly gain access into the deep binding site through hinge movement by twisting of the N- and C-termini (Anthony *et al*., 2010). The structures are helically rich with only six β-sheets seen in the tertiary structures (Natesh *et al*., 2003; Corradi *et al*., 2006). Thus far, structural insights have involved studies of each domain in isolation, with the crystal structure of the full length sACE currently not determined. Kinetic studies have suggested negative cooperativity between the domains in the cleavage of substrates (Binevski *et al*., 2003; Rice *et al*., 2004; Skirgello *et al*., 2005). Other work implicates the N-domain in close proximity to the C-domain, affecting substrate hydrolysis and shedding implying that the domains could be in an intimate orientation to allow for interaction between domains (Woodman *et al*., 2005). The resolution of the sACE crystal structure should assist in a structural perspective of this observed cooperativity.

While the overall topology between domains is very similar, differences in substrate processing and inhibitor binding have been noted and could be attributed to the subtle changes in amino acid composition within the active sites of the domains (discussed below).

Thus, while the domains of sACE are present on the same polypeptide chain, share high sequence identity, have almost identical structural topology, and can influence the function of each other; each domain appears to have distinctive roles in the overall function of sACE.

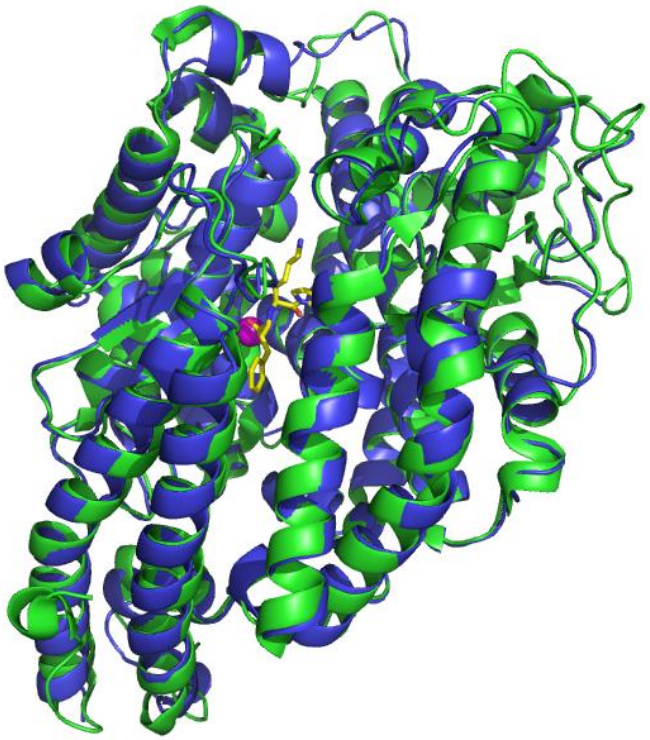

Figure 1.2: A comparison of the overall topology of the sACE N- and C-domains. The coordinates of each domain (PDB accession codes 2C6N and 1O86) were aligned using the program *ALIGN* (Cohen, 1997). The N- (green ribbon) and C-domains (blue ribbon) display marked overall structural topology. A potent ACE inhibitor, lisinopril, and the catalytic zinc ion are shown in yellow sticks and magenta sphere. A deep central cleft can be noted down the centre of the molecules resulting in two sub-domains.

1.2.2.2 The role of the C-domain in vivo

Genetic engineering in mice has allowed for the specific generation of ACE modifications including the complete knockout of both ACE isoforms, the generation of tissue specific ACE expression and production of domain inactivated sACE forms due to mutation of the HEMGH zinc binding motif (Xiao *et al*., 2004; Bernstein *et al*., 2010). Such approaches have allowed for important *in vivo* characterisation of ACE related physiology and assist in an understanding of the distinctive physiological roles of each domain.

ACE null mice, in addition to significantly lowered blood pressure, exhibit additional anatomical and physiological abnormalities including renal defects, anaemia, lower urinary concentration ability and decreased fertility (Krege *et al*., 1995; Esther *et al*., 1996). Significantly lower fertility was attributed to the removal of the tACE isoform. Additional studies indicated that mice lacking tACE had normal anatomy of the testis and showed similar sperm viability, *in vitro* motility and morphology (Hagaman *et al*., 1998). However, sperm of homozygous tACE knockout mice displayed significantly lower transport rates in the oviduct and reduced binding to the zonae pellucidae (Hagaman *et al*., 1998). Reintroduction of tACE expression into an ACE null background restored fertility (Ramaraj *et al*., 1998). Rather than a simple structural contribution to sperm binding, fertility is vitally dependent on the peptidase activity of ACE acting on a currently unknown substrate (Fuchs *et al*., 2005).

More recent elegant studies of C-domain function involved the inactivation of each sACE domain through the conversion of the HEMGH motif to a non-zinc binding sequence. These mice expressed mutant enzymes at comparable levels to wild type mice and allow for an understanding of the physiological contribution of each domain (reviewed by (Bernstein *et al*., 2010)). A study involving inactivation of the N-domain showed that these mice were indistinguishable from wild type in blood pressure, renal function and hematocrit levels (Fuchs *et al*., 2004). Mice containing the inactivated C-domain enzyme showed increased renin and AngI levels and lowered response to AngI infusion; implicating the predominant role of the C-domain in the conversion of AngI to AngII (Fuchs *et al*., 2008). Thus, the C-domain plays a primary role in AngI metabolism and male fertility.

1.2.2.3 The role of the N-domain in vivo

Individual soluble and fully active N-domain has been found in the ileal fluid of patients post surgical colectomy (Deddish *et al*., 1994). Since this discovery, active forms of individual N-domain enzymes at sizes of 65 kDa and 90 kDa have been found in the urine of healthy and hypertensive patients respectively (Casarini *et al*., 2001). Similar results were found in tissue of Wistar-Kyoto and spontaneously hypertensive rats and suggested that the unique presence of 90 kDa form of the N-domain in the hypertensive context could be used as a marker for hypertension (Marques *et al*., 2003; Bueno *et al*., 2004; Ronchi *et al*., 2005). It is possible that the N-domain could be liberated from the sACE molecule by proteolytic action and such an event has been shown, in principle, *in vitro* (Sturrock *et al*., 1997). These findings could suggest an important functioning for the N-domain in physiological regulation.

In addition to a possible isolated or individual role in tissue, the N-domain plays an interesting regulatory role within sACE. Shedding experiments revealed that tACE is shed more efficiently than sACE suggesting that the N-domain prevents proper access to the ACE sheddase (Woodman *et al*., 2000). The significance of the physiological ramifications of this difference is currently unknown.

Due to the domain orientation of sACE, the N-domain may be the first domain in contact with substrates and inhibitors (Deddish *et al*., 1996). While the C-domain is prominent in AngI conversion *in vivo*, the N-domain appears to be involved in the cleavage of other peptides not necessarily involved in the renin-angiotensin system (RAS, see below). Studies with mice have revealed another important role for the N-domain: selective inhibition of the N-domain did not affect blood pressure and AngI conversion but resulted in a six fold elevation of tetrapeptide *N*-acetyl-Ser-Asp-Lys-Pro (AcSDKP) (Junot *et al*., 2001). Such elevation of AcSDKP plasma levels was later confirmed in N-domain inactivated sACE mice and these studies confirmed the selective N-domain function in the clearance of this peptide (Fuchs *et al*., 2004). The involvement and consequences of this peptide are considered below (section 1.3.3.2).

1.3 Substrates of ACE

As mentioned above, ACE is able to cleave substrates other than vasoactive peptides. Further, each substrate is not hydrolysed with the same efficiency between domains and these differences could provide a possible approach in the design of therapeutic strategies of ACE related pathologies.

1.3.1 Mechanism of substrate hydrolysis

The exact mechanism of ACE substrate hydrolysis remains to be fully elucidated. However, since there is high sequence identity and topology between the catalytic centres of ACE and thermolysin, it is assumed to proceed in a thermolysin analogous manner and is described in detail elsewhere (Matthews, 1988; Sturrock *et al*., 2004).

The reaction of thermolysin, and presumably ACE, proceeds through a general-base type mechanism. The substrate is positioned and stabilised through interactions within the active subsites of ACE, in this case the N-domain. Of importance is the interaction of the C-terminal carboxylate with residues Gln259, Lys489 and Tyr498 (Figure 1.3). Optimal interaction of the substrate with residues in the active site leads to the displacement of a water molecule (previously in coordination with the zinc ion) towards Glu362. The displacement results in an enhancement of the nucleophilicity of the water molecule and positions it for nucleophilic attack on the substrate carbonyl carbon (Matthews, 1988). The nucleophilic attack leads to the formation of the tetrahedral intermediate and the proton taken up by Glu362 is immediately transferred to the scissile bond nitrogen atom. This tetrahedral intermediate complex has further interactions with Ala332, Tyr501 and His491; where mutation of the His residue results in drastic loss of transition state stabilisation (Fernandez *et al*., 2001), and the formation of this tetrahedral substrate intermediate has been noted in the crystal structures of ketomethylene inhibitors (Watermeyer *et al*., 2008). Collapse of the tetrahedral intermediate occurs through the transfer of the second water proton by Glu362 to the newly formed N-terminal nitrogen atom and the products are released (Figure 1.3) (Sturrock *et al*., 2004).

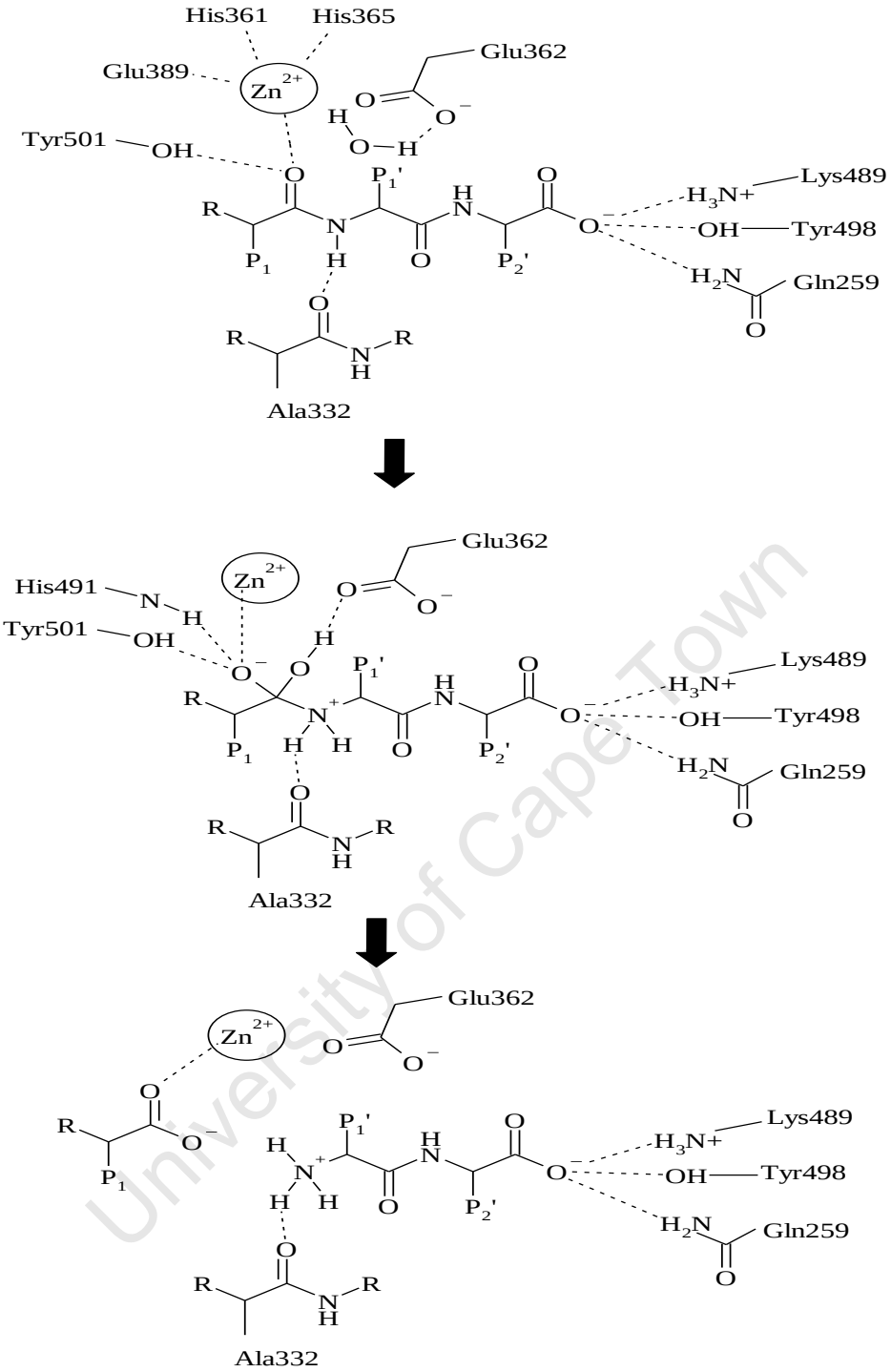

Figure 1.3: Schematic summary of the mechanism of action in substrate cleavage in the N-domain. Cleavage occurs via the nucleophilic attack of the zinc and Glu362 associated water molecule. The subsequent tetrahedral intermediate collapses to result in the cleaved products. Residues of interest are given and significant contacts shown as broken lines. Substrate side chains are designated in the form P_N depending on the position to the scissile bond (Schechter and Berger, 1967). The R group represents the remainder of the substrate peptide chain. Adapted from (Sturrock *et al*., 2004).

1.3.2 Vasoactive peptides: Angiotensin I, bradykinin, angiotensin 1-7 and substance P

ACE was first isolated and characterised on the basis of its ability to convert AngI (DRVYIHPFHL), an inactive decapeptide, to potent vasoconstrictive octapeptide AngII (DRVYIHPF) (Skeggs *et al*., 1954; Skeggs *et al*., 1956). Since then a better understanding of the central role of ACE in the RAS, a system that contributes notably to blood pressure regulation and electrolyte homeostasis, has been elucidated. The potent systemic vasoconstrictive effects of AngII are mediated through the angiotensin type 1 receptor that signals for aldosterone release as well as water and sodium retention (Fyhrquist and Saijonmaa, 2008). The downstream effects of AngII receptor mediated activation go beyond the more direct effect of vasoconstriction, with AngII being associated with increased proliferation, hypertrophy and fibrosis (Turner and Hooper, 2002). With the effects of AngII being described, it is not surprising that ACE is associated with disorders of vascular systems (section 1.1).

BK (RPPGFSPFR), a member of the kallikrein-kinin system and product of kallkrein cleavage (Kakoki and Smithies, 2009), is currently the best known physiological substrate of ACE whereby it has a catalytic efficiency 10-fold higher than the efficiency of AngI hydrolysis (Jaspard *et al*., 1993). In contrast to AngII, BK is a potent vasodilator eliciting its effects largely through the BK type 2 receptor resulting in nitric oxide release and prostaglandin synthesis (Kakoki and Smithies, 2009). Using its classic dipeptidase activity, ACE is able to consecutively produce BK(1-7) and BK(1-5) thus abolishing the vasodilatory effects (Jaspard *et al*., 1993).

Production of sACE enzymes with only one functional domain allowed for the assessment of relative domain contribution to substrate processing. *In vitro* and *in vivo* studies have shown that BK is cleaved with approximately equal kinetics by both N- and C-domains (Jaspard *et al*., 1993; Georgiadis *et al*., 2003; Fuchs *et al*., 2008). While *in vitro* data indicates that AngI is only slightly better cleaved by the C-domain, *in vivo* mouse work suggests that the C-domain active site is physiologically predominant in this process (Wei *et al*., 1991; Fuchs *et al*., 2008).

More recently, the discovery of ACE homologue ACE2 provided a new understanding of the counter-regulatory actions in AngII production. Angiotensin (1-7) (Ang(1-7), DRVYIHP), a product of the carboxypeptidase activity of ACE2 on AngII, is a peptide involved in

vasodilation through specific binding and activation of the Mas receptor (Roks *et al*., 1999; Vickers *et al*., 2002; Santos *et al*., 2003). Ang(1-7) can function as a weak inhibitor of ACE at high concentrations, but is also a substrate of ACE producing angiotensin(1-5) (DRVYI), an inactive peptide (Deddish *et al*., 1998). *In vitro* analysis indicates that both domains can cleave Ang(1-7) with approximately equal kinetics (Rice *et al*., 2004), although another study suggests the cleavage of the peptide is an N-domain specific process (Deddish *et al*., 1998).

Substance P (RPKPQQFFGLM-NH_2) is a C-terminally amidated undecapeptide tachykinin that has vasodilatory properties but also contributes to neurotransmission and pain response (Datar *et al*., 2004). Both *in vitro* and *in vivo* studies indicate that ACE is involved in the cleavage of substance P through the removal of the C-terminal dipeptide and also through unclassical endopeptidase activity (Skidgel *et al*., 1984; Ehlers and Riordan, 1989; Jaspard *et al*., 1993). Kinetic analysis showed that the C-domain is able to hydrolyse this peptide at a modestly faster rate than the N-domain.

One can appreciate the manner in which ACE activity contributes to vasoaction; whereby potent vasoconstrictive peptides are introduced and vasodilatory peptides are removed in a given biological system.

1.3.3 Other substrates not involved in vasoaction

While the most celebrated role of the ACE domains is in the production of AngII and the inactivation of vasodilatory peptides, other peptides are cleaved by ACE that can play key roles in human physiology. These are presented below.

1.3.3.1 Gonadotropin-releasing hormone and amyloid β-peptide

Gonadotropin-releasing hormone (GnRH, pyro-EHWSYGLRPG-NH_2, previously referred to as leutenising hormone-releasing hormone) is a decapeptide hormone containing protected N- and C-termini and is important in fertility and sexual development (Millar *et al*., 2004). As in the case of substance P, cleavage of GnRH occurs through both di- and tricarboxypeptidase ACE activity and novel triaminopeptidase activity was noted whereby ACE cleaved off the N-terminal tripeptide from the substrate (Skidgel and Erdos, 1985). Both domains seem to be involved in C-terminal tripeptide release but N-terminal tripeptidase activity is primarily performed by the N-domain (Ehlers and Riordan, 1991; Jaspard *et al*., 1993). While this is interesting from a mechanistic perspective, no *in vivo* studies have shown

ACE cleavage of GnRH and thus the ACE-GnRH interaction could lack physiological consequence.

Amyloid β-peptide (Aβ) is an oligopeptide in which polymerisation and aggregation are linked to the progression of Alzheimer's disease (Kehoe, 2009). Work by numerous investigators has shown the ability of ACE to cleave Aβ into fragments that lower aggregation ability. While there is agreement that ACE cleaves Aβ *in vitro*, reports differ on the cleavage sites; with some authors describing a number of cleavage sites as a result of ACE endopeptidase activity while others only a single cleavage site (Hu *et al*., 2001; Hemming and Selkoe, 2005; Oba *et al*., 2005; Zou *et al*., 2007; Toropygin *et al*., 2008; Sun *et al*., 2008). Furthermore there is disagreement in the literature regarding the domain specificity of Aβ hydrolysis with some reports showing N-domain specific cleavage (Oba *et al*., 2005; Toropygin *et al*., 2008) and others maintaining that the processing is not domain specific (Hemming and Selkoe, 2005; Sun *et al*., 2008). These disparate results might be due to the different Aβ peptides and ACE forms employed in assays as well as different model experimental systems. Meta-analysis associates the ACE D/D polymorphism (and therefore increased ACE levels) with reduced risk of developing Alzheimer's disease (Lehmann *et al*., 2005) and mice treated with an ACE inhibitor tended to have increased amyloid deposition in the brain (Zou *et al*., 2007). However, other *in vivo* research suggested a limited role of ACE mediated Aβ cleavage (Hemming *et al*., 2007). Thus, the exact molecular nature of Aβ cleavage by ACE remains controversial (Kehoe, 2009).

1.3.3.2 N-acetyl- Ser-Asp-Lys-Pro

French investigators employed a five step purification protocol to identify a tetrapeptide capable of potently inhibiting the proliferation of bovine haematopoietic pluripotent stem cells (Lenfant *et al*., 1989). Various standard characterisation techniques lead to the identification of the peptide as AcSDKP and the activity of the compound confirmed with a synthetically produced molecule resulting in the same biological effects (Lenfant *et al*., 1989). The tetrapeptide was found to be produced from the cleavage of thymosin β-4 through the action of prolyl oligopeptidase (POP) (Grillon *et al*., 1990; Cavasin *et al*., 2004).

ACE was discovered to be specific in the degradation of AcSDKP in plasma, with co-incubation with 1 μM of an ACE inhibitor almost completely preventing AcSDKP hydrolysis (Rieger *et al*., 1993). With the discovery of the two catalytic domains that appear

to differ in substrate specificities (Soubrier *et al*., 1988; Jaspard *et al*., 1993), further investigation probed the domain contribution towards AcSDKP cleavage. This work revealed that, despite similar binding affinities between the two domains, the turnover rate of substrate hydrolysis was 50-fold higher for the N-domain active site (Rousseau *et al*., 1995). Unlike other substrates that might not have *in vivo* significance, studies in both mice and humans have shown an increase in plasma concentrations of AcSDKP when treated with an ACE inhibitor (Azizi *et al*., 1996; Chisi *et al*., 2000; Junot *et al*., 2001). The development of N-selective inhibitors could allow for the treatment of conditions whereby AcSDKP buildup could be desired without affecting the RAS (Dive *et al*., 1999; Junot *et al*., 2001; Azizi *et al*., 2001). The details of the physiological effects of AcSDKP are outlined below and suggest the usefulness of AcSDKP in disease treatment, especially in conditions relating to excessive tissue fibrosis.

1.3.3.2.1 AcSDKP and haematopoiesis

The biological effectiveness of AcSDKP was first discovered in light of the peptide's ability to limit the proliferation of blood stem cells (Lenfant *et al*., 1989) and was found to be synthesised in mice, secreted by the bone marrow in long term culture and had wide tissue distribution (Wdzieczak-Bakala *et al*., 1990; Pradelles *et al*., 1991). These findings encouraged investigations into the molecular functioning of this peptide in proliferation regulation. AcSDKP is able to inhibit the transition from G1 to S phase of the cell cycle thus keeping progenitor cells in the quiescent state (Lombard *et al*., 1990). It was shown that co-treatment with AcSDKP increased survival in mice administered with a lethal dose of cyclophosphamide and thus the investigators could employ higher doses of chemotherapeutic agents in decreasing tumour sizes without causing mouse death (Bogden *et al*., 1991; Masse *et al*., 1998). Other work indicated the ability of AcSDKP to inhibit the proliferation of normal progenitor cells but not already committed leukemic cells (Bonnet *et al*., 1992; Cashman *et al*., 1994).

Since ACE specifically inactivates AcSDKP *in vivo*, administration with ACE inhibitors was anticipated to show similar proliferation inhibition results to AcSDKP infusion. A study by (Chisi *et al*., 2000) indicated that ACE inhibitor captopril was able both *in vitro* and *in vivo* to inhibit murine progenitor cells entering the S-phase during chemotherapeutic treatment or γ-irradiation. This was correlated with increased plasma concentrations and half-life of AcSDKP (Chisi *et al*., 2000). The implications of these studies prompted expectation of the

use of this easily synthesisable peptide or an ACE inhibitor as a co-treatment with chemotherapeutic agents to reduce the severity of cancer treatment due to the ability of AcSDKP to keep progenitor cells in the quiescent state during therapy (Bogden *et al*., 1991; Chisi *et al*., 2000).

A phase I-II clinical study in cancer patients undergoing monochemotherapy sought to establish the usability of AcSDKP as a chemotherapy co-treatment agent that would lower treatment associated severity. Co-administration of AcSDKP with chemotherapeutic agents cytarabine and isofamide showed protection of peripheral blood cells and lowered toxicity (Carde *et al*., 1992). Little development has taken place within the last decade in the literature regarding its use in chemotherapy treatment, suggesting that the translation into the human setting has not been as effective as anticipated (Comte *et al*., 1998). This could be due to the complexities associated with administration timing and dosage which can differ significantly depending on the drug used and could differ in humans compared to mice (Bogden *et al*., 1991; Masse *et al*., 1998). Further, ACE activity has been shown to be elevated upon drug administration or irradiation which could result in AcSDKP clearance prior to taking biological action (Comte *et al*., 1998). No clinical trials have been performed with ACE inhibitors in the assessment of haemoprotection. Thus, the use of AcSDKP as a chemotherapeutic co-treatment agent currently appears to have limited value.

1.3.3.2.2 AcSDKP and tissue fibrosis

Studies over the last decade, particularly by Carretero and co-workers, have resulted in an appreciation of another activity of AcSDKP that could have clinical benefit. An initial tissue culture model system showed that this peptide was able to inhibit DNA and endothelin-1 induced collagen synthesis in rat cardiac fibroblasts, confirming that AcSDKP can mediate its effects on cell types other than the haematopoietic system (Rhaleb *et al*., 2001). Such an effect was shown *in vivo* with aldosterone-salt induced hypertensive rats, whereby co-administration of aldosterone-salt with AcSDKP significantly lowered collagen deposition and cell proliferation in the left ventricle and renal cortex without affecting blood pressure (Peng *et al*., 2001). Since then, a similar effect has been noted for a number of tissues including interstitial and perivascular tissue of the heart (Peng *et al*., 2003; Yang *et al*., 2004; Rasoul *et al*., 2004; Peng *et al*., 2005; Peng *et al*., 2007), aortic tissue (Lin *et al*., 2008) and renal tissue (Liao *et al*., 2010; Wang *et al*., 2010) in mouse models of hypertension and postmyocardial infarction. Inhibition of POP, and therefore inhibition of AcSDKP

production, revealed that the regulation and minimisation of collagen deposition is possibly the peptide's major role at endogenous levels (Cavasin *et al*., 2007). Other mouse models have established that the anti-fibrotic effect of AcSDKP is not limited to cardiovascular dysfunctions, and has been shown to reduce collagen deposition in diabetic rats (Castoldi *et al*., 2010) and drug-induced lung fibrosis (Li *et al*., 2010).

Identification of the predominant anti-fibrotic role mediated by AcSDKP also proposed a new mechanism of action for ACE inhibitors, whereby the reduction of fibrosis is not due to the reduction of profibrotic AngII levels alone but by the elevation of AcSDKP (Rasoul *et al*., 2004). This was further elucidated in an elegant study conducted by (Peng *et al*., 2005) using a monoclonal antibody specific for AcSDKP and able to prevent its physiological action. In AngII induced hypertensive rats, treatment with ACE inhibitor or AcSDKP alone was able to reduce collagen deposition in cardiac tissue. Inclusion of the monoclonal antibody in co-treatment with an ACE inhibitor or AcSDKP restored excessive collagen deposition comparable to untreated controls, suggesting that the decrease in fibrosis in this model is because of AcSDKP buildup due to infusion or ACE inhibition (Figure 1.4). This same effect was repeated in aldosterone-salt induced hypertensive rats (Peng *et al*., 2007). Such work emphasised the role of AcSDKP in prevention of excessive collagen deposition in tissue.

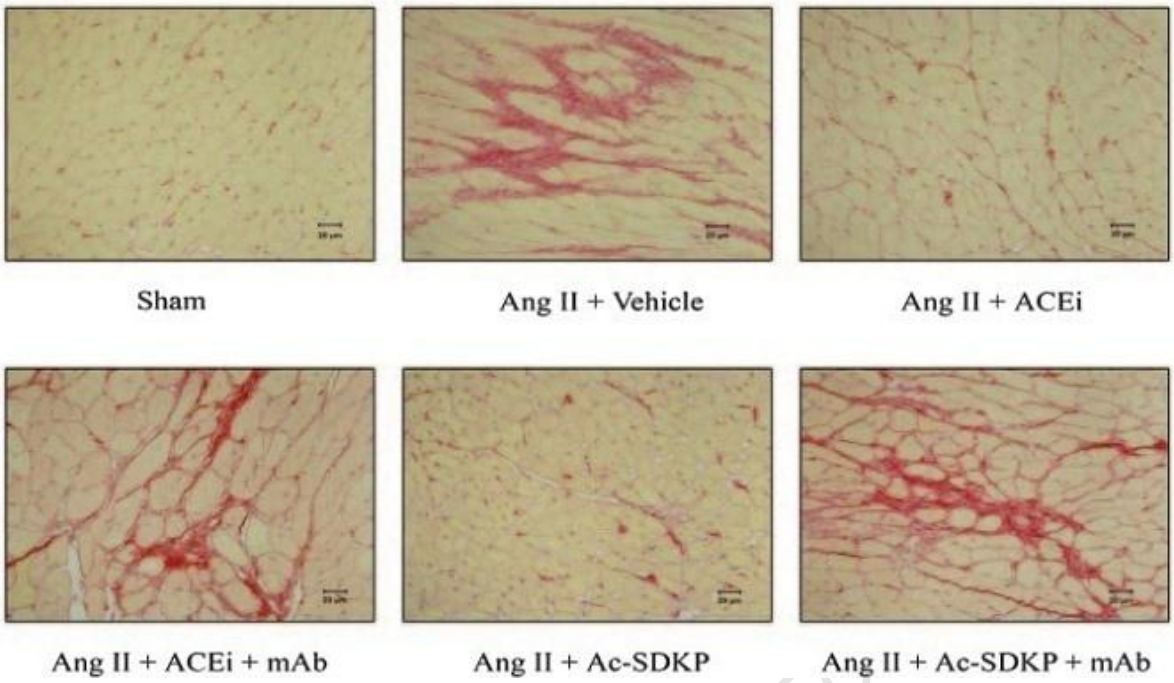

Figure 1.4: A representative experiment emphasising the anti-fibrotic effects of AcSDKP in cardiac tissue (Peng *et al*., 2005). In a study performed by Peng et al (2005), treatment of AngII-induced hypertensive rats with ACE inhibitor captopril (ACEi) or AcSDKP significantly reduced collagen deposition in left ventricle interstitial tissue (collagen stained red with picosirius red solution). Co-treatment with an anti-AcSDKP monoclonal antibody blunted the anti-fibrotic effects of both the ACEi and AcSDKP treatment, implicating the anti-fibrotic effects of ACE inhibition with elevation of AcSDKP levels. Image taken from (Peng *et al*., 2005).

The molecular mechanism of the anti-fibrotic effect of AcSDKP is beginning to emerge. As in the case of haematopoietic stem cell regulation; AcSDKP is able to slow differentiation of bone marrow derived stem cells and thus limited proliferation, migration, activation and cytokine release of macrophages, presenting a novel anti-inflammatory mechanism for the peptide (Sharma *et al*., 2008). AcSDKP was also able to prevent maturation of fibroblasts and subsequent collagen production when fibroblasts were exposed to transforming growth factor β (TGFβ), a fibrosis promoting cytokine (Peng *et al*., 2010). Detailed research shows that AcSDKP blunts the effects of TGFβ signalling through down regulation of the TGFβ/small-mothers-against-decapentaplegic (Smad) and extracellular signal-regulated kinase (ERK 1/2) pathways (Liu *et al*., 2009; Peng *et al*., 2010). AcSDKP induced reduction of fibrosis and cardiac remodelling by galectin-3, a lectin that results in the release of TGFβ and plays a prominent role in macrophage recruitment and cardiac dysfunction, has also been studied and was shown to act through inhibition of the above pathways in mice (Liu *et al*.,

2009). The exact mechanism of Smad pathway downregulation is unknown and does not involve increasing the intracellular levels of inhibitory Smad 7 (Peng *et al*., 2010). However, AcSDKP has been shown to bind specifically to an uncharacterised receptor in rat cardiac fibroblasts and thus could mediate its effects through independent receptor binding (Zhuo *et al*., 2007). Purification and characterisation of this receptor and the signalling pathway this activated receptor utilises is the focus of current research.

Given the findings above, AcSDKP appears to be a promising agent in the treatment of fibrotic tissue conditions without affecting blood pressure. In a mouse model system; treatment with bleomycin, a potent anti-neoplastic agent that often is discontinued in treatment due to increase in lung fibrosis, revealed that N-domain inactivated sACE mice displayed significantly lower pulmonary collagen deposition and increased survival with a lethal dose of the drug compared to their wild type littermates (Li *et al*., 2010). These mice had increased AcSDKP plasma levels compared to controls and were as susceptible to bleomycin induced pulmonary fibrosis when AcSDKP formation was reduced with a POP inhibitor, thus implicating AcSDKP in the prevention of drug related fibrosis of the lung (Li *et al*., 2010). N-domain selective (N-selective) ACE inhibition resulted in 5-fold increases in plasma AcSDKP levels in mice (Junot *et al*., 2001), a concentration similar to that obtained in the bleomycin study with inactivated sACE N-domain mice (Li *et al*., 2010). Thus, N-selective treatment could result in increased plasma concentrations of AcSDKP that could be of therapeutic benefit without affecting blood pressure and could be used in the treatment of pulmonary fibrosis, a condition for which there is currently no approved treatments (du Bois, 2010).

Table 1.1: A summary of selected ACE substrates. Cleavage sites by ACE are indicated by an arrow. The broken arrow indicates the sequential cleavage site after removal of the first dipeptide.

Substrate name	**Biological action of substrate**	**Substrate peptide sequence and ACE cleavage sites**	**Biological action of product**
Angiotensin I	Inactive	D – R – V – Y – I – H – P – F ↓ H – L	Vasoconstriction Hypertrophy Fibrosis
Bradykinin	Vasodilation	R – P – P – G – F ⇣ S – P ↓ F – R	Inactive
Angiotensin (1-7)	Vasodilation	D – R – V – Y – I ↓ H – P	Inactive
Substance P	Vasodilation Pain response	R – P – K – P – Q – Q – F – F ↓ G ↓ L – M -NH_2	Inactive
Gondotropin-releasing hormone	Sexual development	pyro-E – H – W ↓ S – Y – G – L ↓ R ↓ P – G -NH_2	No *in vivo* data published
N-acetyl-SDKP	Anti-fibrosis	Ac-S – D ↓ K – P	Inactive

1.4 Inhibitors of ACE

1.4.1 First generation ACE inhibitors

Currently approved ACE inhibitors are successfully used in the treatment of hypertension, congestive heart failure, post myocardial infarction, left ventricular dysfunction and diabetic nephropathy (Bicket, 2002). Several insights were important to the development of the first ACE inhibitors. Ondetti and co-workers used the crystal structure and functional understanding of carboxypeptidase A (CPA) as a mechanistic model that could be treated as analogous to ACE (although, when the structures of ACE were resolved, this was not found to be the case) (Ondetti *et al*., 1977; Natesh *et al*., 2003). With the discovery and structural determination of the various BK potentiating peptides from snake venom of *Bothrops jararaca* (with the most potent peptides having a Phe-Ala-Pro sequence on the C-terminus) and the development of the benzylsuccinic-Pro inhibitor for CPA, Ondetti and Cushman synthesised an analogue in the form of methylsuccinyl-Pro that was found to have specific but relatively weak ACE inhibition (Cushman *et al*., 1973; Byers and Wolfenden, 1973; Ondetti *et al*., 1977). The conversion of the zinc binding group (ZBG) from a carboxylate to sulphydryl resulted in potent ACE inhibitor captopril that was approved for clinical use in 1981 (Figure 1.5) (Ondetti *et al*., 1977; Cushman *et al*., 1981).

Adverse effects of captopril treatment, including skin rash and loss of taste, resulted in the development of other inhibitors of the Phe-Ala-Pro tripeptide sequence containing a ZBG other than a sulphydryl moiety. This initiated a search for *N*-carboxymethyl dipeptides with comparable inhibition to captopril. The dipeptides showing the greatest ACE inhibition were Ala-Pro and Lys-Pro and the result was the production of enalaprilat and lisinopril, a new class of ACE inhibitors (Figure 1.5) (Patchett *et al*., 1980). Since the finding that ACE inhibition significantly contributes to reduction of blood pressure, 17 ACE inhibitors containing different ZBGs and functionalities have been synthesised and approved for marketing (Redelinghuys *et al*., 2005).

Currently approved ACE inhibitors display binding affinity in the low nanomolar range and bind without any major selectivity between the N- and C-domains (Wei *et al*., 1991). While the major effect of first generation ACE inhibitors is the blockade of AngII production and the elevation of vasodilator BK; other studies indicate a possible cross talk between ACE and

the BK type 2 receptor, agonising the effects of BK as a result of ACE inhibitor binding (Erdos *et al*., 2010)

.

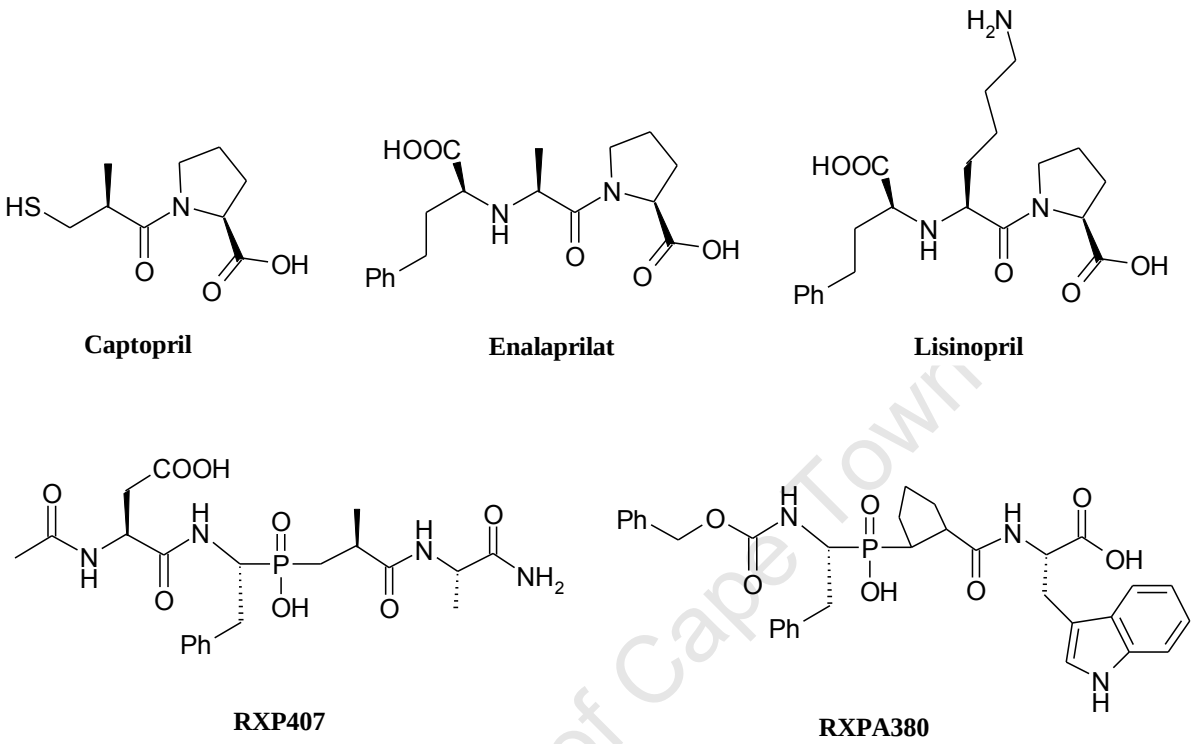

Figure 1.5: Chemical structures of a selection of ACE inhibitors. Captopril, enalaprilat and lisinopril are clinically approved ACE inhibitors for the treatment of hypertension, heart failure and diabetic nephropathy. RXP407 and RXPA380 are phosphinic peptidomimetic inhibitors that are selective for the N- and C-domains respectively.

1.4.2 A structural perspective of ACE inhibitor binding

Side chains of inhibitors and substrates have traditionally been given in the form P_N...P_2, P_1, P_1´, P_2´...P_N´ based on their insertion and interaction with the corresponding S_N...S_2, S_1, S_1´, S_2´...S_N´ subsites (flanking the scissile bond) within the enzyme (Schechter and Berger, 1967). The determination of the crystal structures has allowed for an understanding of inhibitor binding at the atomic level and for the visualisation of the obligatory inhibitor binding sites within the ACE active sites. The resolution of the N-domain and tACE (C-domain, all residues described in tACE numbering) in complex with lisinopril reveals a very similar overall binding mode of the inhibitor in both active sites (Figure 1.6). The inhibitor carboxylalkyl carboxylate in both cases is coordinating the zinc ion and the P_1

phenylalanine extends into the corresponding S_1 subsite to interact with Thr496/Val518 of the N- and C-domains respectively (Natesh *et al*., 2003; Corradi *et al*., 2006). The $P_1´$ lysyl moiety has interactions with unique C-domain $S_1´$ residues Glu162 and Asp377 (replaced by Asp140 and Gln355 in the N-domain respectively) which explains the very slight increase in potency for the C-domain compared to the N-domain and why lisinopril is a slightly more potent inhibitor than enalaprilat which only possesses a methyl in the $P_1´$ position (Natesh *et al*., 2004). The $P_2´$ prolyl carboxylate moiety has significant interactions with conserved residues Gln259/281, Lys489/511 and Tyr498/520 (N/C numbering) and these residues have been suggested to be key in substrate and inhibitor positioning (Natesh *et al*., 2004; Corradi *et al*., 2006; Sturrock *et al*., 2004).

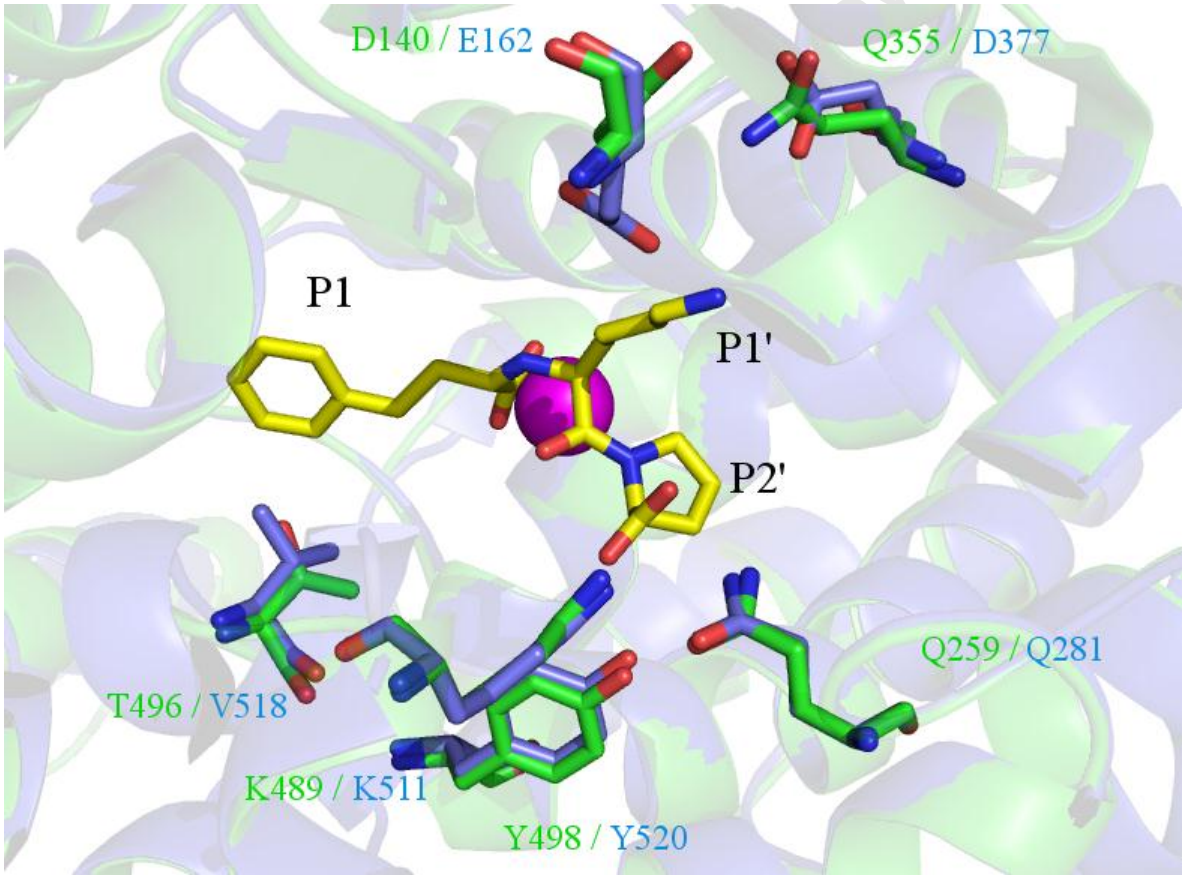

Figure 1.6: Lisinopril binding orientation in the N- (green) and C-domain (blue) active sites. Important contact residues and their corresponding domain counterparts for lisinopril are shown as well as the nomenclature of inhibitor functional group positioning in black (Schechter and Berger, 1967). Lisinopril and the catalytic zinc ion are shown in yellow and magenta respectively. Image generated using PyMOL software (v 0.99, DeLano Scientific).

1.4.3 The need for second generation, N-selective ACE inhibitors

ACE inhibitor treatment is effective in lowering blood pressure. While efficacy is noted in many cases, adverse drug effects (ADEs) have been associated with ACE inhibitor treatment that can lead to discontinuation of drug administration and can be life threatening (Speirs *et al*., 1998; Morimoto *et al*., 2004). The issues pertaining to the molecular basis of ACE inhibitor associated ADEs are complex but the elevation of BK due to ACE inhibition has been implicated as a key contributor to these events (Nussberger *et al*., 1998; Emanueli *et al*., 1998; Adam *et al*., 2002).

First generation ACE inhibitors bind in the low nanomolar range to both domains of sACE (Wei *et al*., 1992). Since BK is cleaved with approximately equal efficiency between domains, and the C-domain active site is the predominant site of AngI conversion *in vivo*, development of low molecular weight inhibitors that selectively inhibit the C-domain (C-selective) have been hypothesised to lower AngII production while leaving the N-domain free to degrade BK (Acharya *et al*., 2003; Ehlers, 2006). Such molecules could have efficacious effects in lowering blood pressure with possibly reduced incidences of ADEs due to lower BK levels.

The domain selective inhibition hypothesis can also be extended to the development of novel N-selective inhibitors. This is due to the compelling *in vivo* evidence describing the buildup of AcSDKP due to general ACE (non-domain selective) inhibition, N-selective inhibition and N-domain inactivation (Azizi *et al*., 1996; Junot *et al*., 2001; Fuchs *et al*., 2004) and the subsequent beneficial effects of elevated AcSDKP in minimising fibrosis in cardiac, renal and pulmonary tissue (Peng *et al*., 2003; Liao *et al*., 2010; Li *et al*., 2010). The development of orally available, clinically relevant inhibitors could be useful in the treatment of fibrotic conditions without affecting blood pressure; with possible use in the treatment of idiopathic and drug-induced pulmonary fibrosis with reduced side effects common to ACE inhibitor administration.

1.4.4 RXP407: an N-selective ACE inhibitor

1.4.4.1 Structural features of RXP407

RXP407 (Ac-Asp-(L)Pheψ(PO_2-CH_2)(L)Ala-Ala-NH_2) is a phosphinic-based peptidomimetic inhibitor that displays three orders of magnitude N-selectivity and can be used as an initial template for the design of novel N-selective compounds (Dive *et al*., 1999). RXP407 utilises

a phosphinate moiety (R-PO_2-CH_2-R´), a functional group analogous to the transition state of a substrate carbonyl, as the ZBG for this inhibitor (Figure 1.5). This is important since the zinc binding ability of phosphinates is lower than hydroxymate and thiolate containing compounds, thus the overall potency is determined by interactions with amino acids within the ACE active sites and not by almost exclusively zinc binding alone (Dive *et al*., 2004).

The discovery of RXP407 involved a combinatorial chemistry approach and the screening of a large phosphinic library. Maintaining a Ac-P_2-Pheψ-(PO_2-CH_2)-Ala-P_2´-NH_2 backbone, all naturally occurring amino acids were tested in the P_2 position for inhibition of the N- and C-domains; with Asp showing the greatest N-selectivity. Assessment of the P_2´ residue best suited for N-selectivity revealed no residues that significantly contributed to selectivity, with an Ala residue in that position having the greatest effect out of a selection of poorly N-selective molecules. This approach allowed for the generation of an inhibitor that possessed unusual structural characteristics compared to other previous ACE inhibitors; namely a C-terminal amide (as opposed to the classic carboxylate) and the extension of an acetylated N-terminal Asp residue into the P_2 position (Figure 1.5) (Dive *et al*., 1999).

The synthesis of RXP407 analogues containing changes of significant inhibitor functional groups revealed important structural determinants for N-selective binding, with a free N- or C-terminus and the replacement of the Asp residue with Ala causing a substantial decrease in N-selectivity (Dive *et al*., 1999). The relative extent of contribution of these groups can be summarised as C-terminal amide > P_2 Asp > *N*-acetyl (Dive *et al*., 1999). These findings not only implicate the importance of these functional groups in N-selectivity, but also implicate the N-domain S_2 and S_2´ subsites in providing significant interactions for N-selective binding.

1.4.4.2 The RXP407–N-domain structure

Prior to the determination of the RXP407–N-domain co-crystal structure, investigators made use of the other available structures to gain insight as to the binding mode of RXP407 in N-selective binding. Tzakos and Gerothanassis (2005) performed homology modelling of the newly solved tACE structure to generate a three dimensional structure of the N-domain and modelled RXP407 on the basis of the positioning of a phosphinic inhibitor analogue in the crystal structure of astacin, another zinc peptidase (Tzakos and Gerothanassis, 2005). These authors found that the *N*-acetyl group of RXP407 was in position to interact with unique residues Tyr369 and Arg381. These interactions are lost in the C-domain with these residues

being replaced by Phe391 and Glu403, respectively (tACE numbering). The P_2 Asp, also important for selective binding, had a salt bridge interaction with conserved residue Arg500 while the C-terminal amide made contact with Glu431 in the N-domain. Glu431 is replaced by Asp354, an acidic residue that has a shorter side chain length (Tzakos and Gerothanassis, 2005). Corradi *et al.* (2006) utilised the newly solved N-domain crystal structure (PDB accession code 2C6N) to perform approximate inhibitor positioning using molecular docking techniques and found an inhibitor binding orientation similar to that presented above (Corradi *et al*., 2006). Jullien *et al*. (2006) also performed homology modelling of the C-domain followed by energy minimisations of the RXP407 ligand in the active site and showed the C-terminal amide in contact with Glu431 and within 5 Å of residues Ser357 and Thr358 (Jullien *et al*., 2006). These hydrophilic residues are replaced by bulkier, hydrophobic residues Val379 and Val380 and optimisation of interaction with these valines are considered important for the C-selectivity of RXPA380 (Corradi *et al*., 2007). All models agree with each other regarding the approximate positioning of the inhibitor P_2' amide, however, the model proposed by Jullien *et al*. suggests that the P_2 Asp interacts with residues Tyr369 and Arg381 as opposed to the *N*-acetyl group of the inhibitor (Jullien *et al*., 2006). Recently, overlay of the RXP407–AnCE (an ACE homologue in *Drosophila melanogaster*) crystal structure with the N-domain resulted in investigators making a similar observation (Akif *et al*., 2010a). This presents a possible structural basis for the greater contribution of the P_2 Asp to N-selectivity whereby the inhibitor residue interacts with unique residues in the N-domain as opposed to a conserved Arg residue.

The recently solved RXP407–N-domain co-crystal structure sheds light on the appropriateness of the models proposed previously and is in more agreement with the model reported by Jullien *et al*. (2006) and Akif *et al*. (2010a), whereby Tyr369 and Arg381 contact the P_2 Asp of RXP407 (PDB accession code 3NXQ) (Anthony *et al*., 2010). In the crystal structure, the inhibitor has 12 direct hydrogen bonds with residues in the S_2, S_1' and S_2' subsites (Figure 1.7). In the S_2 subsite, the P_2 Asp is noted to have up to four hydrogen bonds with residues Tyr369 and Arg381. Of all the direct hydrogen bonds detected, Tyr369 and Arg381 are the only residues that differ to their corresponding C-domain counterparts. Interestingly, the two molecules of the asymmetric unit of the crystal cell show two different positions of the *N*-acetyl group of RXP407, with this functional group not making direct contact with the protein. The C-terminal amide (in the P_2' position) of the inhibitor makes direct contact with Tyr498, His491 and Gln259 in the S_2' subsite. These three residues are

conserved between domains and have traditionally been considered important for inhibitor binding (Natesh *et al*., 2003). In addition, a water mediated hydrogen bond is possible between the amide oxygen of the inhibitor and Thr358, and this interaction could be lost in the C-domain due to the replacement with Val380 (Anthony *et al*., 2010). The exact and significant contribution of the S_2' subsite to N-selectivity is thus not very clear from the crystal structure but suggested from the RXP407 analogues (Dive *et al*., 1999). The crystal structure provides strong evidence for the contribution of the S_2 subsite to N-selective binding of RXP407.

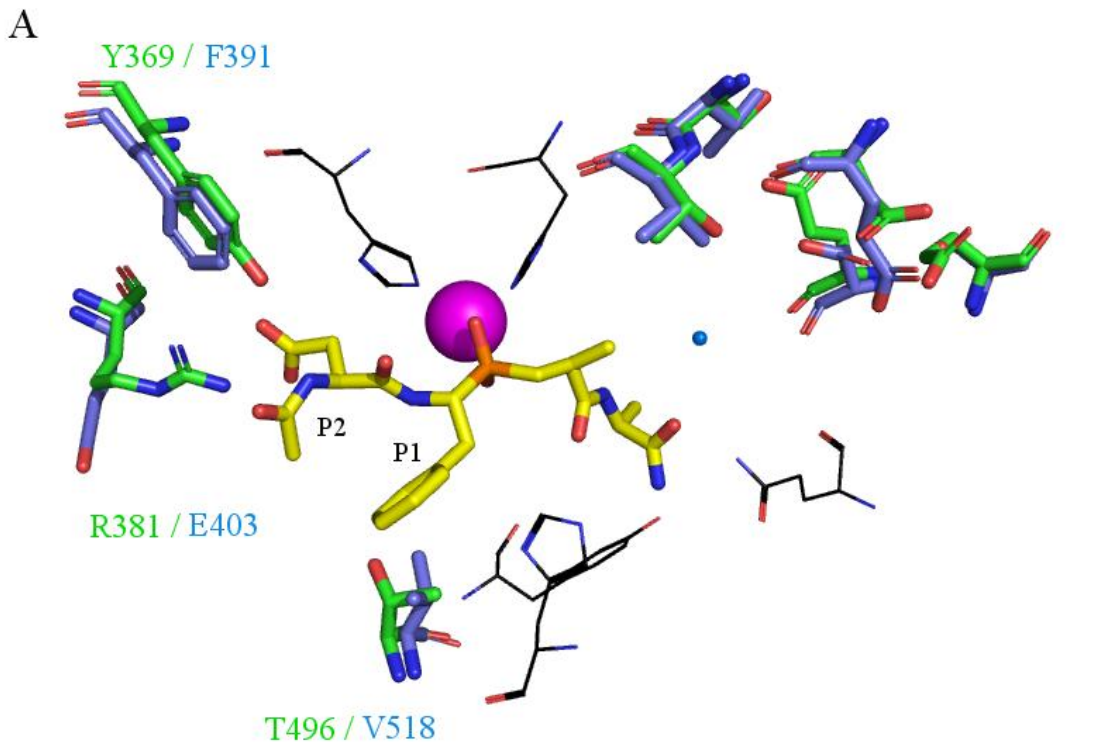

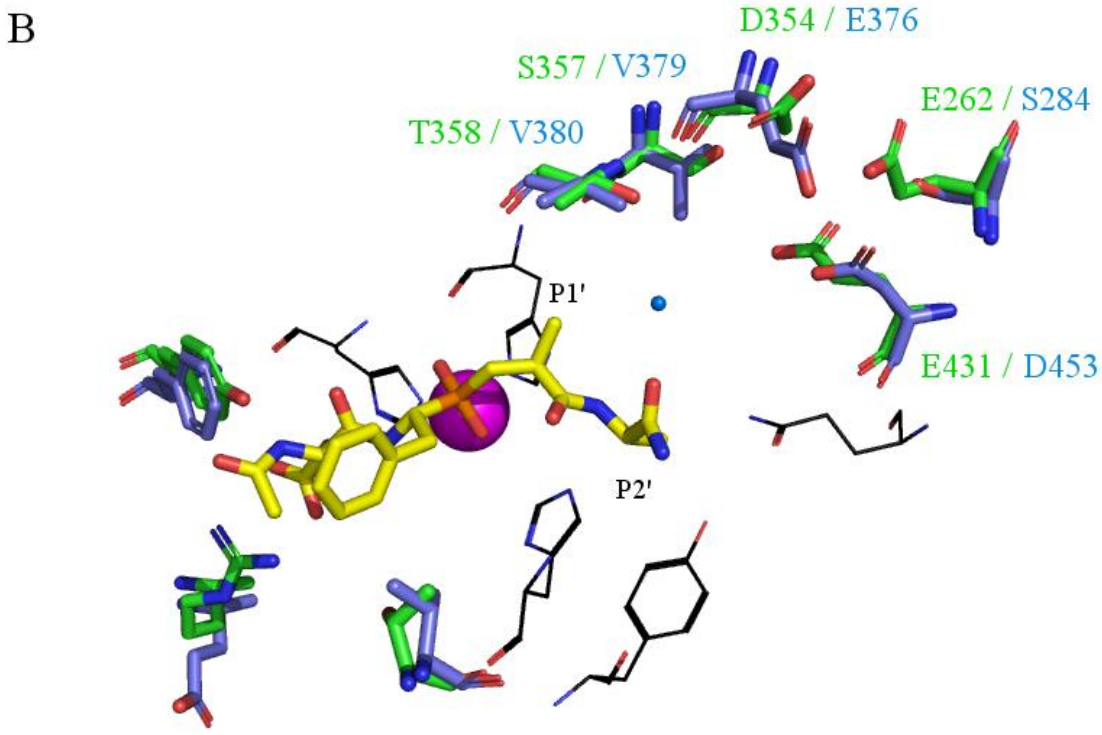

Figure 1.7: The RXP407–N-domain co-crystal structure (PDB accession code 3NXQ). Residues of interest for the N- and C-domains are shown as green and blue sticks respectively in the S_2 (A) and S_2' (B) subsites. The catalytic zinc ion is shown in magenta, RXP407 in yellow and residues conserved between domains in black. A water molecule that could possibly be involved in an interaction between the C-terminal amide and Thr358 is given as a small blue sphere. The RXP407–N-domain crystal structure was structurally aligned to the RXPA380–tACE co-crystal structure (PDB accession code 2OC2) using the program *ALIGN* (Cohen, 1997). tACE numbering used for all C-domain residues. Image generated using PyMOL software (v 0.99, DeLano Scientific).

1.5 Molecular basis for N-selectivity of substrates and inhibitors

1.5.1 The S_2´ subsite

The removal of the P_2´ C-terminal amide from RXP407 and the subsequent drastic loss of N-selectivity implicates residues in the S_2´ subsite providing interactions for N-selective binding (Dive *et al*., 1999). While it is not clear from the crystal structure as to the exact nature of this involvement, the S_2´ subsite contains several residues that differ to their corresponding C-domain amino acids (Corradi *et al*., 2006).

Residues Ser357 and Thr358 are found on the border of the S_2´ subsite and, when compared to the C-domain S_2´ subsite, result in a spatially smaller and more hydrophilic environment (Figure 1.7). The change in subsite size and hydrophobicity in selectivity is emphasised with inhibitors containing P_2´ Trp residues, as in the case of RXPA380, being orders of magnitude more C-selective (Georgiadis *et al*., 2004; Corradi *et al*., 2007).

There are a host of acidic residues present in the S_2´ subsite that differ from their C-domain counterparts in length or polar nature. Glu262, Asp354, Glu431 residues are replaced by Ser, Glu and Asp residues respectively in the C-domain and such changes in acidic nature within this subsite could possibly contribute to preferred binding of RXP407 in the N-domain active site (Figure 1.7 and 1.8) (Corradi *et al*., 2006).

1.5.2 The S_2 subsite

The removal of the RXP407 *N*-acetyl group and P_2 Asp residue result in molecules with markedly reduced N-selectivity (Dive *et al*., 1999). The co-crystal structure of RXP407 in the N-domain active site shows the ability of the P_2 Asp to make significant contacts with unique N-domain residues Tyr369 and Arg381 (Anthony *et al*., 2010). Further work on a keto-ACE inhibitor template indicated the presence of a phenyl group in the P_2 position allowed for improved C-domain inhibition, with molecules containing aliphatic moieties being less C-selective (Nchinda *et al*., 2006b). This change in selectivity was attributed to repulsion of the P_2 phenyl by Tyr369 thus not allowing for stronger binding affinity in the N-domain, whereas the corresponding Phe391 in the C-domain can better accommodate such a group. An aliphatic group could presumably fit into the slightly smaller N-domain S_2 subsite (Nchinda *et al*., 2006b).

In addition to inhibitor functionalities, previous reports studying the synthetic modifications of substrates have implicated the S_2 subsite in contributing to N-selective substrate processing. Michaud *et al*. (1997) reported that AcSDKP analogue hippuryl-Lys-Pro was cleaved with equal efficiency between domains and thus the determinants for N-selective processing lay beyond the C-terminal dipeptide (Michaud *et al*., 1997). Extension analogues were synthesised and extension into the P_1 and P_2 positions was able to partially restore N-selective processing (Michaud *et al*., 1999). Production of an internally quenched fluorogenic equivalent of AcSDKP, Abz-SDK(Dnp)P, confirmed the involvement of the S_2 subsite in substrate selectivity (Araujo *et al*., 2000). Modification of the P_2 Ser to a Thr residue had little effect on selective substrate processing, and conversion to more hydrophobic Tyr and Phe residues resulted in sequential decreases of N-selective processing, suggesting that the presence of an aliphatic alcohol in the P_2 position was a major contributor to N-selective substrate processing (Araujo *et al*., 2000). Thus, although general ACE substrate specificity can be determined by the prospective substrate C-terminal tripeptide (Bunning *et al*., 1983), a large requirement for N-domain specific cleavage appears to lie beyond the S_1 subsite (Michaud *et al*., 1999).

The presence of Tyr369 and Arg381 as unique N-domain residues that appear to have potentially substantial contributions to the selective binding of inhibitor RXP407 has been emphasised above. Another residue, Thr496, is present on the border of the S_2 and S_1 subsites and is replaced in the C-domain by hydrophobic Val518 (Figure 1.7 and 1.8) (Corradi *et al*., 2006). This allows for an extra potential hydrogen bond which could provide an important contact for the binding and positioning of substrates and novel inhibitors.

Thus previous literature reports implicate both the S_2 and S_2' subsites, and residues located within these subsites, in N-selective binding and processing. Unique residues are present in other subsites; Asp140 and Gln355 of the S_1' subsite have been presented above whereby their replacement (with Glu162 and Asp377 in the C-domain) could account for a slight increase in the potency of lisinopril for the C-domain compared to enalaprilat (Figure 1.6). Two residues in the S_1 subsite, namely Ser119 and Asn494, are replaced by Glu143 and Ser516 in the C-domain (Corradi *et al*., 2006). However, these residues have not been implicated in N-selectivity for two main reasons. Firstly, structural modification of inhibitors and substrates suggest the S_2 and S_2' subsites contribute to N-selective binding (as discussed above). Secondly, the available crystal structure indicates that the residues in the S_1 and S_1'

subsites are distant from RXP407 (Anthony *et al*., 2010). Therefore, an analysis of residue contribution to N-domain selective binding and processing by mutagenesis, a study not performed before, should commence with a thorough investigation of the S_2 and S_2' subsites.

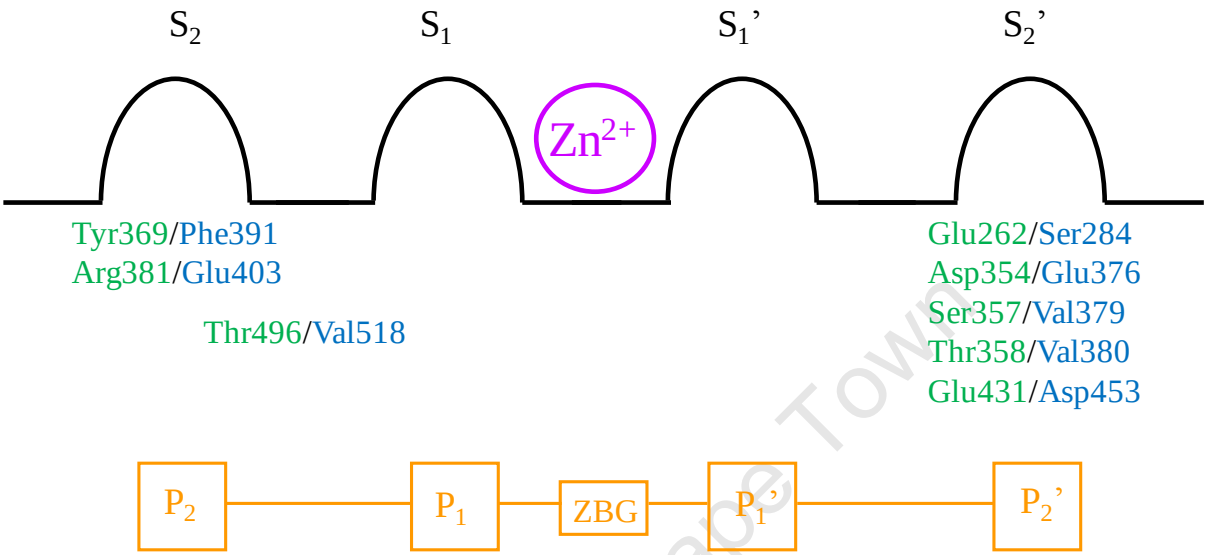

Figure 1.8: Schechter and Burger representation of subsites and residues implicated in N-selectivity. N-domain residues and their corresponding C-domain counterparts are shown in green and blue respectively (tACE numbering for C-domain residues). Catalytic zinc ion represented as a magenta sphere and a representative backbone of an inhibitor with corresponding functional groups that insert into the respective subsites is shown in dark yellow. Thr496/Val518 is represented between the S_1 and S_2 subsites due to this residue being classed as a residue that borders the two subsites.

1.6 Hypothesis statement

The presence of unique N-domain active site residues (that is, with different corresponding C-domain counterpart residues) provide distinct and important interactions with substrates and inhibitors to allow for N-selective binding and processing.

1.7 Aims and objectives

The two domains of sACE display high sequence identity and structural topology but differ in inhibitor binding and substrate processing abilities, suggesting that subtle changes in amino acid composition between the domains confer differences in domain selectivity. The aim of this work is to further elucidate the structure-function relationship of ACE N-selectivity by kinetically assessing residue contribution towards substrate processing and inhibitor binding.

The objectives of the current studies are as follows:

1. To generate mutations of N-domain residues implicated in N-selectivity (outlined in section 1.5) by the conversion into the corresponding C-domain counterparts via site-directed mutagenesis and heterologous protein expression.
2. To kinetically assess the effect of these mutations on the processing of domain selective substrates.
3. To further test the effect of these mutations on the binding of RXP407 and to use this information in the design of novel N-selective inhibitor analogues.

Chapter 2

Mutagenesis, cloning, expression and purification of N-domain enzymes

2.1 Introduction

Whilst sACE contains two domains that are similar in both sequence identity and structural topology, each domain possesses different inhibitor binding and substrate catalysis abilities. This suggests that the unique amino acid residues present in each of the domain active sites could provide distinctive interactions and thus contribute to the observed domain selectivity of the ACE molecule. Identification of residues important for such selectivity would not only aid in understanding of ACE domain substrate specificity but, perhaps more importantly, aid in the structure based design of domain selective ACE inhibitors. Specifically, N-selective ACE inhibitors could be useful in the clinical setting for the potential treatment of pulmonary fibrosis (reviewed in Chapter 1).

Mutagenic conversion of amino acids is a standard approach used to identify key amino acids in enzyme function and has been used to successfully elucidate the structure-function relationships of both the C-domain of ACE and homologue ACE2 (Rushworth *et al*., 2008; Watermeyer *et al*., 2008). Such an approach involves the conversion of key amino acids to their corresponding domain counterparts by codon modification using site-directed mutagenesis; an approach utilising a modified polymerase chain reaction (PCR) and complementary primers to introduce the mutation followed by mutation identification with restriction endonuclease selection (Papworth *et al*., 1996; McPherson, 1990). Residues in both the S_2 and S_2' subsites of the N-domain active site have been implicated in the contribution toward substrate and inhibitor specificity (reviewed in Chapter 1). Thus, these residues have been converted to their corresponding C-domain counterparts (Table 2.1). Enzymes are expressed in mammalian cell tissue culture to fulfil the glycosylation requirements for ACE folding and activity and purified using a simple affinity chromatographic procedure for further kinetic analysis (Bull *et al*., 1985).

Table 2.1: Summary of proposed mutants produced and subsequent naming nomenclature.

Subsite	Mutant name	N-domain residue converted	Introduced C-domain residue (tACE numbering)
S_2	Y369F	Tyr369	Phe391
	R381E	Arg381	Glu403
	YR/FE	Tyr369, Arg381	Phe391, Glu403
	T496V	Thr496	Val518
S_2'	E262S	Glu262	Ser284
	D354E	Asp354	Glu376
	S357V	Ser357	Val379
	T358V	Thr358	Val380
	ST/VV	Ser357, Thr358	Val379, Val380
	E431D	Glu431	Asp453

The objectives for the production of N-domain enzymes with mutations in the S_2 or S_2' subsites were as follows:

1. Conversion of N-domain (*D629*) codons to corresponding C-domain counterparts using a site-directed *Dpn*I approach and confirmation of mutation incorporation by nucleotide sequencing.
2. Cloning of *D629* coding regions containing mutations of interest into mammalian expression vector pcDNA 3.1 (+).
3. Transfection and bulk expression of N-domain enzymes in a mammalian cell culture system.
4. Enzyme purification by lisinopril-sepharose affinity chromatography.

2.2 Methods

2.2.1 Enzymes employed and preparation of pBS-D629

A modified tACE construct, *tACEΔ36NJ,* that lacks the transmembrane region and unique 36 amino acid N-terminus (and therefore identical to the sACE C-domain; hereon referred to as C-domain) had been generated and transfected previously (Ehlers *et al*., 1996). A soluble form of the N-domain, consisting of amino acids 1 to 629 of somatic ACE (hereon referred to as *D629* to refer to the DNA coding region or N-domain to refer to protein), in vector pECE was a kind gift from Dr S. Danilov and was cloned into sequencing vector pBlueScript SK+ (pBS, Invitrogen) as previously described (Balyasnikova *et al*., 2003; Corradi *et al*., 2006). This plasmid was transformed into competent DH5α *E. coli* bacteria and plated onto ampicillin (50 µg/ml) agar plates (Appendix A1). A single ampicillin resistant clone was selected, grown overnight in ampicillin containing medium (luria broth containing 50 µg/ml ampicillin) and plasmid DNA extracted and purified using the Qiagen Mini-prep kit (Qiagen Corp). Purity, integrity and identity of the *pBS-D629* construct was assessed through *Eco*RI and *Xba*I (Fermentas Life Sciences) restriction digests followed by agarose gel electrophoresis with ethidium bromide staining.

2.2.2 Site-directed mutagenesis of soluble N-domain

2.2.2.1 Design of mutagenic primers

One hundred percent complementary primer pairs were designed containing two key features: the mismatch containing the desired codon change and silent mutation(s) that introduces an additional restriction site into the primer incorporated plasmid. Primers were designed according to Stratagene guidelines (Papworth *et al*., 1996) and synthesised by the Inqaba DNA Synthesis Unit (Inqaba Biotech Ltd.). Primers are detailed in Table 2.2. The two primer sets for Y369F and R381E were used in sequential mutagenesis runs for the double mutant YR/FE; while a new primer, eliminating the *Pvu*II site of the S357V primer template was used to generate ST/VV.

Table 2.2: Details of primers utilised for site-directed mutagenesis. Primers were designed using Stratagene guidelines. The codon changed is indicated in bold lower case letters and the restriction enzyme recognition sequence is underlined. In the case of ST357,358VV primer; primer design resulted in the removal of the *Pvu*II restriction site of the S357V template.

Subsite	Mutation	Sequence (5´→3´)	T_m (°C)	Screening enzyme
S_2	Y369F	CCATATACAGTAC**ttc**CTGCAATACAAAGATCTGCCCG	74.2	*Bgl*II
	R381E	GGATCTGCCTGTATCCTTGCGT**gag**GGGGCCAACC	76.6	*Bfu*I
	T496V	GCTAAGTTTCATGTTCCAAATGTG**gta**CCATACATCAGG	75.9	*Kpn*I
S_2´	E262S	GCCCAGAGCTGG**tca**AATATTTACGACATGGTGGTGCC	74.8	*Ssp*I
	D354E	CGGGTCACGATG**gag**CAGCTGTCCACAGTGCACC	82.3	*Pvu*II
	S357V	CGATGGACCAGCTG**gtc**ACAGTGCACCATGAGATGG	78.3	*Pvu*II
	T358V	CGATGGACCAGCTGTCC**gta**GTGCACCATGAGATGG	78.3	*Pvu*II
	ST357,358VV	CGATGGACCAGCTCGTC**gta**GTGCACCATGAGATGG	81.1	*Pvu*II removed
	E431D	GCTAAAAATGGCACTG**gac**AAAATTGCATTCCTGCC	75.4	*Bsm*I

2.2.2.2 Site-directed mutagenesis approach

Reactions were performed using a modified *Dpn*I method (Quick Change® Site-directed mutagenesis, (Papworth *et al*., 1996). Final concentrations of 0.2 µM primers, 0.4 mM dNTPs (Sigma-Aldrich Co.), 5% DMSO (Merck Ltd) and 3 units high fidelity *Pfu* polymerase (Roche Pharmaceuticals) with a total mass of 100 ng *pBS-D629* were used in each mutagenic reaction. Polymerase chain reactions were carried out with the following thermal cycling parameters: denaturation at 94°C (5 min); followed by 16 cycles of 94°C (30 s), 55°C (30 s), 72°C (12 min); final elongation at 72°C (20 min). Aliquots of reactions at various Mg^{2+} concentrations (for optimal polymerase activity and primer specificity) (McPherson, 1990) underwent agarose gel electrophoresis and visualised by ethidium bromide staining. Mutagenic runs showing the greatest specific amplification were selected and digested with 30 units of methylation specific restriction enzyme *Dpn*I (Fermentas Life Sciences) for 4 hours at 37°C to remove remaining template DNA. This was followed by transformation of an aliquot of PCR product reaction mixture into competent DH5α *E. coli* cells and transformants plated onto ampicillin agar plates (Appendix A1).

2.2.2.3 Mutation confirmation

Resistant *pBS-D629* mutant clones were picked and grown overnight in ampicillin containing media. Plasmid DNA was crudely isolated, digested with the appropriate restriction enzyme and visualised with agarose gel electrophoresis (Appendix A1). Positively incorporated mutants were identified by differences in DNA banding patterns compared to template DNA. The presence of the desired mutations, and absence of spurious introductions, was confirmed by nucleotide sequencing of the entire *D629* coding region using internal *D629* and flanking vector (T3 and T7) primers (sequencing performed by DNA Sequencing Unit, Department of Molecular and Cell Biology, UCT).

2.2.3 Cloning of mutant D629 constructs into mammalian expression vector pcDNA 3.1(+)

The cloning strategy served to take the *D629* coding region present in a sequencing vector and successfully incorporate it into another vector effective in mammalian protein expression (Figure 2.1). Approximately 300 ng of each successfully mutated *pBS-D629* template was doubly digested with 15 units *Eco*RI and 10 units *Xba*I. This allowed for the expulsion of the *D629* insert out of the sequencing vector. Following enzymatic digestion, fragments were separated out through agarose gel electrophoresis, visualised and inserts of the correct size excised. Excised insert was purified from the agarose gel using the Wizard® SV Gel and PCR Clean-Up System (Promega Ltd) with supplied protocol and resuspended in 50 µl nuclease free dH_2O. Singly digested *pBS-D629* mutants were produced to control for ligation experiments. Approximately 400 ng of empty vector pcDNA 3.1(+) (Invitrogen Corp.) was doubly digested as above to provide suitable sites for ligation of the insert in the correct orientation. Ligation reactions were set up using a ratio of 1:3 (vector:insert) in the presence of T4 DNA ligase (Fermentas Life Sciences) for several hours at room temperature. Ligation reactions were transformed into competent DH5α *E. coli* and transformants grown on ampicillin selective agar plates (Appendix A1). Screening with cloning enzymes and restriction enzyme sites mutagenically produced allowed for the identification of positive clones containing the mutated insert in pcDNA 3.1(+), thus *pcDNA-D629*. Identified positive constructs were bulk purified using a medium scale plasmid preparation kit (Qiagen Corp.). Prior to transfection, correct mutation and purity of each plasmid was confirmed by restriction enzyme digestion and subsequent agarose gel electrophoresis.

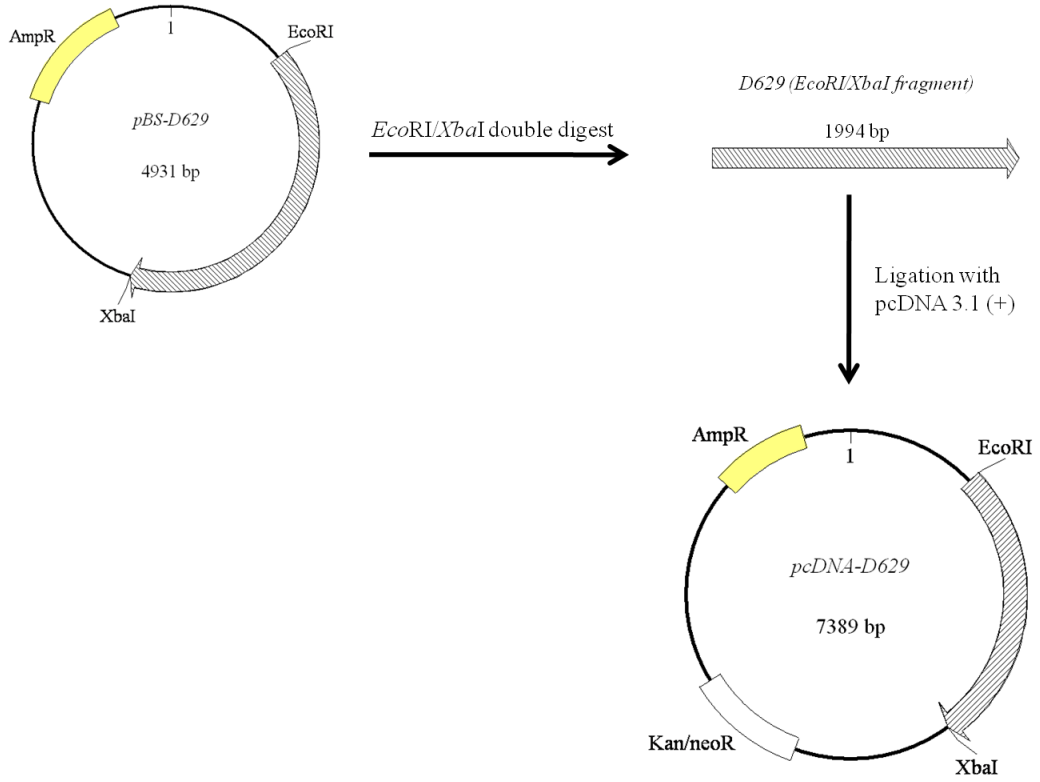

Figure 2.1: A schematic representation of the cloning strategy employed for incorporation of *D629* mutant coding regions into mammalian expression vector pcDNA 3.1 (+). pBS (Invitrogen Corp.) containing the wild-type *D629* coding region (hashed bar) was mutated to codons of interest via site-directed mutagenesis and confirmed by nucleotide sequencing. The *D629* coding region was excised from *pBS-D629* through double digestion of cloning enzymes *Eco*RI and *Xba*I (Fermentas Life Sciences). Pure insert was ligated with prepared vector pcDNA 3.1(+) (previously *Eco*RI and *Xba*I doubly digested, Invitrogen Corp.) to produce *pcDNA-D629* constructs. Incorporation and orientation of the *D629* insert were confirmed by restriction enzyme digests.

2.2.4 Mammalian cell expression of N-domain enzymes

Chinese hamster ovary (CHO) mammalian cell line CHO-K1 was used as the model system for transfection and expression of N-domain enzymes. CHO-K1 cells were cultured at 37°C, 5% CO_2 and 80% relative humidity levels.

CHO-K1 cells were grown to 60% confluency in 100 mm transfection dishes (all tissue culture dishes and flasks supplied by Nunc Ltd) and transfected using the calcium phosphate Profection® Mammalian Transfection System (Promega Corp.) according to the manufacturer's protocol. Briefly, fresh growth medium (constituents of tissue culture medium

employed detailed in the Appendix A2) was applied to the untransfected cells 3 hours prior to transfection. Approximately 15 µg of *pcDNA-D629* construct was finely precipitated by dropwise addition of the DNA solution to $CaCl_2$ (as per manufacturer's guidelines). Following a 30 minute room temperature incubation of the DNA precipitate, the DNA suspension was added dropwise to the cultured cells and incubated at culturing conditions for about 4 hours. To increase transfection efficiencies, cells underwent exposure to glycerol shock solution for 2 minutes followed by extensive washing with wash solution (constituents outlined in the Appendix A2) and subsequent replacement of growth medium.

Twenty four hours after transfection, normal growth medium was replaced with growth medium containing mammalian anti-biotic geneticin (G418; 0.9 mg/ml, Sigma-Aldrich Co.). Colonies showing resistance to G418 were picked and grown in 12 well plates, with high activity clones being selected based on ACE activity via *Z*-Phe-His-Leu (*Z*-FHL) assay (Section 2.2.5). Highest expressers of each construct were seeded from 12 well plates and grown to confluency in T-175 cm^2 flasks; followed by addition of harvesting medium (Appendix A2). Medium was harvested every 72 hours and stored at -20°C until purification.

2.2.5 Z-Phe-His-Leu assay

The cleavage of ACE substrate *Z*-FHL is useful in determining the extent of ACE activity and expression in a given cell culture system or protein solution and was performed as previously described (Friedland and Silverstein, 1976; Schwager *et al*., 2006). Briefly, 5 µl of medium solution was added to 30 µl of a 1 mM *Z*-FHL (Bachem Ltd) in phosphate buffer (100 mM $KHPO_4/KH_2PO_4$ pH 8.3, 300 mM NaCl, 10 µM $ZnSO_4$) on ice in triplicate in a 96-well plate. This enzyme-substrate mixture was incubated at 37°C for 20 minutes and stopped by the addition of 120 µl 0.4 M NaOH. Derivitisation of the liberated His-Leu moiety commenced with the addition of *o*-pthaldialdehyde (Sigma-Aldrich Co., 24 mg/ml in methanol) and the subsequent mixture incubated at room temperature for 10 minutes. Derivitisation was stopped through the addition of 30 µl 3 M HCl and fluorescence intensities measured at λ_{ex}= 360 nm and λ_{em}= 485 nm using a fluorescence spectrophotometer (Varian Inc.). Enzymatic activity was calculated through the use of a His-Leu standard curve (section 3.2.4.1 and Appendix A4).

2.2.6 Purification of N-domain enzymes

Lisinopril, a potent ACE inhibitor, coupled by its free P_1' lysine to sepharose beads was employed to conduct a one-step affinity chromatography purification protocol (El Dorry *et al*., 1982; Bull *et al*., 1985). Medium harvests were defrosted, pooled and NaCl added to bring the final salt concentration to 800 mM NaCl to ensure sufficient binding of the N-domain to the lisinopril beads (Deddish *et al*., 1994). The lisinopril-sepharose affinity column was first washed with wash buffer (20 mM HEPES pH 7.5, 800 mM NaCl, 10 µM $ZnSO_4$) for 20 minutes. The salted harvest medium was loaded on the prepared column and allowed to pass through. Once the harvest medium had been loaded onto the column, the column was washed overnight with wash buffer to remove unbound material. Elution proceeded with the washing of the column with elution buffer (50 mM borate pH 9.5) and eluted fractions collected. Fractions displaying ACE activity (in a Z-FHL assay, section 2.2.5) were pooled into SnakeSkin® pleated dialysis tubing (Pierce Biotechnology Ltd) and placed into dialysis buffer 1 (5 mM HEPES pH 7.5, 0.05 mM PMSF (in ethanol)) at 4°C for 6 hours. The pooled dialysed enzyme solution was then placed into dialysis buffer 2 (50 mM HEPES pH 7.5, 0.05 mM PMSF (in ethanol)) and dialysed overnight at 4°C. Protein concentration after dialysis was determined via a Bradford assay (Bradford, 1976) using BioRad protein reagent (BioRad Laboratories Inc.) and albumin as a standard. Protein purity was assessed via sodium dodecyl sulphate polyacrylamide gel electrophoresis (SDS-PAGE) using a 10% acrylamide gel and stained with Coomassie stain (Appendix A2). Wild type C-domain was purified in a similar manner with the exception of lower NaCl concentrations in the wash buffer (buffer contained 500 mM NaCl).

2.3 Results

2.3.1 Preparation of pBS-D629

The coding region of the N-domain of ACE had previously been inserted into the plasmid pBlueScript SK+ (Balyasnikova *et al*., 2003). Transformation and plasmid DNA isolation allowed for identification of a *pBS-D629* clone. Double digestion with cloning enzymes *Eco*RI and *Xba*I reveals the vector (2.9 kb) and *D629* coding region (2.0 kb) after agarose gel electrophoresis (Figure 2.2).

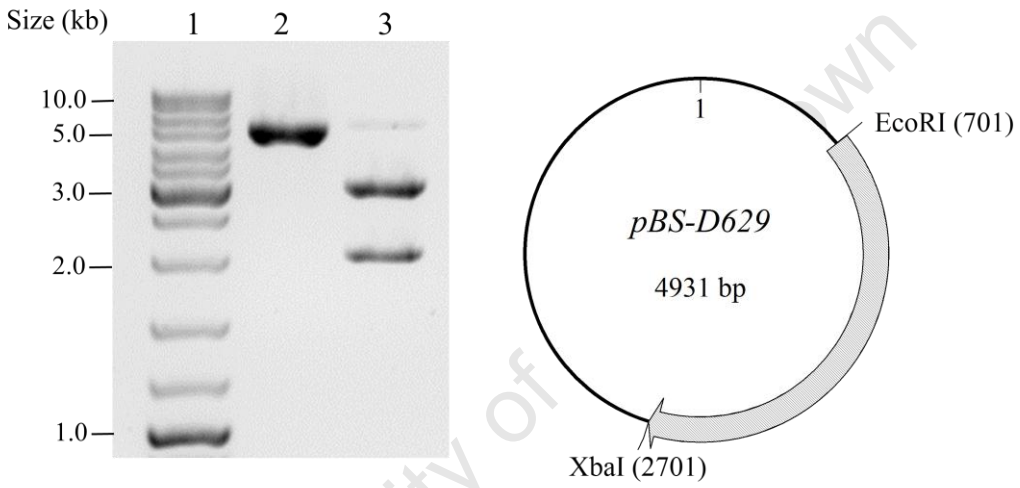

Figure 2.2: Restriction enzyme analysis of *pBS-D629* mutagenesis construct. Unmutated *pBS-D629* was digested with *Xba*I or doubly with *Eco*RI and *Xba*I to confirm plasmid and insert sizes. A plasmid size of 4.9 kb, vector of 2.9 kb and insert of 2.0 kb were confirmed. Lane 1, molecular weight marker (O'Gene™ Ruler DNA Ladder Mix, Fermentas); lane 2, *pBS-D629 Xba*I digest; lane 3, *pBS-D629 Eco*RI/*Xba*I double digest.

2.3.2 Site-directed mutagenesis

Using mutagenic primers and cycling parameters as outlined in Methods (section 2.2.2), a clear amplicon at predicted plasmid size (4.93 kb) for all mutant *D629* constructs was obtained (Figure 2.3).

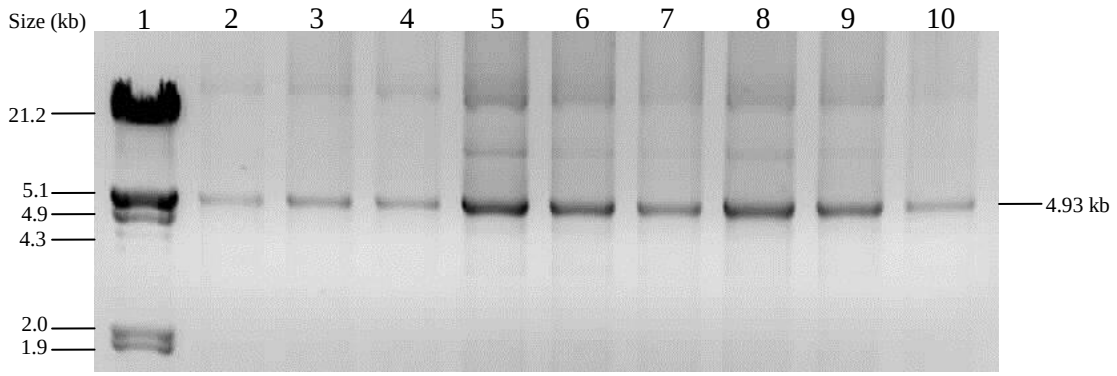

Figure 2.3: A representative gel indicating site-directed mutagenesis products of mutations R381E (lanes 2-4); S357V (lanes 5-7) and T358V (lanes 8-10). pBluescript SK(+) containing wild type N-domain (*D629*), *pBS-D629*, was used as a template and mutagenic constructs amplified using high fidelity *Pfu* DNA polymerase. Expected product migrates at a size of approximately 5 kb. Lane 1, molecular weight marker (*Eco*RI/*Hind*III λ DNA); lane 2, R381E 2 mM $MgCl_2$ run; lane 3, R381E 3 mM $MgCl_2$ run; lane 4, R381E 4 mM $MgCl_2$ run; lane 5, S357V 2 mM $MgCl_2$ run; lane 6, S357V 3 mM $MgCl_2$ run; lane 7, S357V 4 mM $MgCl_2$ run; lane 8, T358V 2 mM $MgCl_2$ run; lane 9, T358V 3 mM $MgCl_2$ run; lane 10, T358V 4 mM $MgCl_2$ run. Products from lanes 3, 5 and 8 were selected for further screening.

Mutagenic reactions showing the greatest visualised amplification were digested with *Dpn*I, transformed, plasmid DNA isolated of selected clones and digested with the appropriate restriction enzyme that contained the newly introduced mutagenic primer restriction site. Screened *pBS-D629* mutant constructs displayed a DNA banding pattern different to that of wild type *pBS-D629* with sizes as predicted by computational methods (DNAMAN v. 4.13, Lynnon Biosoft, 1994).

Nucleotide sequencing of the entire *D629* coding region confirmed the correct introduction of codon change and silent restriction site without any spurious mutations incorporated.

2.3.3 Cloning of mutant D629 constructs into mammalian expression vector pcDNA 3.1(+) and plasmid confirmation

Confirmed mutant coding regions of *D629* in *pBS-D629* were excised through double endonuclease digestion with cloning enzymes *Eco*RI and *Xba*I and isolated fragments inserted into mammalian expression vector pcDNA 3.1(+) as described above (section 2.2.3). Screening of *pcDNA-D629* mutants using appropriate restrictions enzymes (those incorporated into *D629* during mutagenesis) revealed banding patterns that indicated the desired vector, the presence of the incorporated primer and correctly orientated insert.

Banding patterns of mutant plasmids predictably differed compared to wild type digests of the corresponding screening endonuclease (Figures 2.4-2.6). Double S_2´ construct ST/VV contained two consecutive mutations in the same coding region and required the removal of the *Pvu*II from the S357V template to facilitate mutation screening. Thus, restriction screening of *pcDNA-ST/VV* with enzyme *Pvu*II differed from S357V and T358V mutants and had the same banding pattern as that of unmutated plasmid (Figure 2.5). Positively identified plasmids were individually bulk purified for transfection.

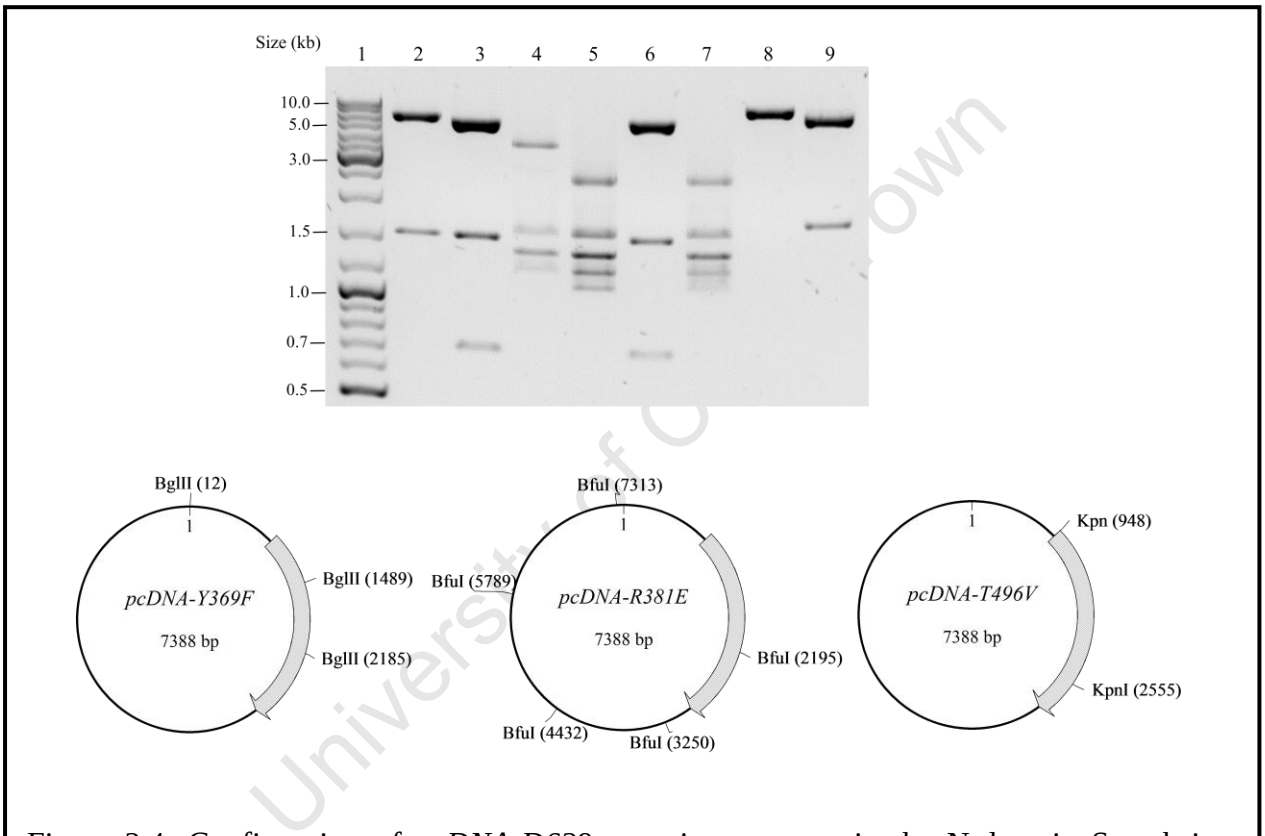

Figure 2.4: Confirmation of *pcDNA-D629* mutations present in the N-domain S_2 subsite. Successfully cloned mutant *D629* coding regions underwent restriction enzyme screening with endonucleases that recognise the primer introduced restriction site to confirm both the correct vector size and presence of the desired mutation. Lane 1, molecular weight marker (O'Gene™ Ruler DNA Ladder Mix, Fermentas); lane 2, unmutated wild type *pcDNA-D629 Bgl*II digest; lane 3, *pcDNA-Y369F Bgl*II digest; lane 4, unmutated wild type *pcDNA-D629 Bfu*I digest; lane 5, *pcDNA-R381E Bfu*I digest; lane 6, *pcDNA-YR/FE Bgl*II digest; lane 7, *pcDNA-YR/FE Bfu*I digest; lane 8, unmutated wild type *pcDNA-D629 Kpn*I digest; lane 9, *pcDNA-T496V Kpn*I digest. Construct *pcDNA-YR/FE* contains both Y369F and R381E mutations in the same *D629* coding region.

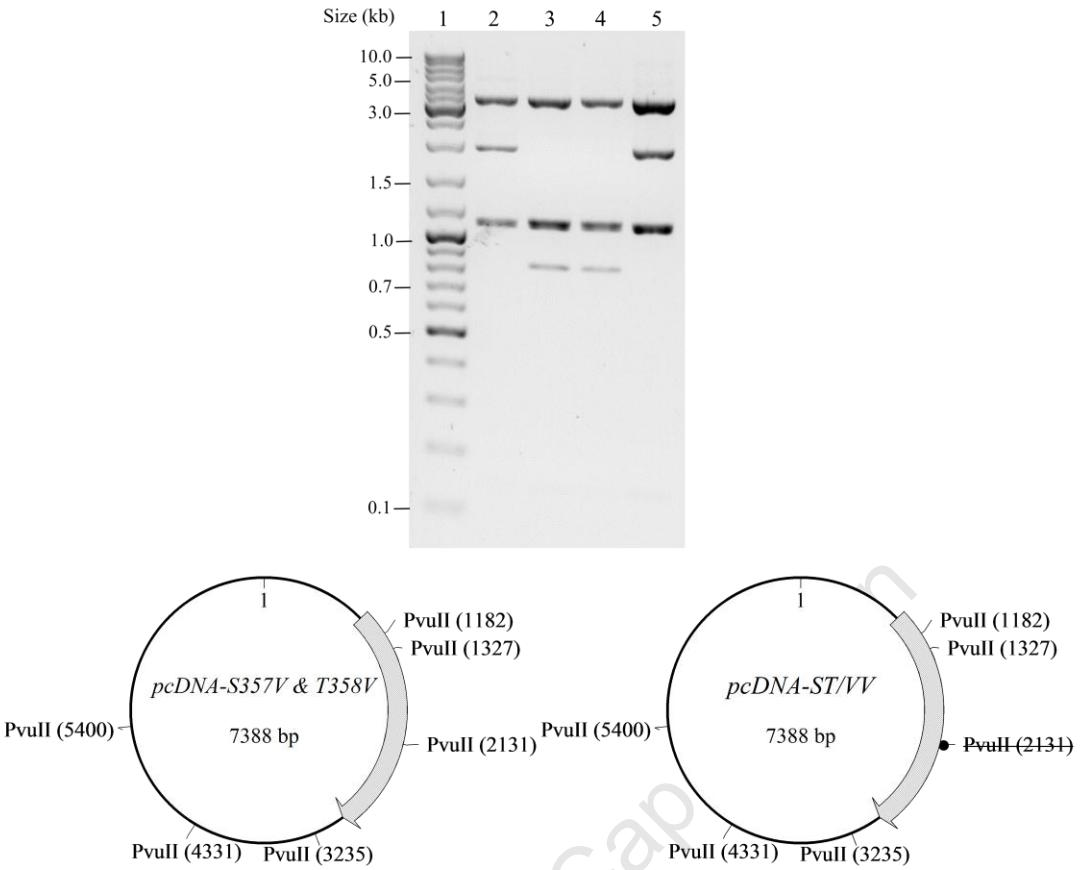

Figure 2.5: Confirmation of *pcDNA-D629* hydrophobic mutations present in the N-domain S_2´ subsite. Restriction enzyme screens were performed as in Figure 2.4. Lane 1, molecular weight marker (O'Gene™ Ruler DNA Ladder Mix, Fermentas); lane 2, unmutated wild type *pcDNA-D629 Pvu*II digest; lane 3, *pcDNA-S357V Pvu*II digest; lane 4, *pcDNA-T358V Pvu*II digest; lane 5, *pcDNA-ST/VV Pvu*II digest. Construct *pcDNA-ST/VV* contains both S357V and T358V mutations in the same *D629* coding region. Primer incorporation resulted in the loss of the *Pvu*II (2131) site of the S357V template.

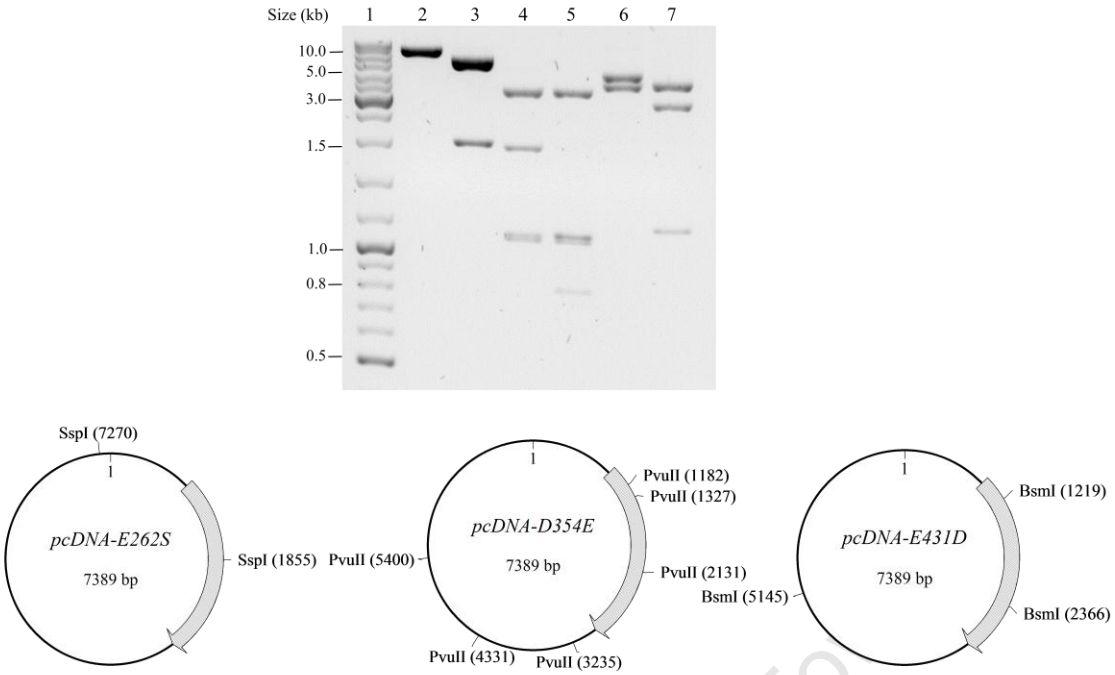

Figure 2.6: Confirmation of *pcDNA-D629* mutations of acidic amino acids present in the N-domain S_2´ subsite. Restriction enzyme screens were performed as in Figure 2.4. Lane 1, molecular weight marker (O'Gene™ Ruler DNA Ladder Mix, Fermentas); lane 2, unmutated wild type *pcDNA-D629 Ssp*I digest; lane 3, *pcDNA-E262S Ssp*I digest; lane 4, unmutated wild type *pcDNA-D629 Pvu*II digest; lane 5, *pcDNA-D354E Pvu*II digest; lane 6, unmutated wild type *pcDNA-D629 Bsm*I digest; lane 7, *pcDNA-D629 Bsm*I digest.

2.3.4 Expression and purification of enzymes

Successfully produced plasmids were transfected into CHO-K1 cells using a calcium-phosphate precipitation protocol as outlined in section 2.2.4. Transfection of *pcDNA-D629* plasmids yielded high expressing clones that had detectable *Z*-FHL hydrolysis activity in the culture medium (Table 2.3). Medium activity of untransfected CHO-K1 cells was negligible. Post lisinopril affinity chromatography (section 2.2.6), yields of protein per litre of harvest medium were calculated. Protein yields were variable between enzymes ranging from 0.8 to 17.9 $mg.L^{-1}$. Several N-domain enzymes (R381E, T496V, D354E and T358V) displayed better expression than wild type enzymes while other derivatives (YR/FE and ST/VV) showed marked reduction in expression profile. In all cases there was sufficient enzyme to proceed with kinetic analysis (presented in Chapters 3 and 4).

Table 2.3: Expression levels of C-domain, N-domain and N-domain protein derivatives. Transfection and expression was performed as detailed in section 2.2.4. Protein yield was calculated post-purification.

Subsite	**Enzyme**	**Activity** ($mU.ml^{-1}$ medium)	**Protein yield** ($mg.L^{-1}$ medium)
-	N-domain	163.4	9.06
	C-domain	156.9	2.12
S_2	Y369F	326.0	7.88
	R381E	191.7	13.6
	YR/FE	74.49	0.90
	T496V	360.4	19.1
S_2'	E262S	215.9	10.2
	D354E	414.9	12.6
	S357V	45.2	2.35
	T358V	412.7	17.9
	ST/VV	50.1	0.81
	E431D	157.0	5.30

All purified enzymes were subjected to SDS-PAGE and visualised with Coomassie staining (section 2.2.6). The predicted molecular mass of unglycosylated N-domain is 72.25 kDa and, taking into account glycosylation (approximately 30%), was predicted to result in a total mass of approximately 90 kDa (Deddish *et al*., 1994; Gasteiger *et al*., 2003). Visualised protein

bands revealed enzymes migrating at the correct predicted size, in agreement with a previous publication expressing soluble N-domain in CHO cells (Rice *et al.*, 2004), and in a homogenous state (Figure 2.7).

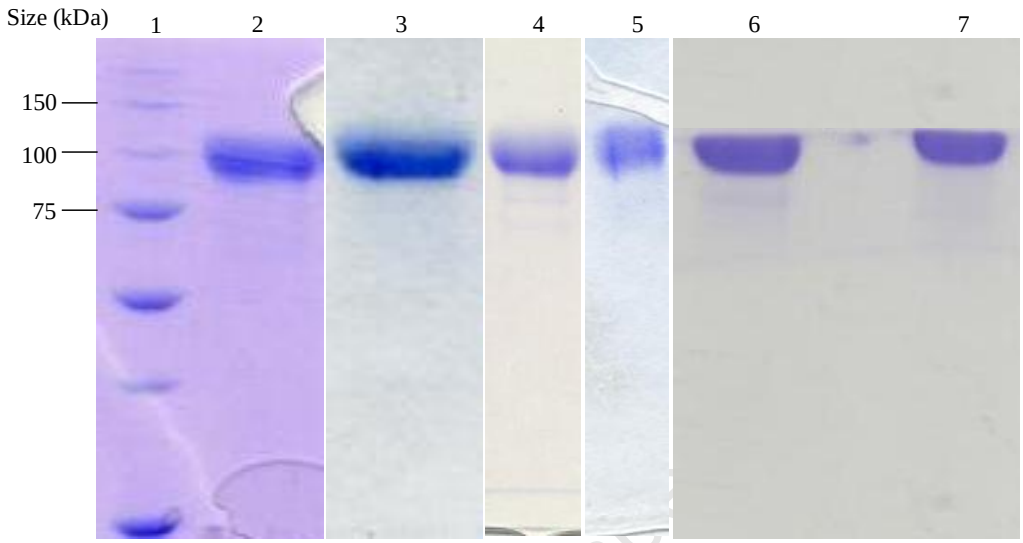

Figure 2.7: Representative acrylamide gels indicating enzyme size and purity. Approximately 10 µg of protein was electrophorised at 50 mA in a 10% denaturing acrylamide gel until suitable separation was achieved. The gel was stained with Coomassie Brilliant Blue and destained with destaining solution as described in Methods and Appendix A2. Lane 1, low molecular weight marker (sizes displayed in kDa, BioRad); lane 2, purified N-domain; lane 3, purified Y369F; lane 4, purified R381E; lane 5, purified YR/FE; lane 6, purified E431D; lane 7, purified T496V. In all cases a single stained band of approximately 90 kDa was observed. Each gel underwent electrophoresis with a molecular marker and aligned.

2.4 Discussion

Site-directed mutagenesis is a powerful molecular biology technique effective in the production of DNA constructs with desired mutations. Many technique variations have been designed ranging from single nucleotide substitution protocols to recombinant approaches whereby large fragments are inserted in cassette-like fashion (McPherson, 1990). While original procedures required single stranded DNA as a template and *in vitro* completion of the complementary strand, use of PCR methodologies allowed for the use of double stranded DNA as a starting template, permitting the use of standard plasmids from organisms other than viruses. Identification of primer incorporated plasmids has traditionally taken four approaches; namely restriction selection, restriction purification, the use of uracil-containing vectors and recognition of phosphorothioate containing plasmids (from the original primer set) (McPherson, 1990). In this study, extensive digestion with methylation specific endonuclease *Dpn*I prior to screening digest removed almost all methylated parental DNA (Papworth *et al*., 1996). This provided simplicity of screening whereby most of the transformants screened were positive for the desired mutation. Restriction selection remains one of the simplest approaches in identification of positive clones without the use of radio labelled probes and is considerably more cost effective than total gene synthesis (Carter, 1986).

A simple cloning strategy allowed for confirmed mutants to be successfully cloned into a mammalian expression vector through the unique restriction sites of *Eco*RI and *Xba*I in the correct insert orientation. Such a cloning strategy had been designed previously to allow for uncomplicated orientation of the insert in the vector (Balyasnikova *et al*., 2003; Corradi *et al*., 2006). All expression plasmids were confirmed by restriction enzyme digestion and transfected into CHO-K1 cells.

Heterologous protein expression has allowed the bulk expression of numerous recombinant proteins that otherwise would require laborious extraction procedures and large amounts of tissue to obtain suitable quantities of enzyme. A number of expression systems have been developed with each having its own set of advantages and disadvantages (reviewed in (Yin *et al*., 2007). Whilst expression in the *E. coli* bacterial system is considered simplest and most cost effective, such a system is not appropriate for the expression of ACE domains due to prokaryotes lacking the molecular machinery for *N*-linked glycosylation and chaperone

mediated protein folding (Yin *et al*., 2007; Mus-Veteau, 2002). Thus, eukaryote cells are required for ACE expression. Indeed, ACE has previously been reported to be expressed in *E. coli* but inactive while expression in yeast *Pichia Pastoris* or cancer cell line HeLa produced active enzyme albeit with different glycosylation patterns (Sadhukhan and Sen, 1996; Williams *et al*., 1997). CHO cells (along with other mammalian cell lines) provide the appropriate machinery for the expression of ACE and this system has been used in our research group to produce ACE proteins in amounts sufficient for crystallisation studies (Natesh *et al*., 2003; Gordon *et al*., 2003; Corradi *et al*., 2006). This optimised system was sufficient for the need of relatively small amounts of protein required for this study.

Transfection of the CHO-K1 cell line produced stable cell lines expressing assay detectable amounts of enzyme activity, with higher culture medium activity generally corresponding to higher protein yields. Variable expression was obtained for protein derivatives with some active site mutants resulting in higher expression than that of wild type controls while both N-domain double mutants had considerably lower activities and yields. Although the conversion of one or more amino acids could result in a more (or less) stable protein structure; these data are most likely due to variable transfection efficiencies. This is suggested since enzymes (with the exception of ST/VV) display comparable catalytic efficiencies to wild-type controls with substrate Abz-Phe-Arg-Lys(Dnp)-Pro (Chapter 3). The ST/VV mutant could have lowered medium activity probably due to decreased overall catalytic ability (presented in Chapter 3). The C-domain enzyme displayed similar activity but reduced yield when compared to the N-domain and is most likely due to its increased catalytic efficiency with the substrate *Z*-FHL (Chapter 3). Thus, less enzyme is required for similar activities.

Purification of both isoforms of ACE has involved purification techniques of ion exchange and size exclusion (Cheung *et al*., 1980; Stewart *et al*., 1981; Ronchi *et al*., 2005), the use of ACE specific antibodies (Lanzillo *et al*., 1980) and affinity chromatography using modified ACE inhibitor structures (Harris *et al*., 1981; El Dorry *et al*., 1982; Pantoliano *et al*., 1984; Bull *et al*., 1985). Affinity chromatography allows ACE to be purified to much higher fold purification from tissue and plasma in only a few steps. Such an approach can also be used, as in this setting, in the purification of recombinant ACE from tissue culture medium in a single purification step. In each case, N-domain and mutant enzymes were purified to

homogeneity as observed by gel electrophoresis, thus yielding sufficiently pure protein for subsequent kinetic analyses.

In summary, implicated residues in the N-domain S_2 and S_2´subsites were converted to corresponding C-domain counterparts via site-directed mutagenesis and confirmed by nucleotide sequencing of the N-domain coding region. An effective cloning strategy allowed for incorporation of the *D629* coding region in a mammalian expression vector and plasmids were transfected. Variable protein expression was observed and, following affinity chromatographic purification, in all cases there was sufficient protein for the required substrate and inhibitor kinetic analysis.

Chapter 3

Mutations in the N-domain and their effects on substrate processing

3.1 Introduction

Somatic ACE is able to cleave a variety of physiologically relevant peptides (reviewed in Chapter 1). In addition, despite 90% sequence identity between the N- and C-domain active sites (Soubrier *et al*., 1988), domain substrate specificity exists for a number of these peptides. *In vivo* mouse studies have demonstrated the primary role of the C-domain in AngI conversion, while inactivation of the N-domain through gene targeting or selective inhibition resulted in elevated AcSDKP levels (Junot *et al*., 2001; Fuchs *et al*., 2004; Fuchs *et al*., 2008).

Several previous publications sought to define the determinants of N-selective substrate processing. Such analysis involved the generation of AcSDKP analogues and their subsequent effects on N-selective processing (Michaud *et al*., 1997; Michaud *et al*., 1999; Araujo *et al*., 2000). Mutational analyses of unique amino acids present in the enzyme active subsites and the consequent catalytic effects have not been performed with regards to N-domain substrate processing.

Five substrates relevant to this study are outlined below.

Abz-Phe-Arg-Lys(Dnp)-Pro (Abz-FRK(Dnp)P) is a fluorogenic substrate that is processed with similar ability by both domains (Araujo *et al*., 2000). Thus, conversion to N-domain residues to their corresponding C-domain counterparts should not abolish enzymatic ability towards this substrate. This is useful in assessing the extent of inhibition by small molecule inhibitors toward mutant N- and C-domain enzyme derivatives without drastic changes in substrate cleavage activity (to be presented in Chapter 4).

Z-Phe-His-Leu (*Z*-FHL) and hippuryl-His-Leu (HHL) are short, synthetic and relatively inexpensive ACE substrates. Each domain displays differing kinetic capacities for these two substrates; HHL is a relatively poor substrate of the N-domain compared to C-domain processing while *Z*-FHL is the better bound and cleaved of the two substrates for both

domains (Wei *et al*., 1991; Danilov *et al*., 2008). This suggests that unique residues present in the N-domain contribute to the less efficient hydrolysis of HHL.

AcSDKP, and its internally quenched fluorogenic derivative Abz-SDK(Dnp)P, have been shown to be the substrates most specifically cleaved by the N-domain (Rousseau *et al*., 1995; Araujo *et al*., 2000). Synthetic substrate analogues of the AcSDKP template and their catalysis by the N- and C-domains implicated the substrate P_2 (*N*-acetyl-Ser) group in being a predominant determinant for substrate selective processing (Michaud *et al*., 1999; Araujo *et al*., 2000). Thus, unique residues in the N-domain could be providing distinct interactions with substrate molecules to allow for differential domain substrate processing preferences.

Previous characterisation of AcSDKP binding and hydrolysis has involved the use of recombinant full length human sACE with inactivated domains (Rousseau *et al*., 1995) or individual soluble domains of human ileal ACE (N-domain) and rabbit tACE (C-domain) (Deddish *et al*., 1996). Importantly, no kinetic characterisation of the soluble human N- and C-domains has been performed with this peptide. This is important due to many experiments having been performed with the soluble human forms, especially with inhibitor binding (Corradi *et al*., 2006; Nchinda *et al*., 2006a; Nchinda *et al*., 2006b; Watermeyer *et al*., 2008). Furthermore kinetic characterisation of AcSDKP processing has involved the use of paper electrophoresis or high pressure liquid chromatography (HPLC), both of which are time consuming and lack the high throughput approach required for screening numerous mutant enzymes and novel inhibitors. Alternatively, since AcSDKP has a protected N-terminus, an appropriate derivatising agent that could recognise the formation of a new N-terminus could allow for the quantification of kinetic parameters. Such an approach, using *N*-acetylated AngI with fluorescamine, has been reported and could be used to assess AcSDKP processing in a plate adapted assay (Conroy and Lai, 1978).

The objectives for the assessment of residue contribution to selective substrate processing were as follows:

1. To kinetically characterise N-domain active site mutants and wild type N-domain hydrolysis of the non-domain selective substrate Abz-FRK(Dnp)P.
2. To utilise the *Z*-FHL/HHL ratio to identify residues potentially contributing to poor HHL cleavage by the N-domain; and subsequent kinetic characterisation of such mutants with *Z*-FHL and HHL.
3. To kinetically assess the effects of active site mutations on the binding and hydrolysis of Abz-SDK(Dnp)P.
4. To establish a novel assay for AcSDKP cleavage and to subsequently perform kinetic analyses with the human N- and C-domains of ACE.

3.2 Methods

3.2.1 Active enzyme concentration determination

While traditional methods are useful for quantification of protein concentration, such approaches provide no quantification of active enzyme amount. This information is necessary because of degradation after purification due to long term storage and/or protein instability due to mutation (Knight, 1995). Assuming a 1:1 binding ratio, incubation of enzyme with a potent inhibitor at varying molar ranges with subsequent activity assay can provide an indication of remaining enzyme molar amount and has been successfully used to confirm active ACE concentrations (Binevski *et al*., 2003; Rice *et al*., 2004; Skirgello *et al*., 2005). A modified *Z*-FHL assay (section 2.2.5) was employed for the determination of active enzyme concentration. Briefly, a serial dilution of ACE inhibitor lisinopril was incubated with 40 nM enzyme in phosphate incubation buffer (100 mM $KHPO_4/KH_2PO_4$ pH 8.3, 300 mM NaCl, 10 µM $ZnSO_4$, 1 mg/ml albumin) for 120 minutes at room temperature. Following 20 µl aliquots of the enzyme-inhibitor complex in triplicate, the enzyme-inhibitor complex and substrate (2 mM *Z*-FHL) were separately pre-warmed to 37°C and assay commenced with addition of 20 µl substrate. After 5 minutes incubation the assay was stopped, free His-Leu dipeptides derivatised and fluorescence determined as described previously (section 2.2.5). Data was analysed for the determination of equimolar inhibitor required to achieve 0% enzyme activity and the active enzyme concentration therefore determined (Figure 3.1).

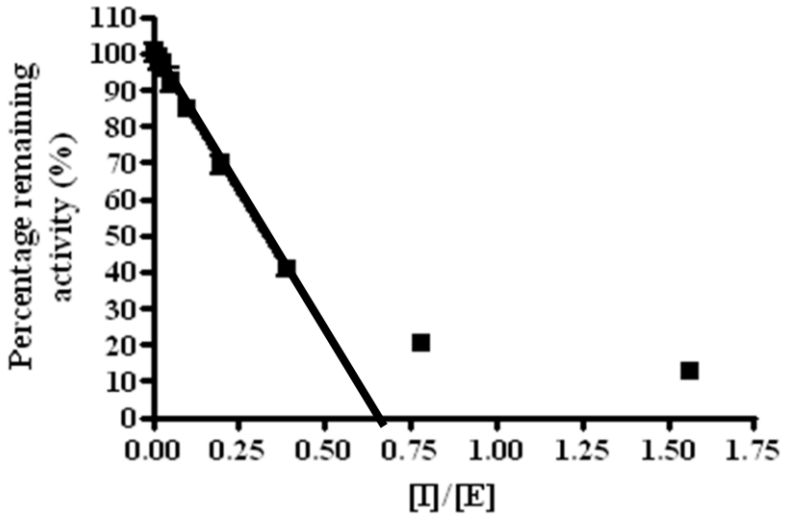

Figure 3.1: A representative curve displaying the calculation of active enzyme in a given buffer storage solution. Assays of the enzyme-inhibitor complexes were performed as described in section 3.2.1. Percentage remaining activity is plotted against the molar ratio of inhibitor to enzyme and linear regression analysis performed on the linear range. The *x* intercept of the extrapolated curve is taken as the theoretical amount of inhibitor for zero remaining enzyme activity.

3.2.2 Internally quenched fluorogenic substrates: Construction of standard curve and determination of correction values

3.2.2.1 Construction of Abz-Gly standard curve

A free donor *o*-aminobenzoic acid fluorescent group coupled to Gly, Abz-Gly (Bachem Ltd.), was used to correlate fluorescence intensity to free donor group amount. A 2 µM stock of Abz-Gly was serially diluted in Tris assay buffer (50 mM Tris-HCl pH 7.0, 100 mM NaCl, 10 µM $ZnCl_2$) and 300 µl volumes aliquoted in triplicate into a 96-well plate (0-600 pmols). Fluorescence intensities were determined using 320 nm and 420 nm excitation and emission wavelengths respectively using a Cary Eclipse spectrofluorimeter (Varian Inc.) and linear regression analysis performed (v 4.01, GraphPad Prism®) (see Appendix A4).

3.2.2.2 Determination of correction values

3.2.2.2.1 The "inner filter effect"

Fluorescence resonance energy transfer (FRET) peptides have been successfully utilised for the continuous monitoring of activity of numerous enzymes, including ACE (Dive *et al*., 1999; Araujo *et al*., 2000; Wang *et al*., 1993). FRET peptides emit a detectable fluorescence

upon separation of the donor (donor group used in this study: *o*-aminobenzoic acid, Abz) and acceptor (acceptor group used in this study: 2,4-dinitrophenyl, Dnp) groups through proteolytic activity. However, higher substrate concentrations result in less distance between uncleaved substrate and Abz-product molecules resulting in product quenching by neighbouring uncleaved groups and thus a decrease in observed fluorescence signal. Such an effect on fluorescence observation hampers the accurate determination of enzymatic kinetic parameters and is generally referred to as the "inner filter effect" (IFE) (Liu *et al*., 1999; Araujo *et al*., 2000). Correction of the IFE requires empirical methods.

3.2.2.2.2 Empirical determination of correction values

A simple empirical procedure for the correction of the IFE in a plate assay has been described by (Liu *et al*., 1999). Baseline fluorescence readings of different Abz-SDK(Dnp)P substrate concentrations (0-50 µM) were measured as above (Section 3.2.2.1) in a 297 µl volume in Tris assay buffer. Three microlitres of 50 µM Abz-Gly was added to the substrate solutions, mixed thoroughly and fluorescence reread as before. Ratios of change in fluorescence with increasing substrate concentration compared to zero substrate were calculated and a non-linear equation used to fit the values up to 50 µM substrate. This correction curve was used to correct all further kinetic experiments with Abz/Dnp donor/acceptor group substrates.

3.2.3 Non-selective fluorogenic substrate Abz-FRK(Dnp)P: Kinetic parameters

Variable volumes of a 50 µM Abz-FRK(Dnp)P substrate solution were aliquoted in triplicate into a 96-well plate on ice. Enzyme solution in HEPES assay buffer (50 mM HEPES pH 6.8, 200 mM NaCl, 10 µM $ZnCl_2$) was added to bring the final assay volume to 300 µl and 0.2 pmols enzyme. This buffer system was used to mimic the conditions required for RXP407 binding kinetics assays (described in Chapter 4). Fluorescence intensities were monitored continuously at ambient temperature (λ_{ex}= 320 nm; λ_{em}= 420 nm) for 20 minutes. Initial changes in intensities over time were corrected with correction values and converted to reaction velocities by use of the standard curve (section 3.2.2.1). Kinetic constants K_m and k_{cat} were determined by the direct linear plot method (Eisenthal and Cornish-Bowden, 1974).

3.2.4 Synthetic substrates: Z-FHL and HHL

3.2.4.1 Construction of His-Leu standard curve

Construction of a standard curve of enzymatic cleavage product of *Z*-FHL and HHL; dipeptide His-Leu (HL) was carried out as described by (Schwager *et al*., 2006). Commercially available HL (Sigma-Aldrich Co.) was dissolved in dH_2O to yield a 5 mM HL stock solution and subsequently diluted to a 0.5 mM working solution in phosphate buffer (100 mM $KHPO_4/KH_2PO_4$ pH 8.3, 300 mM NaCl, 10 µM $ZnSO_4$). HL working solution was diluted in a 96-well plate with phosphate buffer producing increasing amounts of HL per 30 µl. The assay for HL fluorescence was carried out as described in section 2.2.5 and commenced with the addition 0.4 M NaOH. Change in fluorescence was correlated to nanomoles HL by using linear regression analysis as in section 3.2.2.1 (see Appendix A4).

3.2.4.2 Z-FHL/HHL ratios

Differences in catalysis of *Z*-FHL and HHL by the N- and C-domains allow the ratio of rates of hydrolysis of these two substrates to be used to describe "domain-likeness". Due to the N-domain cleaving HHL poorly compared to the C-domain, one would expect a higher *Z*-FHL/HHL ratio for the N-domain and mutation of important substrate binding residues causing a decrease in ratio. *Z*-FHL/HHL assays were performed as described in (Danilov *et al*., 2008). Three microlitres of purified enzyme was added to 30µl of either *Z*-FHL (1 mM) or HHL (5.7 mM) (Appendix A3) in phosphate buffer triplicate in a 96-well plate. The enzyme-substrate solution was incubated at 37°C for 20 minutes followed by addition of 120µl of 0.4 M NaOH to stop catalysis. Derivitisation, subsequent termination of derivitisation and fluorescence intensities determination were performed as outlined in section 2.2.5. Fluorescent values were converted into enzymatic activity and the ratio of activities (*Z*-FHL/HHL) of the enzyme towards the two substrates was calculated.

3.2.4.3 Kinetic parameter determination of Z-FHL and HHL hydrolysis

A modified *Z*-FHL assay was employed to assess the kinetic behaviour of several mutants that displayed changes in *Z*-FHL/HHL ratio towards a C-domain-like ratio. Two N-domain mutant enzymes showing the greatest shift towards the C-domain ratio (Y369F and ST/VV) were selected for further kinetic analysis. Five microlitres of enzyme stock solution in phosphate buffer was aliquoted in triplicate into a 96-well plate and pre-warmed to 37°C. The assay commenced through the addition of 30 µl pre-warmed substrate (either *Z*-FHL or HHL)

at varying concentrations. Following incubation at 37°C for 15 minutes, 120 µl of 0.4 M NaOH was added to stop the enzymatic reaction. Subsequent assay steps were carried out as described previously (section 2.2.5). Enzymatic reaction rates were calculated using a standard curve correlating moles HL to fluorescence intensities and kinetic parameters (k_{cat} and K_m) determined using Michaelis-Menten kinetic curves drawn by nonlinear regression analysis (v 4.01, GraphPad Prism®).

3.2.4.4 Molecular docking of Z-FHL and HHL into the N- and C-domains

Molecular modelling experiments to dock substrates *Z*-FHL and HHL into the N- and C-domain active sites were conducted in a manner described previously using INSIGHT II (v 98.0, Accelrys Inc.) (Corradi *et al*., 2006). Crystal structures of the N-domain (PDB accession code 2C6N containing RXP407 previously docked) (Corradi *et al*., 2006) and C-domain (PDB accession code 1O86) were used as molecular templates. Active site ligands were modified to the required substrate structure and charge potentials of the new ligand fixed. Hydrogen atoms were added to the entire structure, incomplete residues corrected and charge of the receptor domain zinc ion was assigned the +2.0 charge. Once the charge potentials of the entire assembly were accepted; ligand-receptor energy molecular minimisation runs were commenced. The Constant Valence Force Field and Extendable Systematic Force Field (metal adapted) were used for minimisation runs. Three thousand iterations of molecular minimisation cycles were carried out at 300 K with dielectric constant 1.00 and cut off distance of 9.5 Å. An average pose of 100 frames was taken as the minimised ligand positioning. Interaction distance between the substrate carbonyl oxygen and zinc ion, as well as C-terminal interaction with Lys489/511 of the N- or C-domain confirmed the reasonableness of the minimised pose. The coordinates of docked substrate poses of the N- and C-domains were structurally aligned using *ALIGN* (Cohen, 1997) and orientations compared.

3.2.5 N-selective fluorogenic substrate: Abz-SDK(Dnp)P

Fluorogenic substrate Abz-SDK(Dnp)P is an internally quenched peptide that has been previously shown to be cleaved 350-fold more efficiently by the N-domain of ACE (Araujo *et al*., 2000). Assays were done in an approach similar to that of section 3.2.3 and, for comparison, done under conditions similar to that outlined by (Araujo *et al*., 2000); with variable volumes of a 100 µM Abz-SDK(Dnp)P substrate solution aliquoted into a 96-well

plate on ice. Enzyme solution in Tris assay buffer (100 mM Tris-HCl pH 7.0, 50 mM NaCl, 10 µM $ZnCl_2$) was added to bring the final assay volume to 300 µl and 0.2 (N-domain, T496V, R381E, C-domain S_2´), 0.8 (YR/FE), 1.2 (Y396F) or 2 (tACE) pmols enzyme. The C-domain S_2´ protein was kindly made available by Dr W.L. Kröger. This protein contains conversion of all unique C-domain S_2´ residues into N-domain counterparts and has been experimentally assessed to confirm kinetic ability comparable to wild type C-domain (Kroger *et al*., 2009). Baseline fluorescence intensities were measured (λ_{ex}= 320 nm; λ_{em}= 420 nm) followed by incubation of the assay at 37°C for 20 minutes (N-domain enzymes and C-domain S_2´) or 45 minutes (tACE) using a Cary Eclipse spectrofluorimeter (Varian Inc.). Samples were reread at the above parameters and changes in intensities compared to baseline were converted to reaction velocities by use of the standard curve (Appendix A4). Kinetic constants K_m and k_{cat} were determined by nonlinear regression analysis (v 4.01, GraphPad Prism®).

3.2.6 Physiological substrate: AcSDKP

3.2.6.1 The development of a novel AcSDKP assay using fluorescamine

An adapted plate assay was designed based on previously published approach for *N*-acetyl-AngI (Conroy and Lai, 1978) using fluorescamine (4-phenylspiro[furan-2(*3H*),1´-phthalan]-3,3´-dione), a reagent that forms fluorescent adducts exclusively with primary amines (Udenfriend *et al*., 1972). In order to clarify the effect of enzyme and substrate on basal fluorescence, the following conditions were set up: 15 nmols of AcSDKP and 0.3 pmols of N-domain were separately aliquoted into triplicate wells of a 96-well plate to a final volume of 40 µl. Additionally; enzyme and substrate were incubated together to note the change compared to basal fluorescence. Plates were incubated at 37°C for 15 minutes and stopped by the addition of 50 µl 1 M HCl. The solution was neutralised by the addition of 50 µl 1 M NaOH and the pH increased to 8.3 by the addition of 100 µl 500 mM K_2HPO_4/KH_2PO_4 buffer pH 8.3. Ten microlitres of fluorescamine (2 mg/ml in acetone, Sigma-Aldrich Co.) was added and the resulting mixture incubated for 3 minutes at room temperature. Fluorescence intensities were measured at λ_{ex}= 390 nm and λ_{em}= 475 nm using a Cary Eclipse spectrofluorimeter (Varian Inc.).

3.2.6.2 Construction of Lys-Pro standard curve

A range of AcSDKP (0 to 30 nmols) was incubated in HEPES buffer (50 mM HEPES, pH 7.5, 100 mM NaCl, 10 µM $ZnSO_4$) with 2 pmol N-domain enzyme at 37°C overnight. Thirty microlitre aliquots were transferred into a 96-well plate followed by addition of 10 µl assay buffer. The addition of HCl, NaOH, buffer, fluorescamine and measurement of fluorescence intensities was measured as above (section 3.2.6.1). Fluorescence intensities were subtracted from 0 nmol baseline readings and a subsequent curve was constructed correlating change in fluorescence with product amount (Appendix A4).

3.2.6.3 Determination of kinetic parameters

Thirty microlitres of AcSDKP substrate in HEPES buffer, ranging in concentration from 0 to 1000 µM, were warmed to 37°C in a 96-well plate. The assay was commenced by the addition of 10 µl pre-warmed enzyme (0.2 pmols in HEPES buffer) and incubated for 15 minutes for N-domain and sACE and 30 minutes for the C-domain. The assay was stopped, neutralised, buffered, derivitised and read as above (section 3.2.5.1). Changes in fluorescence compared to unhydrolysed substrate were converted to reaction velocities by the use of a standard curve (as constructed in section 3.2.6.2) and kinetic constants calculated from nonlinear regression analysis (v 4.01, GraphPad Prism®).

3.3 Results

3.3.1 Inner filter effect correction values

Increasing substrate concentrations in the presence of a fixed concentration of free donor (Abz-Gly) caused a non-linear decrease in measured fluorescence intensities. Correction values were calculated as described in section 3.2.2.2.2. The fitting and determination of a polynomial derived trend line and equation allowed for the correction of quenching substrate concentrations ranging from 0 to 50 µM (Figure 3.2).

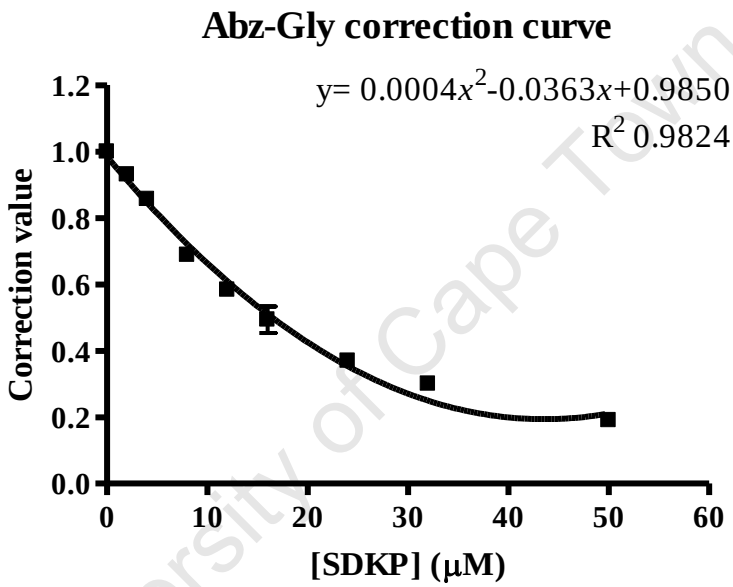

Figure 3.2: Graph of correction value versus increasing intact substrate Abz-SDK(Dnp)P with 0.5 µM Abz-Gly. Ratios of changes in fluorescence compared to a zero substrate control (containing 0.5 µM Abz-Gly alone) were calculated and plotted. A quadratic equation was fitted that best described the data obtained and the equation was subsequently used for correction of kinetic experiments with substrates containing Abz and Dnp moieties. Data represented as mean ± SEM.

3.3.2 Non-selective fluorogenic substrate: Abz-FRK(Dnp)P

Initial kinetic assessment was performed in order to confirm catalytic integrity of enzymes containing active site mutations. Non-selective fluorogenic substrate Abz-FRK(Dnp)P had similar binding affinities between the two wild type domains and a slightly higher turnover rate for the C-domain, consistent with the original publication (Table 3.1) (Araujo *et al*., 2000). Overall catalytic efficiencies for N-domain mutant derivatives were found to be within range of controls with the exception of ST/VV which displayed a 10-fold lower catalytic efficiency compared to the N-domain.

Table 3.1: Binding affinity (K_m), turnover rates (k_{cat}) and catalytic efficiencies (k_{cat}/K_m) of C-domain, N-domain and selected N-domain mutant enzymes in the processing of substrate Abz-FRK(Dnp)P.

Enzyme	**k_{cat} (s^{-1})**	**K_m (µM)**	**k_{cat}/K_m ($s^{-1}.\mu M^{-1}$)**
N-domain	1.51	10.23	0.148
C-domain	8.72	11.91	0.732
Y369F	1.31	10.99	0.119
R381E	8.47	27.66	0.306
YR/FE	12.8	13.51	0.947
T496V	1.47	3.808	0.386
E262S	2.40	10.35	0.232
D354E	1.04	4.146	0.251
S357V	0.892	12.24	0.0729
T358V	3.54	13.41	0.264
ST/VV	0.196	15.21	0.0129
E431D	0.830	4.674	0.178

3.3.3 Synthetic substrates: Z-FHL and HHL

3.3.3.1 Z-FHL/HHL ratios

Z-FHL/HHL ratios of rates of hydrolysis for the N-domain were approximately 11-fold greater than those for the C-domain (Figure 3.3). Comparison of relative rates of hydrolysis for both substrates indicated that conversion of N-domain residues to their corresponding C-domain counterparts resulted in a change in ratio. Most mutations in both the S_2 and S_2' subsites resulted in a decrease toward a more C-domain-like ratio (Figure 3.3). The mutants Y369F (together with its double mutant YR/FE) and double S_2' mutant ST/VV caused the greatest decrease in ratio.

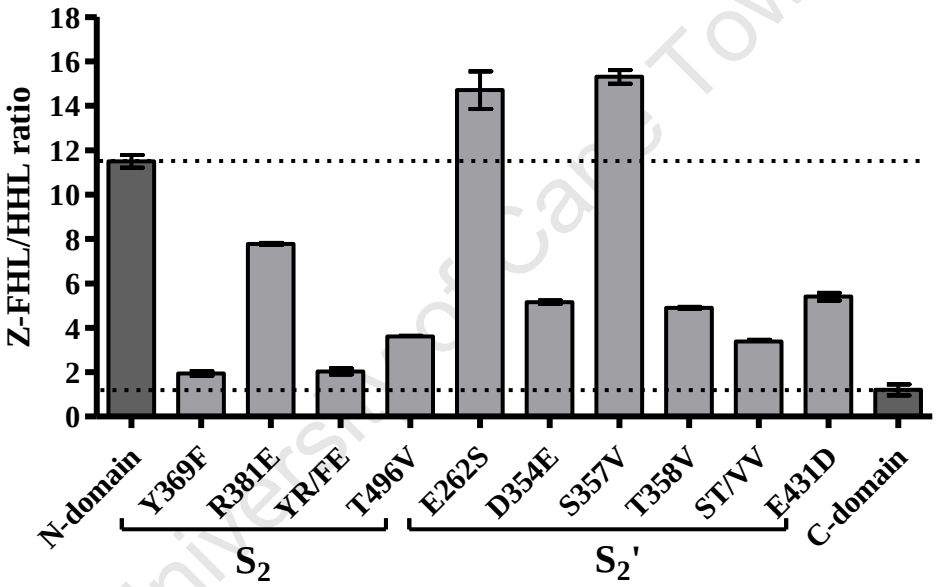

Figure 3.3: Ratios of rates of hydrolysis of substrates *Z*-FHL and HHL by different N-domain mutants. Hydrolysis rates of each enzyme toward substrates *Z*-FHL and HHL were determined as described in section 3.2.4.2 and ratios calculated. Wild type N-domain and C-domain are shown in dark grey, N-domain active site mutants are shown in light grey and the subsite location of residues also indicated. Data represented as mean ± SD.

3.3.3.2 Determination of kinetic parameters

The active site mutants displaying the greatest change in ratio in each subsite (Y369F and ST/VV) were further analysed for their kinetic capabilities toward substrates *Z*-FHL and HHL. N-domain enzymes analysed processed *Z*-FHL with superior binding affinity and turnover rate compared to HHL (Table 3.2). The C-domain displayed considerably better

catalytic efficiencies for both substrates. Ratios of turnover rates between substrates were approximately equal to the ratios of rates of hydrolysis by the enzymes presented above (section 3.3.3.1).

When compared to wild type, N-domain active site mutant Y369F showed similar turnover rates of *Z*-FHL, and markedly improved catalysis of substrate HHL. N-domain mutant ST/VV, as with Abz-FRK(Dnp)P, displayed substantial decreases in k_{cat} values for both substrates compared to wild type N-domain. These N-domain mutants that display similar ratios to the C-domain did not display similar kinetic abilities, as is evinced by noticeably lower k_{cat} values when compared to wild type C-domain (Table 3.2).

Table 3.2: Binding affinity (K_m), turnover rates (k_{cat}) and catalytic efficiencies (k_{cat}/ K_m) of C-domain, N-domain and selected N-domain mutants (Y369F and ST/VV) with substrates *Z*-FHL and HHL. Data given as mean ± SEM.

Enzyme	**Substrate**	k_{cat} **(s^{-1})**	K_m **(mM)**	k_{cat}/K_m **($s^{-1}.mM^{-1}$)**
N-domain	Z-FHL	48.7 ± 3.55	0.78 ± 0.023	62.2 ± 2.79
	HHL	7.57 ± 0.37	1.31 ± 0.04	5.76 ± 0.20
Y369F	Z-FHL	42.8 ± 0.77	0.467 ± 0.012	91.65 ± 1.10
	HHL	26.5 ± 1.62	1.754 ± 0.13	15.13 ± 0.32
ST/VV	Z-FHL	7.36 ± 0.40	0.446 ± 0.0128	16.5 ± 0.89
	HHL	2.94 ± 0.11	1.250 ± 0.1021	2.37 ± 0.126
C-domain	Z-FHL	99.96 ± 3.74	0.071 ± 0.014	1495.6 ± 214.7
	HHL	107.5 ± 6.44	0.780 ± 0.04	137.7 ± 5.2

3.3.3.3 Molecular modelling of Z-FHL and HHL substrates

To investigate the interactions between N-domain active site residues and substrates *Z*-FHL and HHL, molecular docking was performed and substrates successfully minimised in both domains. Interaction distances between the scissile carbonyl group of the substrates and the catalytic zinc ion, as well as bonding distances between substrate C-termini and the conserved Lys489/511 residues were noted (Figure 3.4). A change in HHL substrate orientation appears to occur with the benzoyl moiety in the N-domain active site possibly due to the presence of the terminal hydroxyl group of Tyr369 and residue Arg381. Substrate *Z*-FHL seemed to appear more constrained in the apparently smaller N-domain S_2 subsite than the C-domain counterpart. For both substrates the P_2' Leu was orientated in the opposite direction compared to the C-domain.

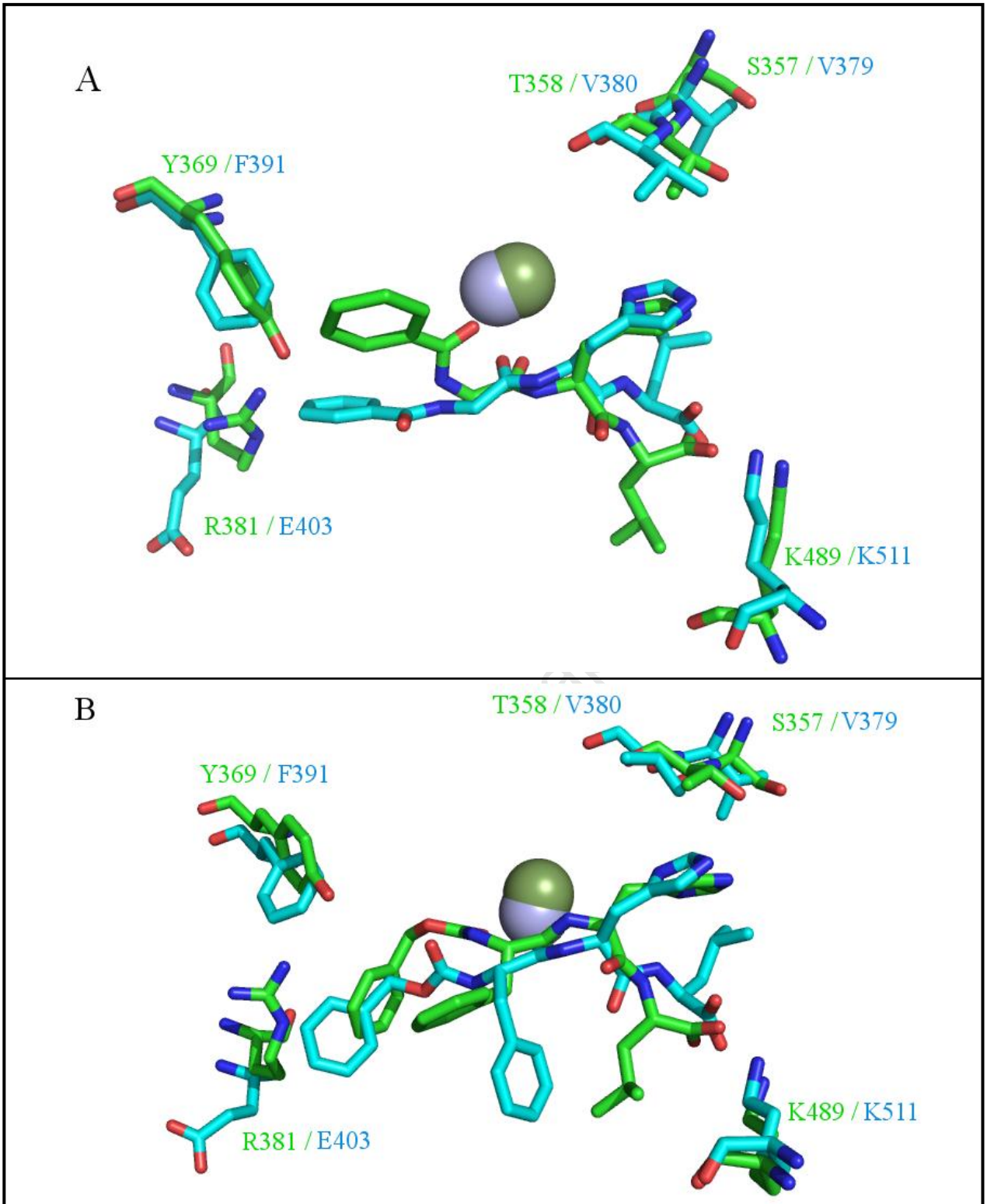

Figure 3.4: Molecular minimisations of synthetic substrates HHL (A) and *Z*-FHL (B) in the N- and C-domains. Minimisations were performed as outlined in section 3.2.4.4 and domains superimposed using the *ALIGN* program (Cohen, 1997). N- and C-domain substrates, residues and zinc ions are shown in green and blue respectively. Interaction distances between the catalytic zinc and conserved lysine residues were noticed for all models. Two major changes in substrate orientation for HHL between domains were noticed; namely the hippuryl group and the P_2' leucine. Image generated using PyMOL software (v 0.99, DeLano Scientific).

3.3.4 N-selective fluorogenic substrate: Abz-SDK(Dnp)P

Assessment of contribution of the S_2 and S_2' subsites in N-selective substrate processing was performed with substrate Abz-SDK(Dnp)P. Catalytic efficiencies of Abz-SDK(Dnp)P binding and hydrolysis were determined for N- and C-domain enzymes and revealed 28-fold more efficient processing by the N-domain (Table 3.3). N-domain enzymes with mutations in the S_2 subsite were analysed under the same kinetic conditions. The S_2/S_1 mutant T496V showed a catalytic efficiency comparable to that of wild-type N-domain; while N-domain S_2 mutants (Y369F, R381E and YR/FE) showed more notable changes in catalytic efficiencies. Mutants containing the R381E mutation (R381E and YR/FE) displayed a large increase in K_m values resulting in lowered overall catalytic efficiencies. The single Y369F mutation showed the greatest alteration in catalytic efficiency, with a 5-fold lower k_{cat}/K_m than wild-type N-domain. Interestingly, a C-domain enzyme containing mutations of all unique amino acids in the S_2' subsite into their corresponding N-domain counterparts showed marked improvement in catalytic efficiency (Figure 3.5).

Table 3.3: Binding affinities (K_m), turnover rates (k_{cat}) and overall catalytic efficiencies (k_{cat}/K_m) for N-domain, C-domain and subsite mutant enzymes in Abz-SDK(Dnp)P processing. All data represented as mean ± SD.

Enzyme	k_{cat} **(s^{-1})**	K_m **(μM)**	k_{cat}/K_m **(s^{-1}/ μM^{-1})**
N-domain	7.41 ± 0.00707	50.6 ± 1.47	0.146 ± 0.00424
Y369F	3.43 ± 0.0523	108 ± 35.4	0.0326 ± 0.0058
R381E	14.1 ± 1.09	265 ± 16.1	0.0529 ± 0.000919
YR/FE	10.8 ± 1.81	254 ± 57.5	0.0428 ± 0.00255
T496V	7.48 ± 0.233	41.2 ± 3.04	0.181 ± 0.00778
C-domain S_2'	7.99 ± 1.08	192 ± 9.76	0.0416 ± 0.00354
C-domain	0.35 ± 0.028	69.0 ± 9.81	0.00512 ± 0.000276

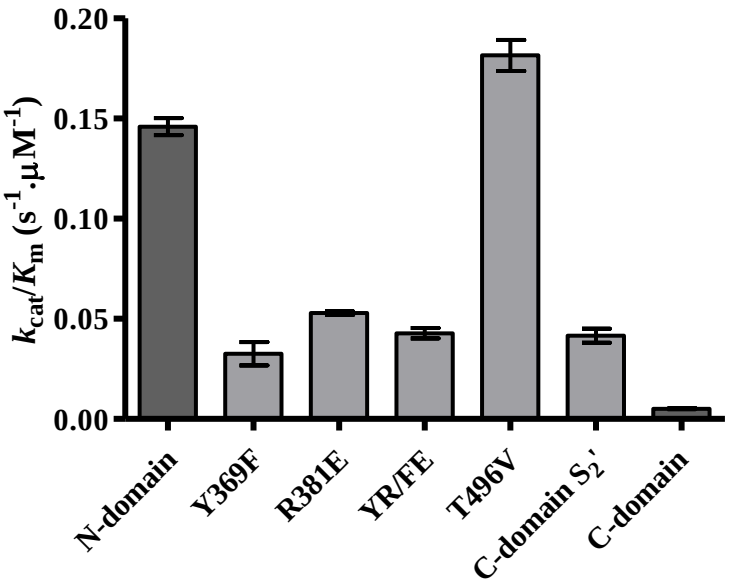

Figure 3.5: Overall catalytic efficiencies (k_{cat}/K_m) of N-domain, C-domain and mutant enzymes in the processing of Abz-SDK(Dnp)P. Enzymatic efficiencies of Abz-SDK(Dnp)P cleavage were determined as outlined in section 3.2.4. Wild type and mutant enzymes are coloured in dark and light grey respectively. Data represented as mean ± SD.

3.3.5 Physiological substrate: AcSDKP

3.3.5.1 Assay development

In order for fluorescamine to be successfully utilised to determine ACE activity, several basic assay requirements needed to be clarified; namely the effect of enzyme on basal fluorescence, the extent of basal substrate derivitization (since AcSDKP has a free amine on the P_1' Lys in the unhydrolysed form); and the need for a reproducibly significant difference between substrate and product fluorescence after derivitisation.

A 5-fold higher amount of enzyme than normally used in standard enzymatic assays (1 pmol) had no difference in fluorescence compared to buffer alone. Also, addition of the same amount of enzyme after the assay was stopped added no additional fluorescence (Figure 3.6). N-domain activity shows a clearly distinguishable difference between product and unhydrolysed substrate. Further, as can be noted in the Lys-Pro standard curve, there was linearity within the range of detection for this study (Appendix A4). Such observations suggested the applicability of the technique in the assessment of ACE activity toward the N-selective substrate and the approach was employed in subsequent AcSDKP experiments.

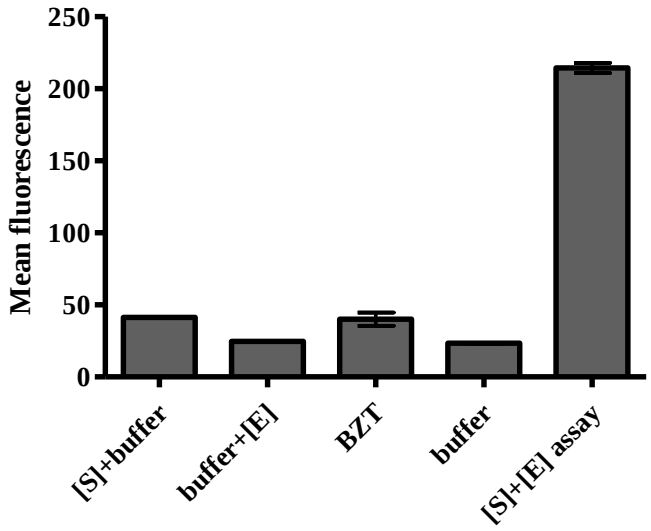

Figure 3.6: Assay development for the use of fluorescamine in the kinetic assessment of AcSDKP hydrolysis. Buffer in the presence of 375 µM AcSDKP ([S]+buffer), 1 pmol N-domain enzyme (buffer+[E]) or substrate and enzyme after the addition of HCl (BZT) were derivitised with fluorescamine and fluorescence intensities determined. Substrate and enzyme co-incubated for 15 minutes ([S]+[E] assay) displayed a marked changed in fluorescence intensity compared to the equivalent of uncleaved substrate, suggesting a usefulness of the assay approach. All data represented as mean ± SEM.

3.3.5.2 Determination of kinetic parameters

Assessment of the binding and hydrolysis of physiological substrate AcSDKP was performed using an assay approach with fluorescamine, a derivitising agent that results in fluorescent signal when derivitised to primary amines. Soluble N-domain analysis with this approach indicated a similar turnover rate compared to the sACE with inactivated C-domain (Table 3.4) (Rousseau *et al*., 1995). A slightly higher K_m than previously reported above was noted; but a higher K_m for soluble N-domain (compared to sACE) is consistent with another report in the literature publishing the kinetic parameters of ileal (soluble N-domain) ACE using an HPLC-based assay (Deddish *et al*., 1996).

K_m values were similar for all enzymes tested, consistent with other reports (Rousseau *et al*., 1995; Deddish *et al*., 1996). While the N-domain had a similar turnover rate to that previously published, the C-domain displayed remarkably higher turnover rate (Table 3.4). Wild-type sACE, with both domains active, displayed the highest k_{cat} value. Comparison of catalytic efficiencies indicated two important observations. Firstly, the N-specificity of the

soluble domains was only 2-fold and, secondly; that soluble domains are additive for the overall catalytic efficiency of sACE (Figure 3.7).

Table 3.4: Binding affinities (K_m), turnover rates (k_{cat}) and overall catalytic efficiencies (k_{cat}/K_m) for N-domain, C-domain and sACE in AcSDKP processing. Data represented as mean ± SEM.

Enzyme	k_{cat} (s^{-1})	K_m (µM)	k_{cat}/K_m ($s^{-1}.\mu M^{-1}$)
N-domain	14.2 ± 1.15	240.5 ± 30.75	0.0601 ± 0.004798
C-domain	4.75 ± 0.68	166.6 ± 29.95	0.0287 ± 0.0011
sACE	25.4 ± 0.721	288.5 ± 35.40	0.0903 ± 0.00984

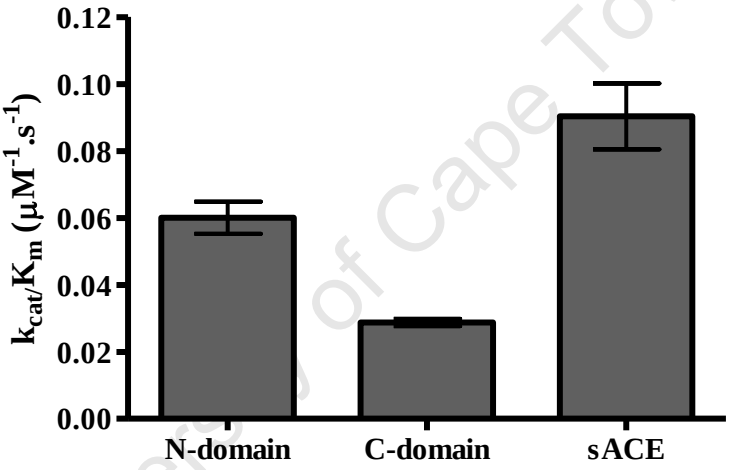

Figure 3.7: Overall catalytic efficiencies (k_{cat}/K_m) of N-domain, C-domain and sACE enzymes in the processing of AcSDKP. Enzymatic efficiencies of AcSDKP cleavage were determined as outlined in section 3.2.6.3. Data represented as mean ± SEM.

3.4 Discussion

Initial assessment of catalytic ability was performed using fluorogenic substrate Abz-FRK(Dnp)P (Araujo *et al*., 2000). Since it is moderately non-specific for the ACE domains, one could anticipate that conversion of N-domain residues into corresponding C-domain counterparts should not drastically affect kinetic ability of mutant enzymes and that the catalytic efficiencies of these mutants should fall within the range of wild type controls. This analysis confirms the catalytic integrity of such N-domain active site mutants.

A minor increased catalytic ability of the C-domain was observed and is consistent with another literature report (Araujo *et al*., 2000). Mutant enzymes displayed catalytic efficiencies that were comparable to the N-domain wild-type control, or alternatively, within the range between N- and C-domain controls. The notable exception was that of double S_2' mutant; ST/VV, which displayed a similar binding affinity for the substrate as wild-type but a 10-fold reduction in turnover rate. This suggests that these two residues are not necessarily directly involved in substrate binding but their conversion could affect the stabilisation of the tetrahedral intermediate (Fernandez *et al*., 2001; Sturrock *et al*., 2004). It is thus suggested that the introduction of hydrophobic valines into an otherwise N-domain pocket (containing other unconserved amino acids) causes changes in subsite architecture (see discussion below regarding molecular minimisations of synthetic substrates).

Previous publications by Danilov and co-workers outlined the usefulness of *Z*-FHL/HHL ratios in assessing the presence of ACE inhibitors in blood and the status of sACE under certain denaturing conditions; and showed an increased N-domain ratio compared to C-domain (Williams *et al*., 1996; Danilov *et al*., 2008). We thus hypothesised that conversion of N-domain residues to C-domain counterparts would tend to cause a decrease in ratio. This trend was noticed, with the majority of mutants displaying decreased ratios. The removal of the tyrosine hydroxyl group and a more hydrophobic S_2' subsite resulted in a ratio close to that of the C-domain, suggesting the important roles of these residues in specific substrate processing. However, ratios do not make it clear as to the exact kinetic nature of the mutant active site in the binding and hydrolysis of HHL and *Z*-FHL. More extensive kinetic analysis was required to assess whether such mutations improve overall catalytic abilities in respect of the substrates *Z*-FHL and HHL.

Wild-type N-domain and mutant Y369F showed similar turnover rates of *Z*-FHL, while improved HHL catalysis by Y369F suggests the importance of the terminal hydroxyl group of tyrosine in minimising HHL catalysis by the N-domain.

The double S_2' mutant ST/VV, despite having a ratio similar to the C-domain, does not in any way resemble the catalytic efficiency of the C-domain. This emphasises the limitations of the above ratios, whereby a decrease in ratio does not necessarily indicate a more "C-domain-like" molecule in the binding and hydrolysis of substrates. Indeed, neither Y369F nor ST/VV display comparable kinetics to the C-domain as could be inferred by the *Z*-FHL/HHL ratios. This study suggests that, while the ratios may be useful for certain applications, more subtle active site amino acid changes can be misleading in modifications of the *Z*-FHL/HHL ratio.

Molecular models of *Z*-FHL and HHL in the domain active sites are in agreement with the above kinetic findings and provide a possible structural perspective of substrate cleavage (Figure 3.4). The benzoyl moiety of HHL is found to be in a different orientation in the N-domain, possibly due to a steric clash with the Tyr369 terminal hydroxyl group. Due to similar binding affinities of HHL between domains it could be suggested that removal of the hydroxyl group allows for the substrate in the C-domain to more readily assume the required positioning in order to be cleaved (that is, to form the tetrahedral intermediate). The presence of a more hydrophilic (due to the presence of Ser357 and Thr358 as opposed to hydrophobic valines) and spatially smaller S_2' subsite could account for the changes in orientation of the P_2' Leu between the two active sites (Corradi *et al*., 2006).

The ST/VV mutant, consistent with the Abz-FRK(Dnp)P kinetics (Table 3.1), is very poor in the cleavage of both synthetic substrates. A possible explanation of this reduced catalysis is that the introduction of bulkier hydrophobic residues into an otherwise N-domain pocket could cause a change in S_2' subsite architecture different to that observed in crystal structures. This could result in decreased contacts with Gln259, Lys489 and Tyr498, residues considered critical in the stabilisation of the substrate molecule during cleavage, and therefore decreased catalytic ability (Matthews, 1988; Sturrock *et al*., 2004). Another ACE mutagenic study supports the above suggestion: conversion of C-domain residue Tyr200 to Phe resulted in a 15-fold reduction in turnover rate with substrate furanacrylolyl-Phe-Gly-Gly and had little effect on substrate binding but a 100-fold decrease in lisinopril binding affinity, suggesting a role of the Tyr residue in contributing to the stabilisation of the tetrahedral

intermediate (Chen *et al*., 1992). Crystal structures show that this residue is distant to bound ligands (greater than 10 Å) and thus, like ST/VV, suggests an indirect role in affecting stabilisation of the tetrahedral intermediate.

Z-FHL has the appearance of being more spatially constrained in the N-domain and this work could provide a structural basis for the observation of *Z*-FHL having improved binding affinity and turnover rates for the C-domain. Again, this could be attributed to the C-domain residues enabling easier positioning of the substrate for hydrolysis (Corradi *et al*., 2006).

The fluorogenic substrate Abz-SDK(Dnp)P had originally been reported to have an N-domain selectivity of more than 300-fold due to the C-domain being very slow in the cleavage of the substrate (Araujo *et al*., 2000). The present study was unable to reproduce such a large degree of selectivity, with a 28-fold N-selectivity noted. Lower than reported selectivity was observed despite the assay being attempted at different temperatures and buffer conditions (data not shown). Differences between enzyme derivatives employed (truncated, individual domains in this study versus full length sACE, domain inactivated enzymes) could be suggested to contribute to the decreased selectivity. Indeed, a 20-fold lower selectivity was also noted in the physiologically relevant substrate AcSDKP using the same truncated enzymes with a completely different assay (section 3.3.4.2). Nonetheless, Abz-SDK(Dnp)P under these conditions can still be considered as a substrate specific for the N-domain and relevant mutations were characterised for their effect on Abz-SDK(Dnp)P binding and turnover.

Implications in the literature of the prominent involvement of the S_2 subsite (see Chapter 1) prompted this study to investigate the effects of mutations in this subsite on Abz-SDK(Dnp)P kinetics. Conversions in the N-domain S_2 subsite (Y369F, R381E and YR/FE) resulted in three to five fold decreases in catalytic efficiencies of the fluorogenic substrate, while S_2/S_1 subsite border mutant derivative T496V had no effect on Abz-SDK(Dnp)P catalysis. This kinetic analysis suggests a modest role of several distinct residues within the S_2 subsite in contributing to the overall selective processing of this substrate and further implies the contribution of several other residues working in concert towards N-selective substrate processing. This study is in agreement with other studies implicating the substrate P_2 group in selective processing of Abz-SDK(Dnp)P derivatives (Michaud *et al*., 1999; Araujo *et al*., 2000). While other unique N-domain residues are present in the S_1 subsite (Ser119, Asn494),

these appear distal from any ligands in the crystal structures available and suggests lack of significant contributions to substrate and inhibitor binding.

In order to compare the role of the S_2 subsite with that of the S_2' subsite in the N-selectivity of Abz-SDK(Dnp)P, a C-domain enzyme containing all unique S_2' residues converted to their N-domain counterparts was kinetically assessed. Such a mutant was utilised due to the seemingly poor kinetics of N-domain mutant ST/VV; which would provide misleading results due to poor overall general cleavage. Unexpectedly; a 10-fold increase in C-domain S_2' mutant enzymatic efficiency compared to wild type C-domain was noted. This was surprising since the above reports suggest that the determinants for N-selective substrate processing lie within the abovementioned unprimed subsites. These kinetic data suggest that, while residues in the S_2 subsite of the N-domain do indeed play a contributing role to selectivity, the determinants for overall Abz-SDK(Dnp)P selectivity involves interplay between a number of enzyme subsites. Such interplay between subsites in contributing to ACE selectivity has been noted in the binding of phosphinic inhibitor RXPA380 (Kroger *et al*., 2009) and will be the focus of future investigation.

In general, mutations in the S_2 and S_2' subsites of the N-domain active site have revealed some important amino acids contributors in substrate processing. ST/VV was a poor enzyme for Abz-FRK(Dnp)P, *Z*-FHL as well as HHL and, while binding affinity for the substrate was comparable to wild type for the substrates tested, the turnover rates were very much lower. Structural suggestions of this phenomenon have been presented above. Y369F, while having a comparable catalytic efficiency with Abz-FRK(Dnp)P to wild type, had improved HHL catalysis and decreased catalysis of N-specific substrate Abz-SDK(Dnp)P and suggests a consistent role of this residue in the specific substrate processing of the N-domain.

Previous work involving AcSDKP kinetics involved the use of paper chromatography or HPLC, neither of which allow for high throughput kinetic characterisation (Rousseau *et al*., 1995; Deddish *et al*., 1996; Michaud *et al*., 1997). Since AcSDKP has an acetylated, and therefore protected, N-terminus it has been identified as a possibly useful substrate for such high throughput analysis using an appropriate derivitising agent.

Fluorescamine is a reagent that forms adducts exclusively with primary amines. Although fluorescamine itself is not fluorescent; derivitisation to primary amines forms fluorescent adducts resulting in a detectable fluorescence signal (Udenfriend *et al*., 1972). Due to the

introduction of a new peptide N-terminus by hydrolysis of an amide bond, fluorescamine has been used to monitor ACE activity in the cleavage of *N*-acetyl-AngI and substance P (Conroy and Lai, 1978; Yokosawa *et al*., 1983), as well as other enzymes (Wang *et al*., 2001; Kang *et al*., 2002). Precedent in the literature therefore suggests a plate adaptation assay of fluorescamine could be used to monitor the conversion of AcSDKP into inactive products.

Basal fluorescence of enzyme and uncleaved substrate was low and N-domain enzyme activity resulted in a large change in fluorescence compared to substrate alone. The negligible effect of enzyme on fluoresence is to be expected due to the amount of enzyme present being below the sensitivity of the derivitising agent (Udenfriend *et al*., 1972). The assay thus appeared feasible to be employed in the analysis of AcSDKP kinetics.

Comparison of wild type soluble human N-domain to the human sACE N-domain active form shows a similar turnover rate (Rousseau *et al*., 1995). The K_m values are higher than Rousseau *et al*. (1995), in agreement with previous work that assessed the soluble ACE domains in ileal ACE (N-domain) and rabbit tACE (C-domain) using HPLC and also showed decreases in substrate binding affinities (Deddish *et al*., 1996). The selectivity of AcSDKP for the domains is markedly reduced with N-selectivity being only 2-fold. Deddish *et al.* (1996) found a similar decrease in selectivity; with AcSDKP having approximately 8-fold N-selectivity. In this study, while the N-domain had a turnover rate similar to a previous report, the C-domain had a considerably higher turnover rate thus decreasing the overall selectivity. Increased C-domain activity could be due to the assay conditions. In the original publication of the N-selectivity of AcSDKP processing (Rousseau *et al*., 1995); salt concentration of 50 mM NaCl was used in the prepared assay buffers despite showing that close to maximal activity of both domains was at a more physiological concentration of 100 mM NaCl. This study sought to mimic the physiological context and therefore utilised conditions of 100 mM NaCl as was the case with other authors (Deddish *et al*., 1996). Thus, a contributor to higher C-domain activity in this study is probably due to the use of an optimal chloride concentration for the C-domain.

Domain cooperativity has been observed whereby the overall activity of sACE empirically equates to the mean activity of the two separate domains, suggesting that the domains do not function in an independent manner. Both human and bovine ACE displayed such functional behaviour with synthetic tripeptides (Binevski *et al*., 2003; Skirgello *et al*., 2005; Woodman *et al*., 2005). Further work with physiological substrates and human ACE enzymes showed a

similar result for AngI and Ang(1-7), but not Ang(1-9) suggesting that this cooperativity is not the case for every ACE substrate (Rice *et al*., 2004). The current study shows that the overall efficiency of sACE in AcSDKP processing is not the mean of the individual N- and C-domains but additive of the respective individual domain efficiencies. Under these conditions, it appears that both domains have the ability to be efficient in the cleavage of AcSDKP. However, numerous other publications support the predominant role of the N-domain in AcSDKP cleavage *in vivo* (Azizi *et al*., 1996; Junot *et al*., 2001; Fuchs *et al*., 2004; Li *et al*., 2010). Further work is required in order to assess the exact molecular basis of this reduced selectivity and additive effect. This study found decreases in both Abz-SDK(Dnp)P and AcSDKP selectivities. The previously established substrate selectivities were performed using the sACE domain inactivated forms of the enzyme (Rousseau *et al*., 1995; Araujo *et al*., 2000), and this work suggests that the individual domains do have different kinetic behaviour that warrants further investigation. The resolution of a sACE crystal structure could assist in providing a structural perspective and the relative domain orientation in sACE substrate and inhibitor binding.

A novel plate adapted assay has been designed and shows promise for the use in studies which require a more high-through put approach in the assessment of AcSDKP. Such an assay approach could be important for the testing of a number N-selective inhibitors and their effect on *in vitro* AcSDKP processing.

Chapter 4

Mutational effects on RXP407 binding and the design of novel N-selective inhibitors

4.1 Introduction

ACE inhibitors have been effectively employed in a wide variety of clinical settings ranging from the management of hypertension to diabetic nephropathy; highlighting the central role of ACE in pathologies relating to vascular function. Whilst ACE inhibitors are very often an efficacious form of treatment, ADEs can cause discomfort to patients and lead to the discontinuation of treatment in more severe cases (Speirs *et al*., 1998; Morimoto *et al*., 2004). Further work has implicated that BK buildup associated with dual blockade of ACE could be a major contributor to the occurrence of ADEs (Nussberger *et al*., 1998; Emanueli *et al*., 1998). This, coupled with the finding of two similar yet distinct functioning ACE domains (Wei *et al*., 1991; Fuchs *et al*., 2004; Fuchs *et al*., 2008), has lead to the hypothesis that selective inhibition of one particular domain could still maintain efficacy whilst leaving the second domain free in the degradation of BK (Acharya *et al*., 2003; Ehlers, 2006).

The N-domain is the principle enzyme for the degradation of haemoregulatory and anti-fibrotic agent AcSDKP and build up of this peptide has been shown to lower collagen deposition in a variety of tissues (reviewed in Chapter 1). Further, elevation of AcSDKP plasma levels through N-domain inactivation reduces pulmonary fibrosis associated with bleomycin administration (Li *et al*., 2010). Thus, selective N-domain inhibition could be utilised in co-administration with chemotherapeutic bleomycin and as a possible treatment for pulmonary fibrosis of which there are currently no approved drugs (du Bois, 2010).

The phosphinic peptidomimetic inhibitor RXP407 is the only inhibitor developed that displays marked N-selectivity of three orders of magnitude (Table 4.1) (Dive *et al*., 1999). The synthesis of RXP407 analogues led to the identification of the P_2 Asp and *N*-acetyl group as well as the amidated C-terminus as structural determinants for the selectivity of this molecule (Dive *et al*., 1999). Such findings provide important information regarding the subsites involved in N-selective binding (that being the S_2 and S_2' subsites) and suggest potential unique interactions of residues within those subsites with the inhibitor. Also, the

above functionalities can be used in the modification of existing inhibitor templates to enhance the N-selectivity of candidates that possess more drug-like characteristics.

The identification of amino acids that possibly contribute to the selective binding of RXP407 made use of available structures and docked models (Tzakos and Gerothanassis, 2005; Jullien *et al*., 2006; Corradi *et al*., 2006; Anthony *et al*., 2010) and has been reviewed in Chapter 1. These residues were converted to their corresponding C-domain counterparts, expressed and purified as described in Chapter 2, and their kinetic abilities assessed using the fluorogenic substrate (Abz)-FRK(Dnp)P (Chapter 3). Such conversions can shed light on active site residue contribution in RXP407 binding and guide the design of N-selective inhibitors. This approach has been used to successfully elucidate the molecular basis of RXPA380 C-selectivity (Kroger *et al*., 2009).

Of the clinically used inhibitors, only captopril displays modest selectivity for the N-domain active site (Wei *et al*., 1992). While several established ACE inhibitors can potently inhibit ACE activity, only captopril was able to differentiate between AcSDKP and AngI hydrolysis further supporting its modest N-selectivity described above (Michaud *et al*., 1997). Since the C-terminal amide is crucial for the N-selectivity of RXP407, the simple addition of a C-terminal amide could result in a clinically relevant N-selective inhibitor (Table 4.1).

Keto-ACE (5-S-5-Benzamido-4-oxo-6-phenylhexanoyl-L-proline) is a ketomethylene derivative that utilises a carbonyl group for zinc coordination and has been shown to be approximately 30-fold C-selective (Table 4.1) (Deddish *et al*., 1998). The synthetic approach for the synthesis of keto-ACE analogues containing different P_2 and P_2' functionalities has been established previously (Nchinda *et al*., 2006b) and provides an appropriate starting point for the synthesis of additional potentially N-selective inhibitors. These inhibitors thus provide templates for the design of novel N-selective inhibitors and modification of these molecules to include an *N*-acetyl group, a P_2 Asp and a C-terminal amide could result in more drug-like molecules with greatly improved N-selectivity (Table 4.1).

Table 4.1: Names, structures and molecular masses of potentially N-selective compounds.

Compound name	**Compound structure**	**Molecular mass (g.mol^{-1})**
	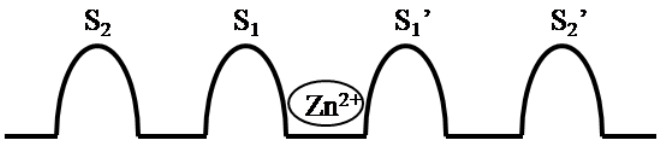	
RXP407	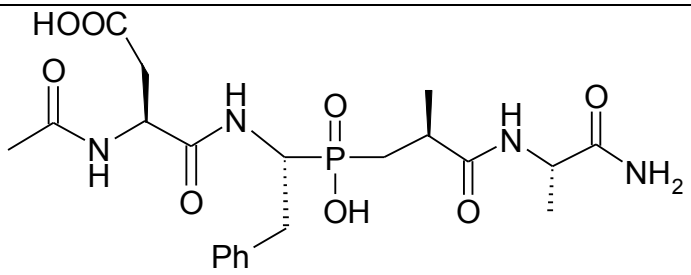	498.48
Captopril	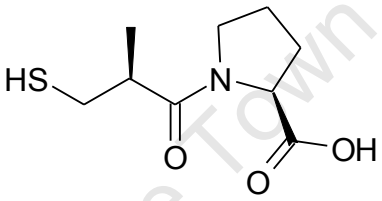	217.29
$CapNH_2$	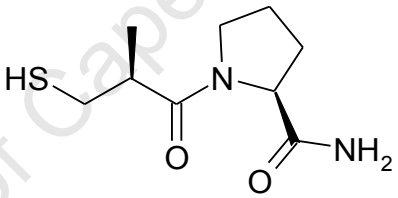	216.30
Keto-ACE	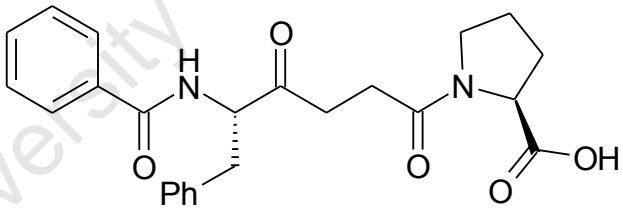	422.49
1	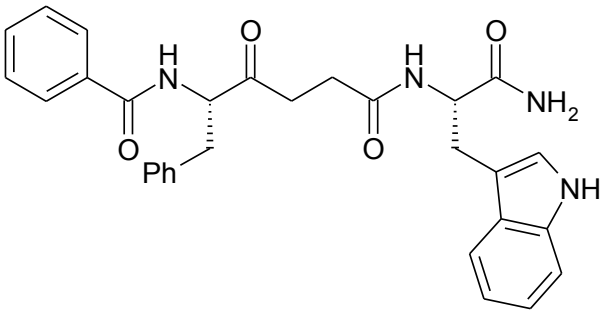	510.60
2	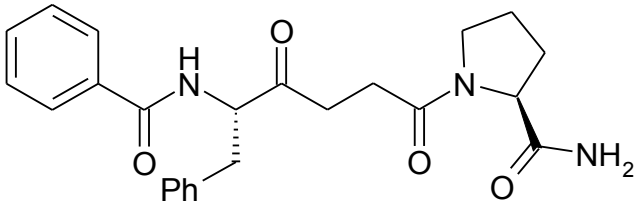	421.50

Table 4.1: *continued*

Compound name	Compound structure	Molecular mass (g.mol^{-1})
	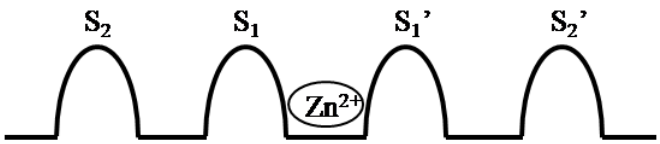	
3	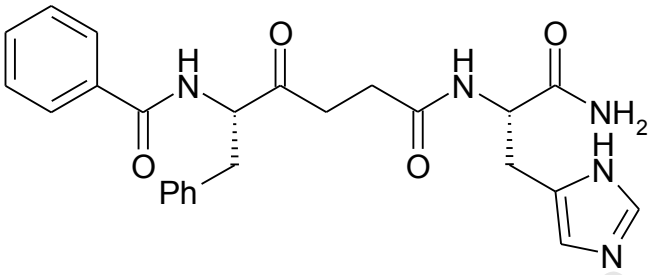	461.53
4	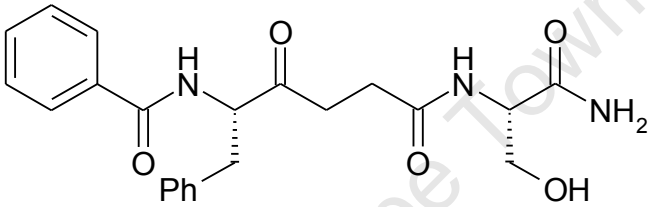	411.46
5	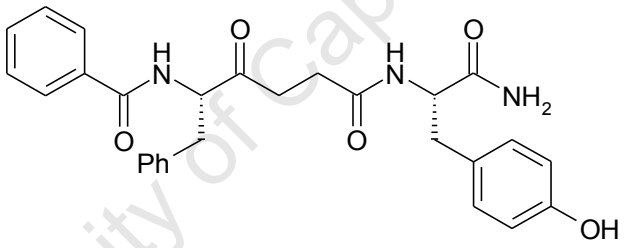	487.56
6	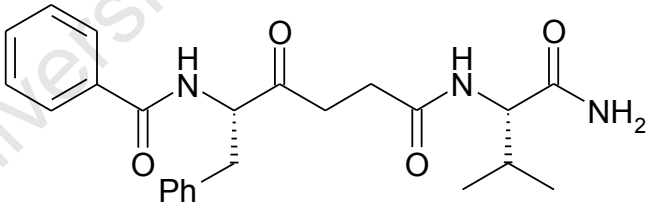	423.52
7	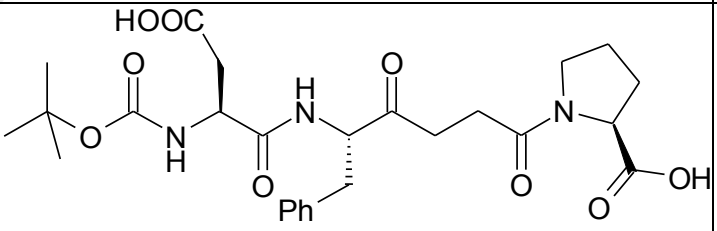	533.58
8	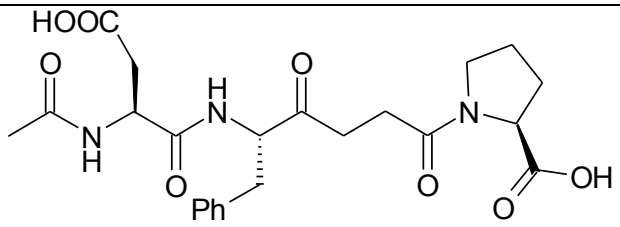	475.50

The objectives for the assessment of residue contribution to selective binding and the design of N-selective inhibitors were as follows:

1. To assess the kinetic binding of RXP407 to N-domain active site mutants using the fluorogenic substrate Abz-FRK(Dnp)P.
2. To assess the N-selectivity of a C-terminally amidated captopril analogue, capNH_2, using the substrate *Z*-FHL.
3. To evaluate the N-selectivity of keto-ACE analogues that contain newly introduced functionalities in the P_2 and P_2' positions; by screening for inhibitory potential and subsequent binding characterisation using the substrate *Z*-FHL.
4. To perform molecular docking studies of enhanced N-selective molecules positioned in the N- and C-domain active sites.

4.2 Methods

4.2.1 Preparation of inhibitors for enzymatic assays

Phosphinic inhibitor RXP407 was a kind gift from Prof V. Dive (CEA, iBiTecS, Service d'Ingénierie Moléculaire des Protéines, France). The solid inhibitor powder was dissolved in sterile dH_2O and subsequently serially diluted in RXP407 assay buffer (50 mM HEPES pH 6.8, containing 200 mM NaCl, 10 µM $ZnCl_2$). ACE inhibitor captopril was purchased from Sigma-Aldrich Co. C-terminally amidated captopril ($capNH_2$) was synthesised by Dr S. Salisu and keto-ACE analogues with differing P_2 and P_2' functionalities synthesised by Dr R.K. Sharma (in collaboration with Prof K. Chibale, Department of Chemistry, University of Cape Town) (Table 4.1). Captopril and $capNH_2$ were dissolved in sterile dH_2O and subsequently diluted in phosphate incubation buffer (100 mM $KHPO_4/KH_2PO_4$ pH 8.3, 300 mM NaCl, 10 µM $ZnSO_4$, 1 mg/ml albumin). Due to solubility issues, keto-ACE analogues were dissolved in 100% DMSO or methanol to yield a 50 mM inhibitor stock solution. Aliquots of stock solutions were diluted to 10 mM working stocks with dH_2O followed by dilution in phosphate incubation buffer.

4.2.2 Inhibition assays

4.2.2.1 RXP407 binding constant determination

Binding affinity of RXP407 was carried out as described previously (Watermeyer *et al*., 2008). Briefly, approximately 20 nM enzyme was incubated with an appropriate RXP407 dilution series in RXP407 assay buffer at room temperature for 90 minutes. Enzyme-inhibitor solutions were then aliquoted in triplicate in 20 µl volumes followed by addition of 280 µl (Abz)-FRK(Dnp)P (in RXP407 assay buffer) to give a final substrate concentration of either 4 or 8 µM. Change in fluorescence intensities over time was subsequently monitored using a Cary Eclipse spectrofluorimeter (Varian Inc.). Initial velocities were calculated using a standard curve correlating moles free Abz produced and fluorescence intensity (Appendix A4), and inhibitory binding affinities calculated with a Dixon Plot of inverse reaction velocity versus inhibitor concentration (Figure 4.1) (Dixon, 1953).

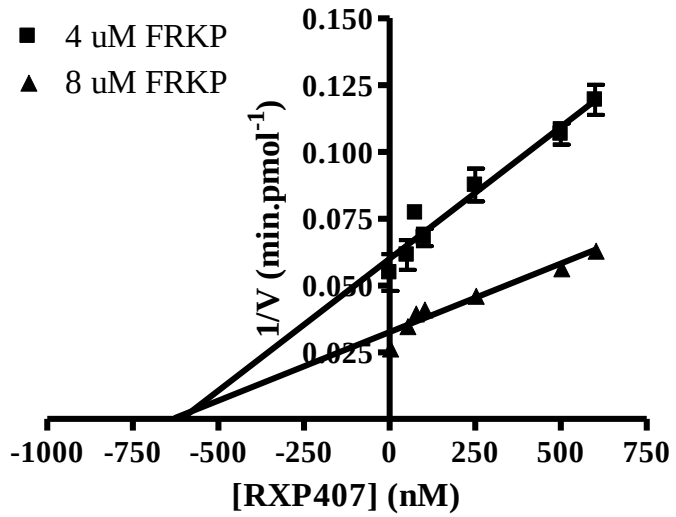

Figure 4.1: A representative Dixon Plot indicating the determination of the K_i value of N-domain mutant derivative YR/FE for RXP407. The corresponding *x*-coordinate of intersection of the two straight lines (extrapolated from two different substrate concentrations) is indicative of the negative of the K_i value in accordance with (Dixon, 1953). Data represented as mean ± SEM.

4.2.2.2 Novel ACE inhibitor analogues

A dilution series of captopril (0-500 nM) and capNH$_2$ (0-25 µM) in phosphate incubation buffer was incubated with N- and C-domains (final concentrations of 2.5 nM and 1 nM respectively) for 60 minutes. Triplicate 20 µl aliquots of the enzyme-inhibitor complex were aliquoted into a 96-well plate and prewarmed to 37°C. Twenty microlitres of pre-warmed substrate (2 mM *Z*-FHL in phosphate buffer) was added, incubated for 20 minutes shaking and subsequent assay steps performed as described previously (section 2.2.5). Percentage remaining activity was plotted against inhibitor concentration (in logarithmic scale) and the concentration required for 50% enzyme inhibition calculated through the use of a sigmoidal dose response curve (GraphPad Prism®, v 4.01, see Figure 4.3).

In order to identify potential N-selective keto-ACE analogues, a broad screen was first conducted to identify compounds with minimum threshold of 50% N-domain inhibition at 250 µM inhibitor concentration. Ten millimolar inhibitor stocks were diluted to 500 µM with phosphate incubation buffer, with the exception of compound 1 that required to be assayed at a higher concentration because of insolubility at lower concentrations due to a lower DMSO concentration. Forty microlitres of inhibitor solution was mixed with 40 µl enzyme (5 nM N-domain or 2 nM C-domain) and incubated at room temperature for 90 minutes and assayed with *Z*-FHL as outlined above. Percentage remaining activity was compared to controls

containing no inhibitor (with the same organic solvent concentration in phosphate incubation buffer). Compounds displaying above threshold inhibition of the N-domain and minimal inhibition of the C-domain were further analysed for N-selective inhibition activity.

Promising inhibitors were further kinetically analysed for their binding affinities toward the N- and C-domains. A serial dilution series was incubated with enzyme (as above) in phosphate incubation buffer and assayed as above at two substrate concentrations (0.1 mM and 1 mM *Z*-FHL). Inhibition constants (K_i) were calculated using Dixon plots as described in section 4.2.2.1.

4.2.3 Molecular docking of novel keto-ACE analogues

Ligand docking of N-selective keto-ACE analogues (compounds 7 and 8) into the N-domain active site was performed using the computational software platform of Discovery Studio (DS, Accelrys Inc., v 2.5). The recently solved RXP407—N-domain co-crystal structure (PDB accession code 3NXQ) was used as reference ligand (RXP407) and receptor (N-domain) respectively (Anthony *et al*., 2010). The receptor was prepared by deletion of the additional chain as solved in the asymmetric unit cell. Water and non-protein molecules of the remaining chain were also deleted. Conformers present in the data file of the N-domain were corrected and hydrogen atoms added through the use of the standard "Clean Protein" utility within the DS suite. Incomplete residues were corrected and charges of the zinc ion and complexing residues assigned. The co-ordinates of the co-crystallised ligand (RXP407) were extracted from the receptor and saved separately as a comparative during analysis. The spatial arrangement of the reference ligand was used to define a sphere for subsequent docking protocols (Figure 4.2). Ligand molecules were drawn using ChemSketch (ACD Laboratories, Freeware Edition) and saved in compatible MDL mol format. Drawn structures had hydrogen atoms added and the CHARMm forcefield (Brooks *et al*., 2009) applied to both ligand and receptor. Grid docking experiments were performed using the CDOCKER protocol (Wu *et al*., 2003) available on the DS platform with a set output of 10 minimised ligand poses. Poses with interaction distance between the zinc ion and carbonyl as well as between the C-terminal carboxylate and residues Lys489 and Tyr498 were selected for further analysis. Best fit poses were then selected on the basis of the lowest mean energy and interaction energy of the selected poses (Wu *et al*., 2003). The same approach was employed with the reference ligand to confirm reasonableness of the docked poses.

Figure 4.2: Representative figure indicating computationally defined active site sphere of the N-domain (PDB accession code 3NXQ) for docking of novel inhibitors. The N-domain protein structure is represented as a white-pink ribbon, the catalytic zinc as a grey sphere and reference ligand RXP407 shown in stick display. The docking sphere is shown in red and was generated by software within DS (Accelrys Inc., v 2.5). Image generated using DS Client Visualiser (Accelrys Inc., v 3.0).

4.3 Results

4.3.1 RXP407 binding affinities

To assess the contribution of N-domain residues towards selective binding of RXP407, inhibition binding assays were carried out on N-domain mutant derivatives using (Abz)-FRK(Dnp)P as a substrate. As shown previously (Dive *et al*., 1999), RXP407 showed marked N-selectivity with a low nanomolar binding affinity for the N-domain active site and micromolar inhibition of the C-domain (Table 4.2). Single amino acid conversions in both the N-domain S_2 and $S_2´$ subsites displayed modest effects on the selective binding of RXP407 (Table 4.2). In the $S_2´$ subsite, S357V and E431D showed a three-to-four fold decrease in affinity toward RXP407 binding (K_i). Additionally, $S_2´$ mutants E262S, D354E, T358V and the double mutation ST/VV showed no effects on inhibitor binding. While S_2/S_1 subsite mutant T496V had no effect on inhibitor affinity compared to wild type control, single mutations in the S_2 subsite (Y369F and R381E) resulted in modest three-to-six fold lower RXP407 binding affinities. Interestingly the double S_2 mutant, YR/FE, resulted in a 122-fold increase in K_i (Table 4.2) and thus a drastic decrease in inhibitor affinity for the mutant active site.

Table 4.2: Inhibitory binding constants (K_i) of RXP407 to enzyme active sites. Enzyme and inhibitor were pre-incubated and activity monitored continuously with substrate Abz-FRK(Dnp)P as outlined in section 4.2.2.1. K_i values were calculated by the Dixon Plot.

Subsite	Enzyme	K_i (nM)
-	N-domain	5.16
	C-domain	2830
S_2	Y369F	18.0
	R381E	33.5
	YR/FE	631
	T496V	5.99
$S_2´$	E262S	3.66
	D354E	3.52
	S357V	20.5
	T358V	3.40
	ST/VV	3.60
	E431D	17.7

4.3.2 C-terminally amidated captopril ($capNH_2$)

Since C-terminal amidation of RXP407 was previously shown to be important for N-selectivity (Dive *et al*., 1999); captopril, a modestly N-selective and clinically relevant drug template was amidated at the C-terminus and assessed for changes in N-selectivity. IC_{50} value determination for these two compounds for each domain was employed as an initial assessment of the degree of N-selectivity of the captopril analogue $capNH_2$. Captopril showed an IC_{50} value in the low nanomolar range and a selectivity of approximately 3-fold for the N-domain, a degree of selectivity consistent with literature reports (Wei *et al*., 1992; Michaud *et al*., 1997). $CapNH_2$ had an increased IC_{50} value compared to controls and showed an N-selectivity of 6-fold (Figure 4.3).

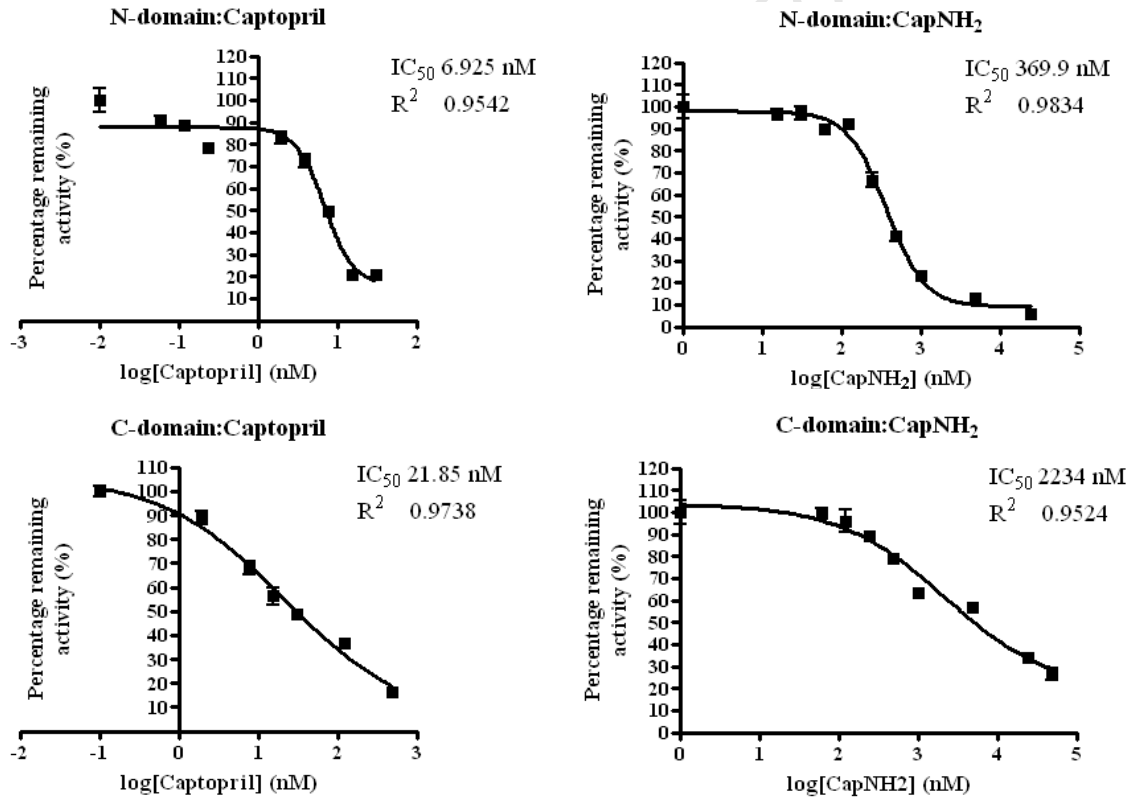

Figure 4.3: IC_{50} inhibition values for captopril and C-terminally amidated analogue, $capNH_2$. Inhibition assays were performed as described in section 4.2.2.2. Captopril displays modest 3-fold N-selectivity consistent with literature reports while $capNH_2$ shows decreased inhibitory potential and 6-fold N-selectivity. Data represented as mean ± SEM.

4.3.3 Keto-ACE analogues

The parent molecule, keto-ACE, has been shown to have binding affinities for both N- and C-domains in the lower micromolar range with a C-selectivity of approximately 30-fold (Deddish *et al*., 1998; Nchinda *et al*., 2006b; Watermeyer *et al*., 2008). As a control for the broad inhibition screen, keto-ACE displayed good inhibition of both domains as evident by the low residual enzyme activity at 250 µM inhibitor concentration (Figure 4.4).

4.3.3.1 Inhibitors containing P_2' functionalities

Keto-ACE analogues containing various amino acids in the P_2' position, as well as an amidated C-terminus, were assessed for inhibitory potential in a broad screen assay (compounds 1-6). All amidated keto-ACE analogues showed poor inhibition of the N-domain at 250 µM inhibitor concentration (Figure 4.4). Several compounds displayed improved inhibition of the C-domain and this inhibitory feature tended to correlate with bulkier and more hydrophobic amino acids in the P_2' position.

4.3.3.2 Inhibitors containing P_2 functionalities

A second group of keto-ACE analogues was generated containing an acidic P_2 Asp residue and either a *t*-Boc group or *N*-acetyl group protecting the N-terminus (compounds 7 and 8). These compounds generally showed improved inhibition of the N-domain compared to the C-domain at 250 µM (Figure 4.4). In both cases, minimal inhibition of the C-domain was noted at this concentration.

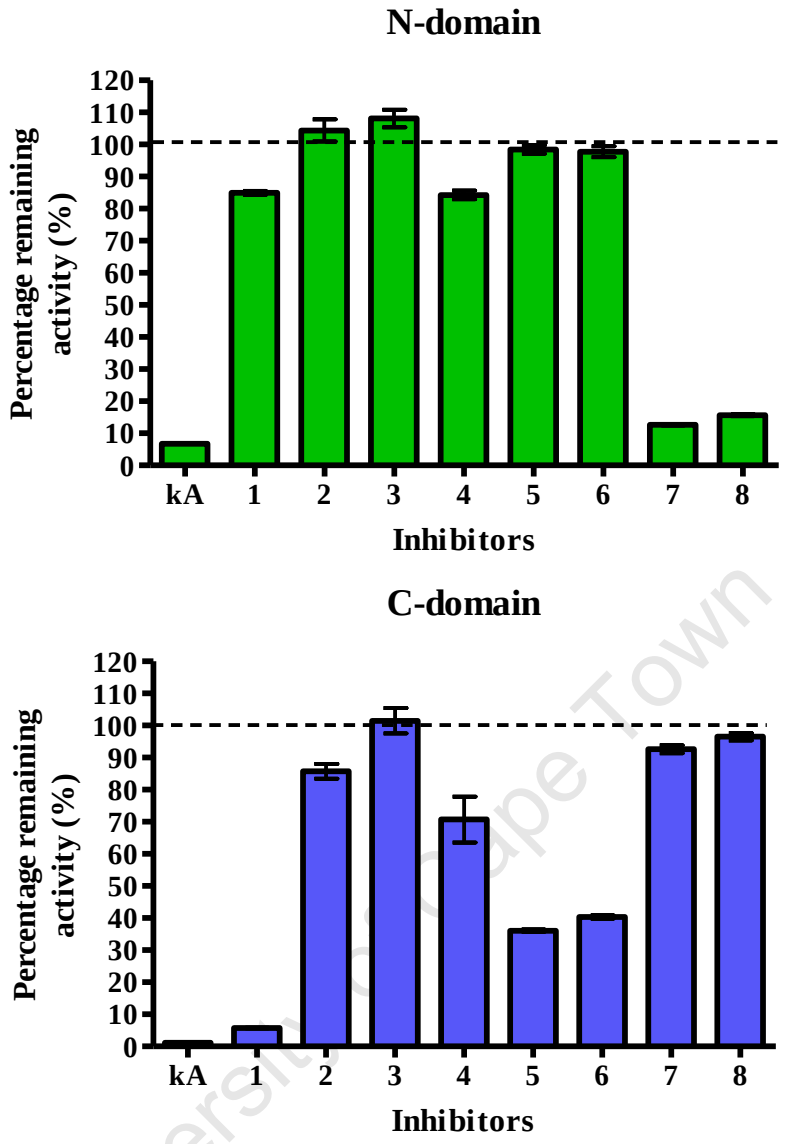

Figure 4.4: Inhibition screen of keto-ACE (kA) analogues and their effect on N- and C-domain activity. Two hundred and fifty micromolar inhibitor (with the exception of compound 1- 2.5 mM) was incubated with 2.5 nM N-domain or 1 nM C-domain and assayed as described in section 4.2.2.2. Percentage remaining ACE activity was calculated from a zero inhibitor control. Data represented as mean ± SEM.

K_i values of the keto-ACE parent molecule were in the lower micromolar range for both domains and displayed 36-fold C-selectivity, consistent with previous reports (Deddish *et al*., 1998; Nchinda *et al*., 2006b; Watermeyer *et al*., 2008). Inhibitor binding affinities of P_2 Asp containing compounds 7 and 8 had improved binding affinity for the N-domain displaying low micromolar inhibition and an approximately 30-fold selectivity for the N-domain (Table 4.3). Thus, the addition of an aliphatic *N*-protecting group and P_2 Asp resulted in an increase of approximately 1000-fold N-selectivity of these molecules (Table 4.3).

Table 4.3: Inhibitory binding constants of keto-ACE and analogues containing P_2 Asp functionalities. K_i values were determined as in section 4.2.2.2 and N-selectivity calculated as the ratio of C-domain K_i over N-domain K_i. Values represented as mean ± SD.

Compound	**Structure**	**N-domain K_i (µM)**	**C-domain K_i (µM)**	**Selectivity (C K_i/N K_i)**
keto-ACE	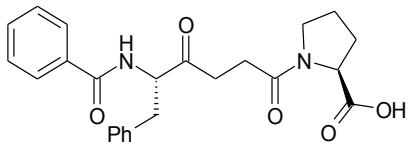	12.74±0.2333	0.3504±0.0089	0.02750
7	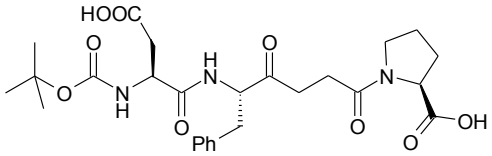	9.790±0.3394	330.0±30.83	33.71
8	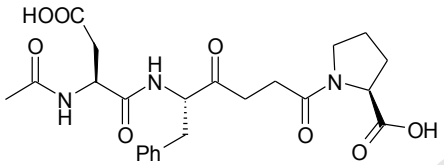	29.11±3.861	913.4±85.23	31.38

4.3.4 Molecular docking of keto-ACE analogues

Molecular docking of keto-ACE analogues was performed to provide a structural perspective of improved N-selective binding. In order to confirm the reliability of the molecular docking approach, reference ligands RXP407 and RXPA380 were removed from the predefined active sites of the N- and C-domains respectively and re-docked back into their crystal structure receptors. Both minimised ligands closely matched the reference poses of the crystal structure reference with RXP407 and RXPA380 displaying root mean square deviation (RMSD) values of 1.31 Å and 1.73 Å respectively (Figure 4.5).

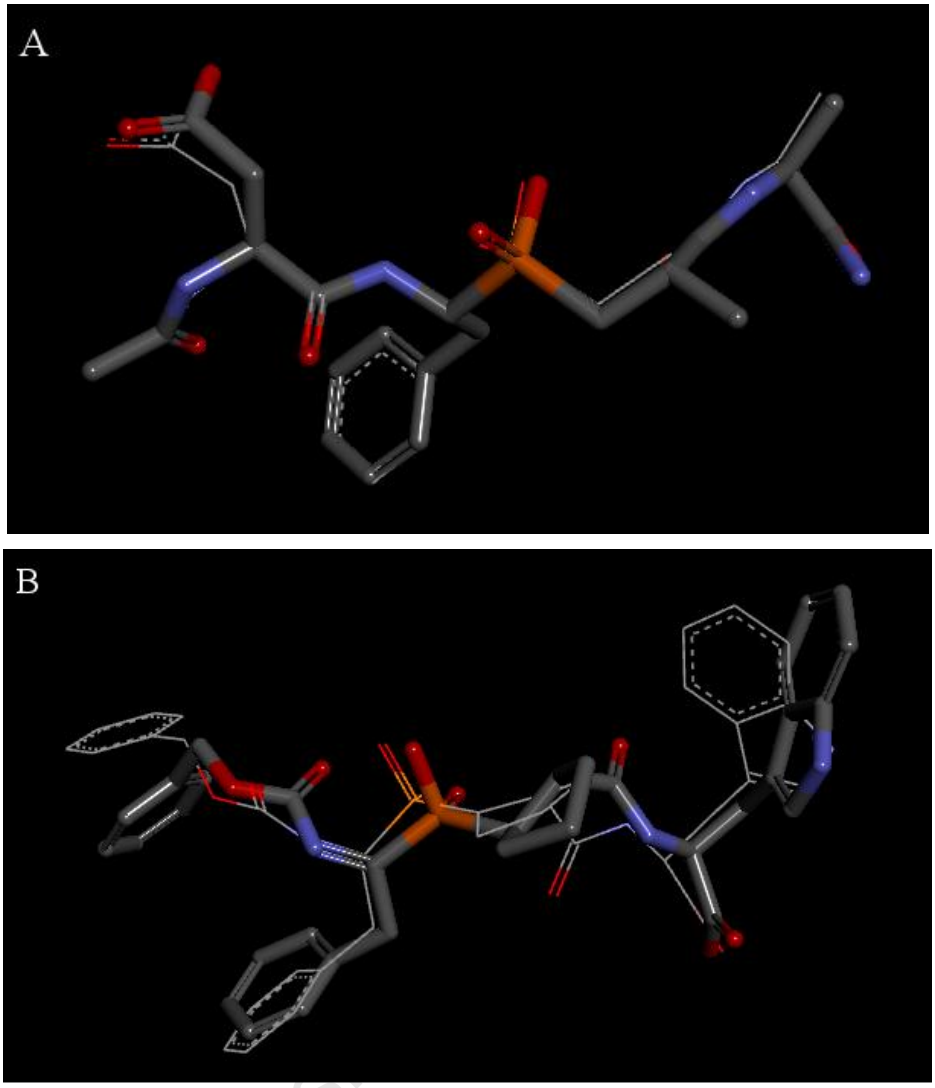

Figure 4.5: Redocked poses of reference ligands compared to the original crystal structure coordinates of RXP407 in the N-domain (A) and RXPA380 in the C-domain (B). Molecular docking was performed and relevant poses selected as outlined in section 4.2.3. Original crystal structure and redocked conformations are shown in line and stick styles respectively. In both cases the RMSD value is less than 2.0 Å. Images were generated using DS Client Visualiser (Accelrys Inc., v 3.0).

Structures of molecules showing the most prominent N-selectivity of the keto-ACE series (compounds 7 and 8) were molecularly docked into the computationally defined active sites of the N- and C-domains and appropriate poses selected on predetermined selection criteria. Two categories of conformations of molecules in the N-domain were noted for both ligands whereby the *N*-protecting groups displayed two possible positions. For compound 7; the *t*-Boc group either positioned downwards toward the large open active site cleft beyond the S_2 subsite to allow for the P_2 Asp to interact with Tyr369 and Arg381 (Figure 4.6 (A), stick

style pose) or the *t*-Boc itself was able to have interactions with the unique S_2 residues and the Asp pointed towards the conserved protein backbone (Figure 4.6 (A), line style pose). For compound 8; the *N*-acetyl appears to either position in the open cleft beyond the S_2 subsite (Figure 4.6 (B), stick pose) or within the S_2 subsite (Figure 4.6 (B), line pose). Compound 8 docks into the N-domain with an apparently conserved P_2 Asp interaction with Tyr369 and Arg381 between poses.

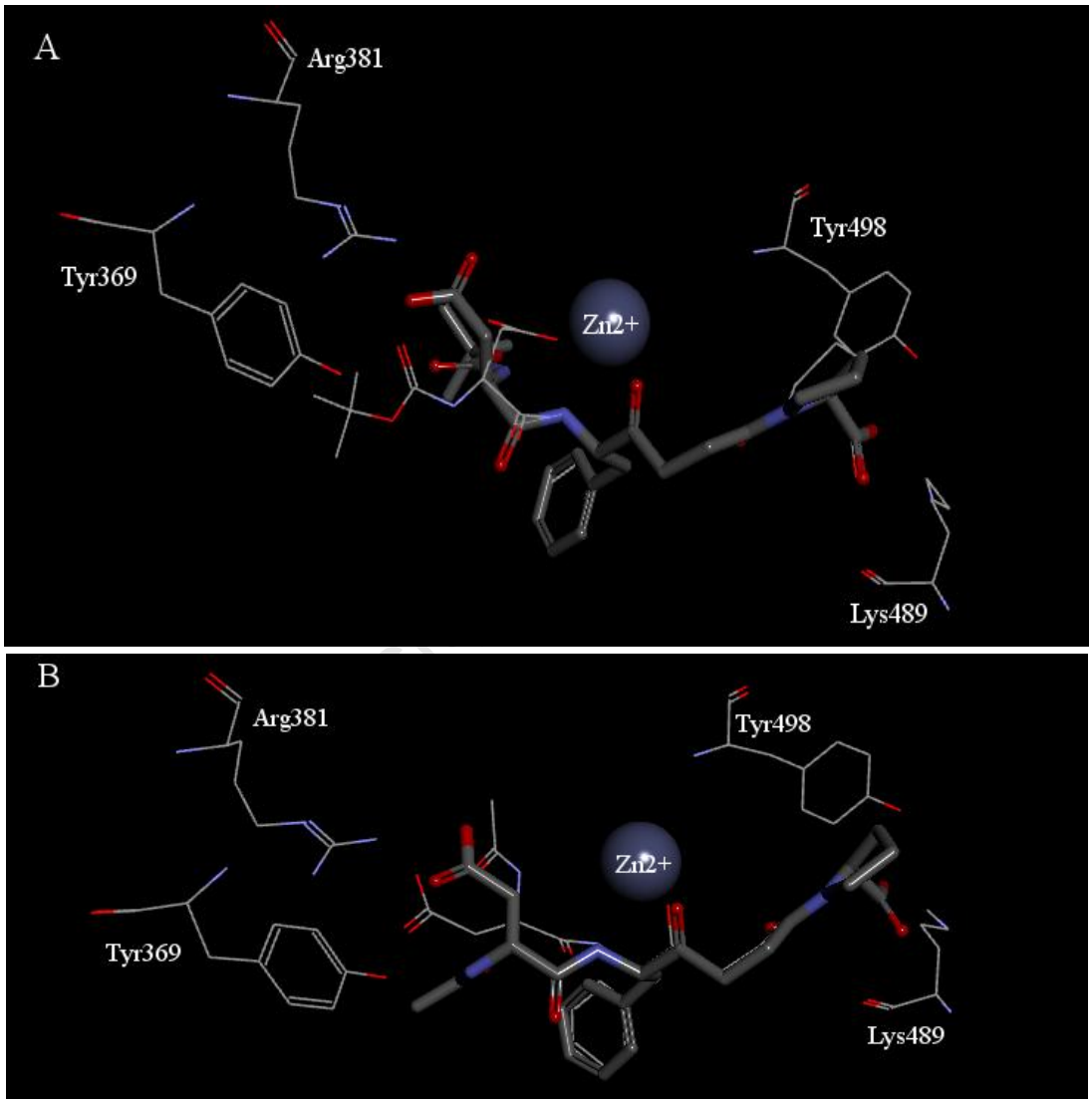

Figure 4.6: Two categories of poses obtained from molecular minimisation experiments and pose selection analysis of compounds 7 (A) and 8 (B) in the N-domain active site. Molecular docking was performed, relevant poses selected as outlined in section 4.2.3 and two representative poses indicated in line or stick bond display. In general two categories of poses were observed with the varied positioning of the *N*-protecting group and indicated possible hydrogen bonding with unique amino acids in the N-domain. Tyr369, Arg381, Lys489, Tyr498 and catalytic zinc ion are included in the diagram. Images were generated using DS Client Visualiser (Accelrys Inc., v 3.0).

In contrast and as expected, molecular minimisation of ligands in the C-domain active site indicated the lack of interactions of compound 7 with amino acids in the S_2 subsite due to a loss of interaction partners (Tyr369 is replaced by Phe391 and Arg381 is replaced by Glu403 in the C-domain). Consistent with a model of RXP407 in the C-domain (Tzakos and Gerothanassis, 2005), the inhibitor P_2 Asp has interactions with Ala356 of the protein backbone, which normally the inhibitor backbone carbonyl contacts (Anthony *et al*., 2010), and thus provides a structural visualisation of the basis of the improved N-selectivity of this compound (Figure 4.7). No poses of compound 8 in the C-domain met with the predetermined selection criteria of this study and were either of wrong orientation or lacked appropriate zinc ion coordination suggesting minimal set contacts between inhibitor and active site. Such docking corroborates the finding of compound 8 being a very poor inhibitor of the C-domain (K_i value close to 1 mM).

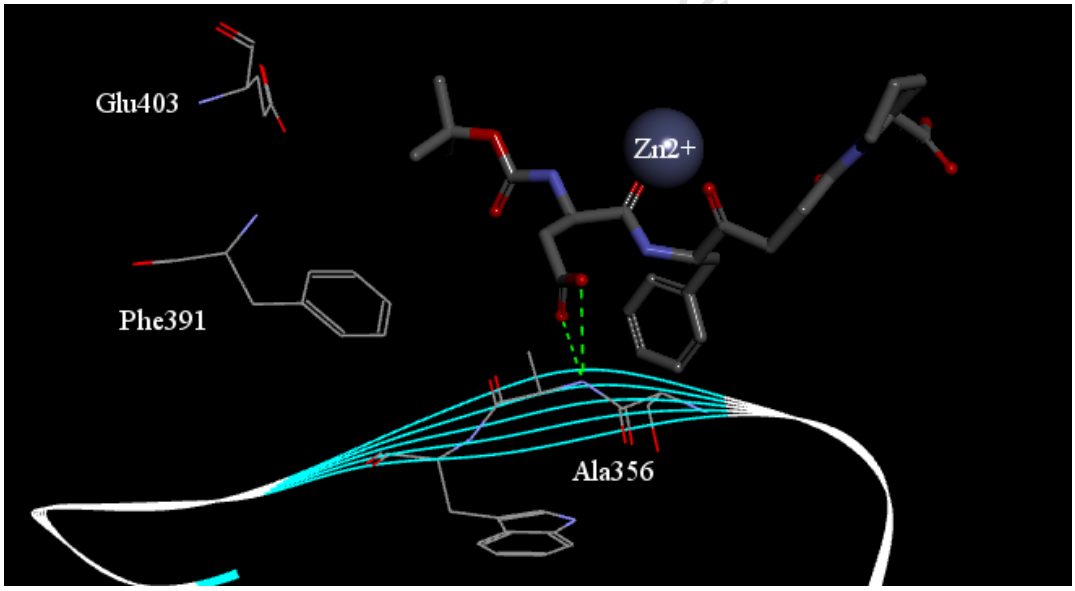

Figure 4.7: Compound 7 docked into the C-domain active site. The inhibitor P_2 Asp and *t*-Boc group lack interactions with unique domain residues, with the Asp seen to interact with the protein backbone of C-domain residue Ala356. Zinc ion and amino acids of interest are given as shown with hydrogen bonds represented as a broken green line. Image was generated using DS Client Visualiser (Accelrys Inc., v 3.0).

4.4 Discussion

Original combinatorial synthesis of RXP407 emphasised the importance of the inhibitor P_2 *N*-acetyl group and Asp residue, and P_2' C-terminal amide in selective binding of the N-domain active site (Dive *et al*., 1999). Such work thus suggested the importance of interactions of unique residues present in the corresponding enzyme subsites and their contribution to N-selectivity.

Numerous single and double mutations in the S_2' subsite of the N-domain resulted in minor changes in RXP407 binding affinity, suggesting limited individual roles of these residues in N-selective binding. All unique residues within possible binding distance in this subsite have been mutated in this study; however, an understanding of the molecular basis of the C-terminal amide interaction remains elusive. All computational models (RXP407 docked into the N-domain) do not show prominent interaction of the C-terminal amide with unique N-domain amino acids (Tzakos and Gerothanassis, 2005; Jullien *et al*., 2006; Corradi *et al*., 2006). In addition, the recently resolved N-domain–RXP407 co-crystal structure indicates that the RXP407 C-terminal amide makes contacts with conserved residues Gln259 and Tyr498 (Figure 4.8) (Anthony *et al*., 2010). Although it has been proposed that the amide might make a water-mediated hydrogen bond with Thr358 (Anthony *et al*., 2010), the significance of this single interaction as a means to selective binding is not supported by the above mutational analysis. With individual interactions in the S_2' subsite apparently not being the major player in N-selective binding, it is hypothesised that perhaps the presence of several unique residues provide the appropriate environment for C-terminal positioning within this subsite. When these residues are removed, as in the C-domain, perhaps subtle changes to this environment results in less favourable C-domain binding affinity. Future work could involve conversion of all S_2' residues in a single active site to further investigate this hypothesis.

Single mutations of residues in the S_2 subsite had little or no effect on RXP407 binding. However, conversion of residues Tyr369 and Arg381 in a single active site (YR/FE) resulted in a binding affinity of RXP407 more comparable to C-domain binding. This suggests that both amino acids make sufficient contact with the inhibitor that, when one residue is converted, the other can provide interaction to still allow potent binding. Such information provided a useful indication of which molecular models better describe the probable binding mode in the N-domain active site (Kroger *et al*., 2009). The recently solved N-domain–

RXP407 co-crystal structure supports the above proposal (Anthony *et al*., 2010). In this structure, the P_2 Asp of RXP407 is within 3 Å of both Tyr369 and Arg381 thus allowing for extensive interaction with both of these residues (Figure 4.8). These findings provide useful information for the design of N-selective inhibitors and suggest that future compounds contain functionalities that can maximise interactions with Tyr369 and Arg381 in the N-domain active site.

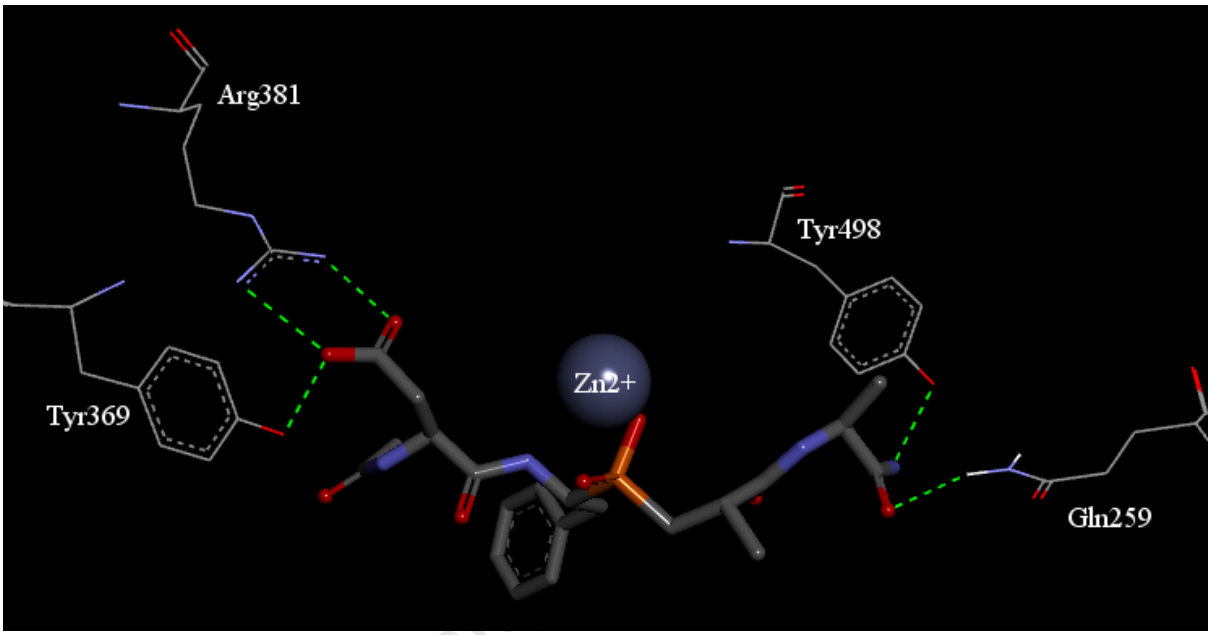

Figure 4.8: The crystal structure of N-selective ACE inhibitor RXP407 in the N-domain (PDB accession code 3NXQ) (Anthony *et al*., 2010). The RXP407 P_2 Asp has prominent hydrogen bond interactions with unique N-domain residues Tyr369 and Arg381 while the crystal structure indicates interactions of the P_2' amide only has interactions with domain conserved residues Gln259, His491 and Tyr498. N-domain amino acids and inhibitor RXP407 are displayed in line and stick style respectively, the zinc ion shown as a sphere and hydrogen bonds represented as broken green lines. Image was generated using DS Client Visualiser (Accelrys Inc., v 3.0).

A concurrent study was performed to initiate the development of novel N-selective inhibitors. With structural determinant investigations of RXP407 revealing the importance of the C-terminal amide in the selective binding of this inhibitor (Dive *et al*., 1999), simple modification of existing and potentially clinically relevant ACE inhibitor templates could help confer N-selectivity. Captopril, the smallest and most accessible in terms of organic synthesis of all the clinical ACE inhibitors, was used as a starting point to investigate this

hypothesis. Captopril displays minor N-selectivity, in agreement with previous work (Wei *et al*., 1992; Michaud *et al*., 1997). While it is difficult to identify the basis of this subtle selectivity from the crystal structures available, it has been suggested that energetic compensations in the active site could be a determinant (Natesh *et al*., 2004). Amidation of the C-terminus of captopril, compound capNH_2, showed no major change in N-selectivity. A possible suggestion is that captopril, being small and largely reliant on the sulphydryl group for potency, can position in a slightly different conformation due to its size and lack of other interactions. Thus, the possible interactions that the C-terminal amide makes in the S_2' subsite of the domains would not be effective in discriminating between domains because captopril could adopt a different position due to its size. Indeed, this drug has been shown to inhibit several other dissimilar zinc metalloproteases implying the lack of specificity of the compound (Thunnissen *et al*., 2002; Yamamoto *et al*., 2010). Further work using a keto-ACE backbone with compounds containing a C-terminal amide with different P_2' functionalities also failed to inhibit the N-domain at 250 µM inhibitor concentration, corroborating the mutational analysis with RXP407 above; that mutations in the S_2' subsite have little or no effect on inhibitor binding compared to wild type N-domain. Even compound 2, identical to the keto-ACE parent molecule with the exception of the C-terminal amide, was a poor inhibitor of both domains. Thus, the addition of a C-terminal amide to captopril and keto-ACE does not increase N-selectivity and appears to reduce inhibitor potency. This decreased inhibitory ability suggests that amidation of the C-terminus of these inhibitors renders a less effective inhibitory molecule possibly due to reduced interaction with Lys489, an interaction considered to be key for ACE inhibitor potency (Natesh *et al*., 2003; Acharya *et al*., 2003). With this possible loss of interaction, both captopril and keto-ACE do not have additional functional groups present elsewhere on the structure to significantly assist in binding. RXP407, that appears to lack an interaction with Lys489 in the crystal structure, utilises other subsite interactions for ACE binding (particularly the S_2 subsite) and thus inhibitory and selectivity potential must obviously be optimised in other pockets (Anthony *et al*., 2010). Therefore cooperative binding between the P_2 and P_2' groups could possibly play a role, that being the C-terminal amide could assist simply in anchoring in a slightly different but unique conformation so as to allow for better binding elsewhere in the molecule. Such interplay between subsites has been noted for another phosphinic inhibitor, RXPA380 (Kroger *et al*., 2009). With this being said, the N-domain co-crystal structure showed no unique interactions with the C-terminus, S_2' subsite mutational analysis indicated that mutations had minimal

affect on RXP407 binding, and the addition of a C-terminal amide to both captopril and keto-ACE analogues did not notably increase selectivity. Thus, the role of the C-terminal amide remains unclear and future work could involve the addition of a C-terminal amide to P_2 Asp compounds and subsequent testing on the resultant compound N-selectivity.

Several compounds containing different P_2' functionalities displayed apparently better inhibition of the C-domain (compounds 1, 5 and 6). This observation is consistent with the rationale that bulkier, more hydrophobic P_2' functionalities are better accommodated by the C-domain S_2' subsite (Georgiadis *et al*., 2003; Georgiadis *et al*., 2004; Watermeyer *et al*., 2008; Watermeyer *et al*., 2010) and shows the predominant role of these types of amino acids in driving C-selectivity.

To further investigate the role of inhibitor functional groups in N-selectivity, another category of keto-ACE analogues was synthesised containing a free C-terminus and P_2 Asp. Two molecules, which differed only in the *N*-protecting group (compound 7 possesses a *t*-Boc while compound 8 contains an acetyl functionality), were able to inhibit the N-domain in the low micromolar range and showed moderate (approximately 30-fold) N-selectivity. This observation is significant since the parent molecule of keto-ACE is shown to be approximately 36-fold C-selective, in agreement with previous studies (Deddish *et al*., 1998; Nchinda *et al*., 2006b; Watermeyer *et al*., 2008). Thus, the conversion of a benzoyl group to an Asp residue and aliphatic *N*-protecting group onto the P_2 position of keto-ACE contributes to a change in selectivity for the N-domain of approximately 1000-fold.

Docked models of compounds 7 and 8 reveal the potential for the *N*-protecting group to position in two orientations. In the case of compound 7, the carbonyl oxygen of the *t*-Boc group had the possible ability to interact with unique N-domain residue Tyr369. This agrees with other studies that suggested that the N-domain could more easily accommodate aliphatic moieties than phenyl groups due to the presence of Tyr369 and Arg381, and provides a structural perspective as to the reason that keto-ACE analogues containing a P_2 *t*-Boc group have improved N-selectivity (Nchinda *et al*., 2006b; Watermeyer *et al*., 2008). The *N*-acetyl group of compound 8, being less bulky, could also rotate to fit into the S_2 subsite while the P_2 Asp made contacts with active site residues. Such an observation is in agreement with the N-domain–RXP407 co-crystal structure where the two solved structures in the asymmetric unit had two different positions of the *N*-acetyl group (Anthony *et al*., 2010). The P_2 Asp in both compounds could position to have close contacts with residues Tyr369 and Arg381, in

agreement with the crystal structure of RXP407 in the N-domain (Figure 4.8). This emphasises the importance of the P_2 Asp in providing contacts that can discriminated between domains. When Tyr369 and Arg381 are removed, in the case of the C-domain, the compounds clearly have minimal contacts with the active site (Figure 4.7). This molecular minimisation study provides a structural indication of the importance of inhibitor functional group contacts with residues Tyr369 and Arg381 to assist in N-selective binding and aids in an understanding as to why such moieties were considered important for RXP407 selectivity (Dive *et al*., 1999).

The current study emphasises the features critical to improved N-selectivity; namely the presence of an *N*-protecting group and a P_2 Asp. Such functional groups appear to make key contacts with residues Tyr369 and Arg381 as evinced by crystal structures, N-domain mutational analysis and molecular docking minimisation studies. Clearly, maintenance or even improvement of these interactions will be required in the next phase of N-selective inhibitor development. Also, novel P_2 groups that are not naturally occurring amino acids could be used to enhance interactions with Tyr369 and Arg381. For example, ketomethylene based inhibitors containing oxadiazoyl rings have been successfully used in the development of selective inhibition of dipeptidyl peptidase IV possibly due to its interaction with a unique Arg residue (Koo *et al*., 2007).

In this study, a combined enzyme mutation analysis and inhibitor modification approach has allowed for the furthering in understanding of the molecular basis of N-domain inhibitor selectivity. This, together with the timely publication of the co-crystal structure of RXP407 in the N-domain, contributes to the rational structure-based design of N-selective inhibitors. In light of this work, it is suggested that aliphatic groups (and not bulky phenyl moieties) in the inhibitor P_2 position inhibitors could allow for better accommodation of the inhibitor in the N-domain active site, resulting in improved binding potency. Furthermore, future generation of N-selective inhibitors should focus to achieve optimal interactions with Tyr369 and Arg381. Such prominent interactions should allow for discrimination between active sites, as is noticed when these two residues are mutated and subsequent binding of RXP407 is more than 100-fold reduced. These future inhibitors have exciting potential application in treatment of various tissue fibrosis conditions due to the potent anti-fibrotic effect of AcSDKP buildup (Cavasin, 2006; Cavasin *et al*., 2007; Li *et al*., 2010).

Chapter 5

Conclusions and Future Directions

This study sought to determine the extent of unique N-domain active site residues in contributing towards N-selective inhibitor binding and substrate processing. The S_2 and S_2' subsites were implicated as important for N-selectivity through the previous generation of substrate and inhibitor analogues (Michaud *et al*., 1997; Michaud *et al*., 1999; Dive *et al*., 1999; Araujo *et al*., 2000), and important residues within these subsites identified through the use of available molecular models and crystal structures (Tzakos and Gerothanassis, 2005; Jullien *et al*., 2006; Corradi *et al*., 2006; Akif *et al*., 2010a; Anthony *et al*., 2010). Amino acids of interest were converted to their corresponding C-domain counterparts, expressed in a mammalian cell culture system and purified to homogeneity. These mutant enzyme derivatives were subsequently tested with N-selective substrates and inhibitors. Information regarding their contributions can be used in the initial design of novel N-selective inhibitors.

Assessment of the effects of these mutations in substrate processing involved substrates *Z*-FHL, HHL and Abz-SDK(Dnp)P. The S_2 mutant Y369F showed markedly improved catalytic efficiency in the hydrolysis of HHL and molecular docking experiments confirmed that the presence of the phenolic hydroxyl group could obstruct the optimal positioning of HHL; thus lowering catalytic ability in the N-domain. The S_2 mutants Y369F, R381E and YR/FE, but not T496V, all showed approximately 5-fold reduction in catalytic efficiencies of Abz-SDK(Dnp)P processing suggesting the cooperation of several other residues in allowing for selective hydrolysis. This was further corroborated with a C-domain S_2' mutant enzyme showing 10-fold improved catalysis compared to the C-domain control, suggesting that N-selectivity involves interplay between subsites for effective processing. Further sophisticated molecular modelling, as performed previously with another fluorogenic substrate (Bersanetti *et al*., 2004), could shed light on the possible interactions and dynamics involved in N-selectivity of substrate processing. Multiple mutations within a given subsite could allow for an investigation into the extent of cooperative binding between residues in allowing for effective catalysis to occur. Future work should also involve multiple mutations

in both subsites which could allow for an understanding of overall contribution across subsites to this process.

A potentially high-throughput assay for AcSDKP kinetic determination was developed and showed similar N-domain catalytic constants to those published in the literature (Rousseau *et al*., 1995; Deddish *et al*., 1996). Surprisingly, the C-domain turnover rate was markedly higher than previous reports (approximately 40-fold) and thus N-selectivity was only approximately 2-fold for AcSDKP. This finding requires further investigation. The use of full length sACE molecules containing only a single functioning active site could assist in understanding the manner of how each domain regulates the other in AcSDKP processing. Other chimeras have been generated in our research group that involved a swap in domain orientation or sACE containing two C-domains (Woodman *et al*., 2005), which could be useful in further characterising the molecular nature of possible domain regulation in the hydrolysis of this important peptide.

N-domain mutations were further assessed in their effect on binding of N-selective phosphinic inhibitor RXP407. This inhibitor showed prominent N-selectivity, displaying low nanomolar inhibition of the N-domain (K_i= 5.16 nM) and micromolar inhibition of the C-domain (K_i= 2.83 µM) consistent with the literature (Dive *et al*., 1999). Several mutations in the S_2' subsite (E262S, D354E, T358V and ST/VV) had no effect on inhibitor binding while S_2' subsite mutations S357V and E431D resulted in slight decreases in inhibitor affinity (S357V K_i= 20.5 nM, E431D K_i= 17.7 nM). Thus, S_2' mutations within plausible binding distance of the inhibitor had no considerable effect on inhibitor binding. The importance of the inhibitor P_2' group has been described elsewhere (Dive *et al*., 1999), thus it is likely that the production of an N-domain mutant containing all unique S_2' residues converted to corresponding C-domain counterparts would give an indication as to the full extent of S_2' subsite contribution in RXP407 binding. Also, the determination of the crystal structure of RXP407 in the C-domain could allow for improved understanding of the differences in P_2' group positioning between domains in this pocket.

Analysis of mutations in the S_2 subsite revealed the important role of this pocket in the N-selectivity of RXP407. Mutant T496V had no effect on inhibitor binding while mutations Y369F and R381E had minor decreases of inhibitor affinity (Y369F K_i= 18.0 nM, R381E K_i= 33.5 nM). However, conversion of both Tyr369 and Arg381 (mutant YR/FE) resulted in a 112-fold decrease in RXP407 binding affinity (K_i= 631 nM). This suggests that

both residues make contact with the inhibitor such that when one is removed the remaining residue can provide interactions to still allow for potent binding, in agreement with the recently solved crystal structure (Anthony *et al*., 2010). Complete loss of binding affinity to a level comparable to the C-domain (that is, in the micromolar range) was not achieved with any of the above mutations suggesting, as with the abovementioned substrate analyses, that interplay between subsites results in a total contribution towards N-selective binding. The next phase of this study should involve, as with substrate processing analyses, the use of mutants with conversions of multiple implicated residues across subsites and subsequent testing. This approach was employed in investigating the molecular basis of ACE C-domain selectivity and has already suggested important interplay between subsites for RXPA380 and RXP407 binding (Kroger *et al*., 2009).

Previously described structural determinants for the N-selectivity of RXP407 were used in the design of novel N-selective inhibitors. C-terminally amidated captopril ($capNH_2$) and keto-ACE molecules did not show improved N-selectivity and appeared to have reduced potency in inhibitor screens compared to controls (amidated keto-ACE failed to inhibit the N- and C-domains at 250 µM concentration whereas the parent molecule showed low micromolar range potency). The substitution of a P_2 benzoyl moiety with an *N*-protecting group and Asp residue resulted in a 1000-fold change in N-selectivity. Structural perspectives in the form of molecular minimisation studies indicated the P_2 Asp or *t*-Boc group had the ability to interact with S_2 residues Tyr369 and Arg381. In agreement with mutational studies above, the S_2/P_2 interaction is considered very important for N-selective binding. Future work should involve the synthesis of a keto-ACE analogue containing both the P_2 Asp/protecting group and an amidated C-terminus to investigate whether there could be cooperative effects between these two groups thereby synergising and improving N-selective binding of this series of compounds.

Taking the analyses of both substrates and inhibitors together reveals the consistent role of the S_2 subsite, particularly residues Tyr369 and Arg381, in contributing to differential domain kinetics. Tyr369 contributes to preventing improved HHL catalysis, both residues appear to assist in positioning Abz-SDK(Dnp)P for selective catalysis and both residues interact significantly with RXP407 and novel N-selective inhibitors. Thus, this study provides functional information involving active site mutation that further implicates the S_2 subsite in providing important interactions for both substrate processing and inhibitor binding.

The current study also gives important direction regarding the design of N-selective inhibitors. Based on the above findings, it is recommended that inhibitor design focus on the optimisation of interactions with Tyr369 and Arg381. The formation of four hydrogen bonds of the P_2 Asp with these residues is a large contributor to its selective binding of the N-domain ((Anthony *et al*., 2010) and this study). Thus, the addition of a P_2 Asp to clinically relevant, non-domain selective inhibitors (for example, enalaprilat) could result in an increase in N-selectivity and produce an important lead in the development of N-selective drug candidates. Combinatorial chemistry resulted in the discovery of the P_2 Asp playing an important role in N-selectivity (Dive *et al*., 1999); however, P_2 functionalities should not be limited to naturally occurring amino acids but extended to the inclusion of other more novel P_2 structures. Such low molecular weight compounds containing novel functionalities have been designed for other dipeptidyl peptidases and, in addition to good *in vitro* inhibition, displayed promising pharmacokinetic properties (Koo *et al*., 2007).

Current ACE inhibitors contain structural similarity in that all inhibitors insert in an orientation on the "primed side" of the zinc ion. Development of new classes of inhibitors involved an extension of these templates into the P_1 and P_2 groups (Redelinghuys *et al*., 2005). While this extension could assist in potency and selectivity, it could possibly introduce issues of reduced drug-like characteristics (Walters *et al*., 1999). K-26, a potent phosphonotripeptide ACE inhibitor, was recently shown to bind exclusively with the S_1 and S_2 subsites of AnCE (Ntai and Bachmann, 2008; Akif *et al*., 2010b). Thus, this molecule provides a template in the development of a new class of low molecular weight ACE inhibitors. Such molecules could be synthetically modified to optimise interactions with Tyr369 and Arg381 and thus increase N-selectivity.

In conclusion, this study has identified N-domain residues that contribute to the observed domain selectivity in substrate processing and inhibitor binding; and thus supplies useful information in the design of novel N-selective ACE inhibitors. The next generation of ACE inhibitors possessing improved N-selectivity could be useful in the treatment of conditions relating to tissue fibrosis without affecting blood pressure regulation.

Appendix

A1. Molecular cloning

A1.1 General information

DH5α *E. coli* cells (genotype: F^-, φ80*lac*ZΔM15, Δ(*lac*ZYA-*arg*F)U169, *deo*R, *rec*A1, *end*A1, *hsd*R17(r_k^-, m_k^+), *pho*A, *sup*E44, *thi*-1, *gyr*A96, *rel*A1, λ^-) (Invitrogen) were used for the transformation and propagation of plasmids. Bacterial culturing was carried out in luria broth medium (LB, 1% (w/v) tryptone, 0.5% (w/v) yeast extract, 1% NaCl) at 37°C and 200 rpm shaking. Ampicillin (final concentration 50 µg/ml) was added to the medium after autoclaving in cases of antibiotic selection as described in the text. Agar plates (1% (w/v) tryptone, 0.5% (w/v) yeast extract, 1% NaCl, 1.5% (w/v) bacteriological agar, 50 µg/ml ampicillin) were used in the plating of *E. coli* cells for single colony selection.

A1.2 Preparation and transformation of competent cells

Procedures regarding the preparation and transformation of DH5α cells were performed as described by (Sambrook *et al*., 1989). A single clone was picked and grown overnight in 5 ml LB medium. Five hundred microlitres of overnight culture was inoculated into 50 ml LB and grown under culturing condition until reaching an optical density at 595 nm (OD_{595}) of 0.5-0.6 units. Cells were harvested by centrifugation at 5000 rpm for 10 minutes at 4°C and the supernatant discarded. The cell pellet was resuspended in ice cold 10 ml 100 mM $MgCl_2$ and incubated on ice for 30 minutes. Cells were centrifuged again as above and the supernatant discarded. The cell pellet was resuspended in 2 ml 85 mM $CaCl_2$ (containing 15% glycerol), aliquoted in 100 µl aliquots into sterile reaction tubes and either used immediately or stored at -80°C for later use.

For transformation, competent cells were thawed on ice and approximately 20 µl DNA solution added directly to the reaction tube. The DNA-cells mixture was incubated on ice for 20 minutes, followed by heat shock of 5 minutes at 37°C and subsequent 1 minute incubation on ice. Four hundred and fifty microlitres of LB was added to the mixture and incubated at 37°C for 60 minutes shaking. Transformants were plated out onto ampicillin agar plates and incubated overnight at 37°C.

A1.3 Crude small scale plasmid preparation (Sambrook *et al*., 1989)

A selection of colonies displaying ampicillin resistance were inoculated into 5 ml LB containing antibiotic and grown overnight under bacterial culturing conditions. Approximately 1 ml of overnight culture was harvested through centrifugation on a bench-top centrifuge and the bacterial pellet re-suspended in 250 µl STET buffer (8% (w/v) sucrose, 5% (w/v) triton X-100, 50 mM EDTA pH 8.0, 50 mM Tris-HCl pH8.0, 20 µg/ml ribonuclease A, 1 mg/ml lysozyme). The resuspension was vortexed and boiled for 1 minute followed by centrifugation for 8 minutes at room temperature. The viscous pellet was removed with a sterile toothpick and the remaining DNA-containing supernatant was precipitated by the addition of 250 µl isopropanol with thorough mixing. The mixture was centrifuged for 8 minutes at room temperature, the supernatant discarded and the DNA pellet air dried for approximately 10 minutes. The dried pellet was gently resuspended by the addition of 20 µl nuclease free dH_2O and 1 to 3 µl used for restriction enzyme digests.

A1.4 Restriction endonuclease digests and agarose gel electrophoresis

Restriction endonuclease digests were performed with prepared plasmid DNA. Approximately 1-10 units of restriction endonuclease activity was used in a buffer system recommended by the appropriate manufacturer of the enzyme. Endonuclease was incubated with the DNA and 1X buffer system in a final volume of 20 µl for 1 hour at 37°C (unless otherwise indicated in the text) and stopped by placement on ice and the addition of loading buffer (0.25% (w/v) bromophenol blue, 0.25% (w/v) xylene cyanol, 30% (v/v) glycerol).

DNA fragments were fractionated and visualised by agarose gel electrophoresis. Prepared samples were loaded into a 1% agarose gel in TBE buffer (90 mM Tris-citrate pH 8.5, 90 mM boric acid, 3.2 mM EDTA, 10 µg/ml ethidium bromide). Samples underwent electrophoresis at 75 V for 60-90 minutes and banding patterns visualised under UV emission.

A2. Heterologous protein expression

A2.1 Mammalian cell culture medium components

Dulbecco's Modified Eagle Medium (DMEM) and Ham's nutrient mixture (Ham's-F12) were purchased from Gibco® (Invitrogen), foetal calf serum (FCS) was purchased from Sigma-Aldrich Co. and penicillin-streptomycin (Pen-Strep) purchased for Lonza Research Solutions. All medium was filter sterilised upon mixture of the components and sterility maintained at all times.

Growth medium:	44% (v/v) DMEM, 44% (v/v) Ham's-F12, 10% (v/v) FCS (heat inactivated- 56°C for 30 minutes), 20 mM Hepes pH 7.5.
Harvesting medium:	48% (v/v) DMEM, 48% (v/v) Ham's-F12, 2% (v/v) FCS (additional heat inactivation- 72°C for 30 minutes), 20 mM Hepes pH 7.5, 100 units Pen-Strep.
Wash solution (PBS):	137 mM NaCl, 2.7 mM KCl, 10 mM Na_2HPO_4, KH_2PO_4 pH 7.5.
Glycerol shock solution:	15% (v/v) glycerol in PBS.

A2.2 SDS polyacrylamide gel electrophoresis

Acrylamide gels were cast and subsequently electrophoresed using the Mini-PROTEAN Tetra Electrophoresis System (BioRad Laboratories Inc.). All running gels were cast with 10% acrylamide. Two and a half millilitres of 40% (w/v) acrylamide/bis-acrylamide (19:1) (Sigma-Aldrich Co.) was mixed with 3.3 ml running gel buffer (1.1 M Tris-HCl pH 8.8, 0.3% (w/v) SDS) and 4.1 ml dH_2O (final volume 9.9 ml). Gel polymerisation was initiated with the addition of 0.1 ml 10% (w/v) AMPS (made fresh) and 7 µl TEMED and the polymerising solution covered with a layer of isopropanol to ensure a flat interface between stacking and running gels. Once the running gel was set, the isopropanol was removed. The stacking gel was prepared by the addition of 0.8 ml 40% (w/v) acrylamide/bis-acrylamide (19:1) to 3.3 ml stacking gel buffer (0.38 M Tris-HCl pH 6.8, 0.3% (w/v) SDS) and 5.6 ml dH_2O (final volume 9.7 ml). Gel polymerisation was initiated with the addition of 0.3 ml 10% (w/v) AMPS (made fresh) and 20 µl TEMED followed by the insertion of the supplied comb for the formation of gel loading wells and allowed to set.

The equipment for gel electrophoresis was assembled according to manufacturer's guidelines. Five microlitres of loading buffer (62.5 mM Tris-HCl pH 6.8, 2% (w/v) SDS, 10% (v/v) glycerol, 5% (v/v) mercaptoethanol, 0.001% (w/v) bromophenol blue) was added to samples of 20 µl volumes and boiled for 5 minutes. The entire prepared sample was then loaded directly into the well of the above prepared acrylamide gels. Electrophoresis was performed in running buffer (25 mM Tris-HCl pH 8.3, 200 mM glycine, 1% (w/v) SDS) at a constant current of 50 mA and stopped when the dye front had eluted through the opposite end of the gel.

After electrophoresis, the apparatus was dismantled and acrylamide gels were stained with Coomassie staining solution (0.25% (w/v) Coomassie brilliant blue, 50% (v/v) methanol, 10% (v/v) acetic acid) for approximately 60 minutes. De-staining was performed by incubation of the gels with de-stain solution (25% (v/v) ethanol, 10% (v/v) acetic acid) for 2 hours.

A3. Preparation of substrates for enzymatic assays

A3.1 Internally quenched fluorogenic substrates (Abz-FRK(Dnp)P and Abz-SDK(Dnp)P)

Substrates were obtained in solid form and were a kind gift from Dr A.K. Carmona (Universidade Federal de São Paulo, Brazil). The powder was dissolved in 100% DMSO to yield a 10 mM stock solution based on the extinction co-efficient ε_{365}= 17300 $M^{-1}cm^{-1}$ (Araujo *et al*., 2000). Substrates were subsequently diluted down in assay buffer to the required working stock concentration and used in enzymatic assays.

A3.2 Z-Phe-His-Leu and Hippuryl-His-Leu

HHL was purchased from Sigma-Aldrich Co. For a 5.7 mM working stock solution, 48.5 mg HHL was dissolved in 4.2 ml 0.025 M NaOH (with heating) followed by addition of 4.0 ml 5X phosphate buffer (500 mM $KHPO_4/KH_2PO_4$ pH 8.3), 2.0 ml 3 M NaCl, 9.8 ml dH_2O and 15 µl 10 mM $ZnSO_4$. The working solution was stored at 4°C until use.

Z-FHL was purchased from Bachem Ltd. For a 20 mM stock solution, 110 mg substrate was dissolved in 1 ml 0.28 M NaOH (with heating) followed by the dropwise addition of 9 ml dH_2O. The stock solution was aliquoted out into reaction tubes at stored at -20°C. Working stock solutions were diluted down to the desired concentration with 5X phosphate buffer, NaCl, dH_2O and $ZnSO_4$ as above and stored at 4°C until use.

A3.3 Ac-Ser-Asp-Lys-Pro

AcSDKP was purchased from Sigma-Aldrich Co. and dissolved in sterile dH_2O to yield a 10 mM stock solution. A 2 mM working stock was obtained by dilution in HEPES buffer (50 mM HEPES, pH 7.5, 100 mM NaCl, 10 µM $ZnSO_4$) and subsequently diluted to appropriate concentrations in the same buffer.

A4. Standard curves

A4.1 Standard curves used for enzymatic assays

Standard curves were empirically determined as described in Chapters 3 and 4.

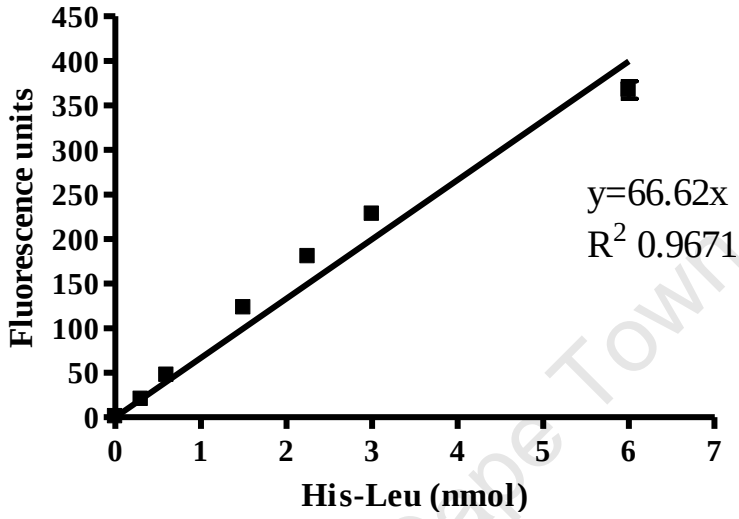

Figure A1: Standard curve of His-Leu correlated with increasing fluorescence.

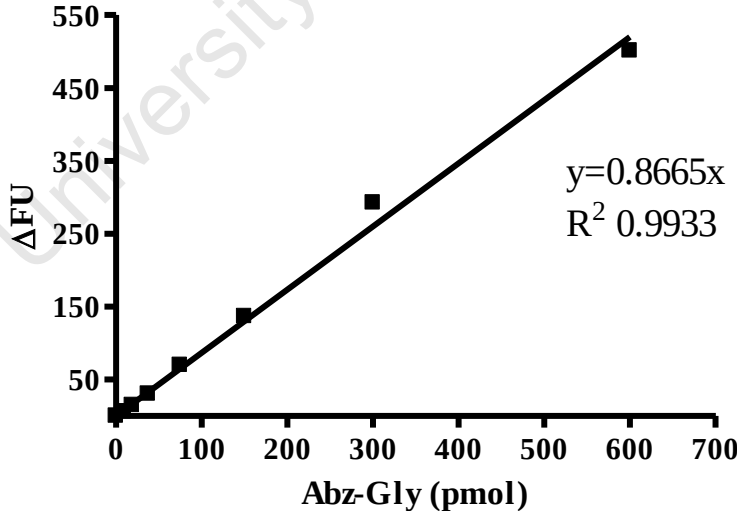

Figure A2: Standard curve of Abz-Gly correlated with increasing change in fluorescence (ΔFU).

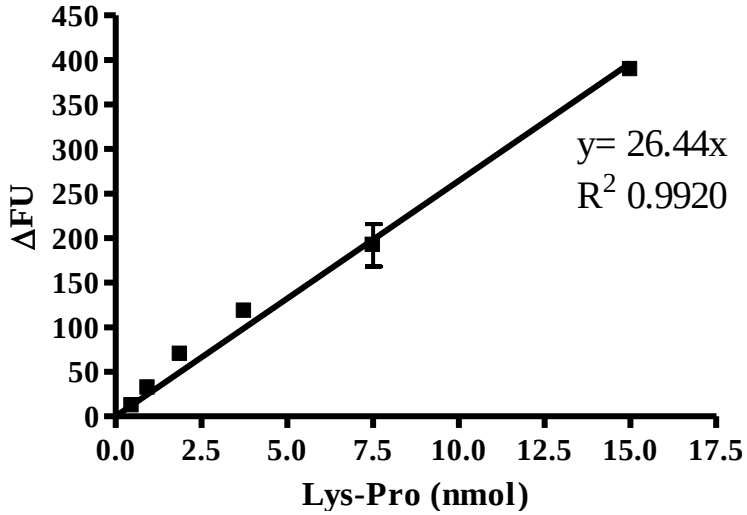

Figure A3: Standard curve of Lys-Pro correlated with increasing change in fluorescence (ΔFU).

References

Acharya, K.R., Sturrock, E.D., Riordan, J.F., and Ehlers, M.R. (2003) ACE revisited: a new target for structure-based drug design. *Nat. Rev. Drug Discov.* **2**, 891-902.

Adam, A., Cugno, M., Molinaro, G., Perez, M., Lepage, Y., and Agostoni, A. (2002) Aminopeptidase P in individuals with a history of angio-oedema on ACE inhibitors. *Lancet* **359**, 2088-2089.

Akif, M., Georgiadis, D., Mahajan, A., Dive, V., Sturrock, E.D., Isaac, R.E., and Acharya, K.R. (2010a) High-resolution crystal structures of Drosophila melanogaster angiotensin-converting enzyme in complex with novel inhibitors and antihypertensive drugs. *J. Mol. Biol.* **400**, 502-517.

Akif, M., Ntai, I., Sturrock, E.D., Isaac, R.E., Bachmann, B.O., and Acharya, K.R. (2010b) Crystal structure of a phosphonotripeptide K-26 in complex with angiotensin converting enzyme homologue (AnCE) from Drosophila melanogaster. *Biochem. Biophys. Res. Commun.* **398**, 532-536.

Anthony, C.S., Corradi, H.R., Schwager, S.L., Redelinghuys, P., Georgiadis, D., Dive, V., Acharya, K.R., and Sturrock, E.D. (2010) The N domain of human angiotensin-I-converting enzyme: the role of N-glycosylation and the crystal structure in complex with an N domain-specific phosphinic inhibitor, RXP407. *J. Biol. Chem.* **285**, 35685-35693.

Araujo, M.C., Melo, R.L., Cesari, M.H., Juliano, M.A., Juliano, L., and Carmona, A.K. (2000) Peptidase specificity characterization of C- and N-terminal catalytic sites of angiotensin I-converting enzyme. *Biochemistry* **39**, 8519-8525.

Azizi, M., Junot, C., Ezan, E., and Menard, J. (2001) Angiotensin I-converting enzyme and metabolism of the haematological peptide N-acetyl-seryl-aspartyl-lysyl-proline. *Clin. Exp. Pharmacol. Physiol.* **28**, 1066-1069.

Azizi, M., Rousseau, A., Ezan, E., Guyene, T.T., Michelet, S., Grognet, J.M., Lenfant, M., Corvol, P., and Menard, J. (1996) Acute angiotensin-converting enzyme inhibition increases the plasma level of the natural stem cell regulator N-acetyl-seryl-aspartyl-lysyl-proline. *J. Clin. Invest.* **97**, 839-844.

Balyasnikova, I.V., Metzger, R., Franke, F.E., and Danilov, S.M. (2003) Monoclonal antibodies to denatured human ACE (CD 143), broad species specificity, reactivity on paraffin sections, and detection of subtle conformational changes in the C-terminal domain of ACE. *Tissue Antigens* **61**, 49-62.

Bernstein, K.E., Shen, X.Z., Gonzalez-Villalobos, R.A., Billet, S., Okwan-Duodu, D., Ong, F.S., and Fuchs, S. (2010) Different in vivo functions of the two catalytic domains of angiotensin-converting enzyme (ACE). *Curr. Opin. Pharmacol.* **In press**

Bersanetti, P.A., Andrade, M.C., Casarini, D.E., Juliano, M.A., Nchinda, A.T., Sturrock, E.D., Juliano, L., and Carmona, A.K. (2004) Positional-scanning combinatorial libraries of

fluorescence resonance energy transfer peptides for defining substrate specificity of the angiotensin I-converting enzyme and development of selective C-domain substrates. *Biochemistry* **43**, 15729-15736.

Bicket, D.P. (2002) Using ACE inhibitors appropriately. *Am. Fam. Physician* **66**, 461-468.

Binevski, P.V., Sizova, E.A., Pozdnev, V.F., and Kost, O.A. (2003) Evidence for the negative cooperativity of the two active sites within bovine somatic angiotensin-converting enzyme. *FEBS Lett.* **550**, 84-88.

Bogden, A.E., Carde, P., de Paillette, E.D., Moreau, J.P., Tubiana, M., and Frindel, E. (1991) Amelioration of chemotherapy-induced toxicity by cotreatment with AcSDKP, a tetrapeptide inhibitor of hematopoietic stem cell proliferation. *Ann. N. Y. Acad. Sci.* **628**, 126-139.

Bonnet, D., Cesaire, R., Lemoine, F., Aoudjhane, M., Najman, A., and Guigon, M. (1992) The tetrapeptide AcSDKP, an inhibitor of the cell-cycle status for normal human hematopoietic progenitors, has no effect on leukemic cells. *Exp. Hematol.* **20**, 251-255.

Bradford, M.M. (1976) A rapid and sensitive method for the quantitation of microgram quantities of protein utilizing the principle of protein-dye binding. *Anal. Biochem.* **72**, 248-254.

Brooks, B.R., Brooks, C.L., III, Mackerell, A.D., Jr., Nilsson, L., Petrella, R.J., Roux, B., Won, Y., Archontis, G., Bartels, C., Boresch, S., Caflisch, A., Caves, L., Cui, Q., Dinner, A.R., Feig, M., Fischer, S., Gao, J., Hodoscek, M., Im, W., Kuczera, K., Lazaridis, T., Ma, J., Ovchinnikov, V., Paci, E., Pastor, R.W., Post, C.B., Pu, J.Z., Schaefer, M., Tidor, B., Venable, R.M., Woodcock, H.L., Wu, X., Yang, W., York, D.M., and Karplus, M. (2009) CHARMM: the biomolecular simulation program. *J. Comput. Chem.* **30**, 1545-1614.

Bueno, V., Palos, M., Ronchi, F.A., Andrade, M.C., Ginoza, M., and Casarini, D.E. (2004) N-Domain angiotensin I-converting enzyme expression in renal artery of Wistar, Wistar Kyoto, and spontaneously hypertensive rats. *Transplant. Proc.* **36**, 1001-1003.

Bull, H.G., Thornberry, N.A., and Cordes, E.H. (1985) Purification of angiotensin-converting enzyme from rabbit lung and human plasma by affinity chromatography. *J. Biol. Chem.* **260**, 2963-2972.

Bunning, P., Holmquist, B., and Riordan, J.F. (1983) Substrate specificity and kinetic characteristics of angiotensin converting enzyme. *Biochemistry* **22**, 103-110.

Burnier, M. and Zanchi, A. (2006) Blockade of the renin-angiotensin-aldosterone system: a key therapeutic strategy to reduce renal and cardiovascular events in patients with diabetes. *J. Hypertens.* **24**, 11-25.

Byers, L.D. and Wolfenden, R. (1973) Binding of the by-product analog benzylsuccinic acid by carboxypeptidase A. *Biochemistry* **12**, 2070-2078.

Carde, P., Chastang, C., Goncalves, E., Mathieu-Tubiana, N., Vuillemin, E., Delwail, V., Corbion, O., Vekhoff, A., Isnard, F., and Ferrero, J.M. (1992) [Seraspenide (acetylSDKP): phase I-II trial study of inhibitor of hematopoiesis protects against toxicity of aracytine and ifosfamide monochemotherapies]. *C. R. Acad. Sci. III* **315**, 545-550.

Carter, P. (1986) Site-directed mutagenesis. *Biochem. J.* **237**, 1-7.

Casarini, D.E., Plavinik, F.L., Zanella, M.T., Marson, O., Krieger, J.E., Hirata, I.Y., and Stella, R.C. (2001) Angiotensin converting enzymes from human urine of mild hypertensive untreated patients resemble the N-terminal fragment of human angiotensin I-converting enzyme. *Int. J. Biochem. Cell Biol.* **33**, 75-85.

Cashman, J.D., Eaves, A.C., and Eaves, C.J. (1994) The tetrapeptide AcSDKP specifically blocks the cycling of primitive normal but not leukemic progenitors in long-term culture: evidence for an indirect mechanism. *Blood* **84**, 1534-1542.

Castoldi, G., di Gioia, C.R., Bombardi, C., Perego, C., Perego, L., Mancini, M., Leopizzi, M., Corradi, B., Perlini, S., Zerbini, G., and Stella, A. (2010) Prevention of myocardial fibrosis by N-acetyl-seryl-aspartyl-lysyl-proline in diabetic rats. *Clin. Sci. (Lond)* **118**, 211-220.

Cavasin, M.A. (2006) Therapeutic potential of thymosin-beta4 and its derivative N-acetyl-seryl-aspartyl-lysyl-proline (Ac-SDKP) in cardiac healing after infarction. *Am. J. Cardiovasc. Drugs* **6**, 305-311.

Cavasin, M.A., Liao, T.D., Yang, X.P., Yang, J.J., and Carretero, O.A. (2007) Decreased endogenous levels of Ac-SDKP promote organ fibrosis. *Hypertension* **50**, 130-136.

Cavasin, M.A., Rhaleb, N.E., Yang, X.P., and Carretero, O.A. (2004) Prolyl oligopeptidase is involved in release of the antifibrotic peptide Ac-SDKP. *Hypertension* **43**, 1140-1145.

Chen, Y.N., Ehlers, M.R., and Riordan, J.F. (1992) The functional role of tyrosine-200 in human testis angiotensin-converting enzyme. *Biochem. Biophys. Res. Commun.* **184**, 306-309.

Cheung, H.S., Wang, F.L., Ondetti, M.A., Sabo, E.F., and Cushman, D.W. (1980) Binding of peptide substrates and inhibitors of angiotensin-converting enzyme. Importance of the COOH-terminal dipeptide sequence. *J. Biol. Chem.* **255**, 401-407.

Chisi, J.E., Briscoe, C.V., Ezan, E., Genet, R., Riches, A.C., and Wdzieczak-Bakala, J. (2000) Captopril inhibits in vitro and in vivo the proliferation of primitive haematopoietic cells induced into cell cycle by cytotoxic drug administration or irradiation but has no effect on myeloid leukaemia cell proliferation. *Br. J. Haematol.* **109**, 563-570.

Cohen, G.H. (1997) ALIGN: a program to superimpose protein coordinates, accounting for insertions and deletions. *J. Appl. Cryst.* **30**, 1160-1161.

Comte, L., Lorgeot, V., Bignon, J., Volkov, L., Dupuis, F., Wdzieczak-Bakala, J., and Praloran, V. (1998) In vivo modifications of AcSDKP metabolism and haematopoiesis in mice treated with 5-fluorouracil and Goralatide. *Eur. J. Clin. Invest.* **28**, 856-863.

Conroy, J.M. and Lai, C.Y. (1978) A rapid and sensitive fluorescence assay for angiotensin-converting enzyme. *Anal. Biochem.* **87**, 556-561.

Corradi, H.R., Chitapi, I., Sewell, B.T., Georgiadis, D., Dive, V., Sturrock, E.D., and Acharya, K.R. (2007) The structure of testis angiotensin-converting enzyme in complex with the C domain-specific inhibitor RXPA380. *Biochemistry* **46**, 5473-5478.

Corradi, H.R., Schwager, S.L., Nchinda, A.T., Sturrock, E.D., and Acharya, K.R. (2006) Crystal structure of the N domain of human somatic angiotensin I-converting enzyme provides a structural basis for domain-specific inhibitor design. *J. Mol. Biol.* **357**, 964-974.

Cushman, D.W., Cheung, H.S., Sabo, E.F., and Ondetti, M.A. (1981) Angiotensin converting enzyme inhibitors: Evolution of a new class of antihypertensive drugs. *Angiotensin converting enzyme inhibitors: Mechanism of action and clinical implications* **1**, 1-25.

Cushman, D.W., Pluscec, J., Williams, N.J., Weaver, E.R., Sabo, E.F., Kocy, O., Cheung, H.S., and Ondetti, M.A. (1973) Inhibition of angiotensin-converting enzyme by analogs of peptides from Bothrops jararaca venom. *Experientia* **29**, 1032-1035.

Danilov, S.M., Balyasnikova, I.V., Albrecht, R.F., and Kost, O.A. (2008) Simultaneous determination of ACE activity with 2 substrates provides information on the status of somatic ACE and allows detection of inhibitors in human blood. *J. Cardiovasc. Pharmacol.* **52**, 90-103.

Danilov, S.M., Balyasnikova, I.V., Danilova, A.S., Naperova, I.A., Arablinskaya, N.E., Borisov, S.E., Metzger, R., Franke, F.E., Schwartz, D.E., Gachok, I.V., Trakht, I.N., Kost, O.A., and Garcia, J.G. (2010) Conformational fingerprinting of the angiotensin I-converting enzyme (ACE). 1. Application in sarcoidosis. *J. Proteome. Res.* **9**, 5782-5793.

Datar, P., Srivastava, S., Coutinho, E., and Govil, G. (2004) Substance P: structure, function, and therapeutics. *Curr. Top. Med. Chem.* **4**, 75-103.

Deddish, P.A., Marcic, B., Jackman, H.L., Wang, H.Z., Skidgel, R.A., and Erdos, E.G. (1998) N-domain-specific substrate and C-domain inhibitors of angiotensin-converting enzyme: angiotensin-(1-7) and keto-ACE. *Hypertension* **31**, 912-917.

Deddish, P.A., Wang, J., Michel, B., Morris, P.W., Davidson, N.O., Skidgel, R.A., and Erdos, E.G. (1994) Naturally occurring active N-domain of human angiotensin I -converting enzyme. *Proc. Natl. Acad. Sci. U. S. A.* **91**, 7807-7811.

Deddish, P.A., Wang, L.X., Jackman, H.L., Michel, B., Wang, J., Skidgel, R.A., and Erdos, E.G. (1996) Single-domain angiotensin I converting enzyme (kininase II): characterization and properties. *J. Pharmacol. Exp. Ther.* **279**, 1582-1589.

DeRemee, R.A. and Rohrbach, M.S. (1980) Serum angiotensin-converting enzyme activity in evaluating the clinical course of sarcoidosis. *Ann. Intern. Med.* **92**, 361-365.

Dive, V., Cotton, J., Yiotakis, A., Michaud, A., Vassiliou, S., Jiracek, J., Vazeux, G., Chauvet, M.T., Cuniasse, P., and Corvol, P. (1999) RXP 407, a phosphinic peptide, is a potent inhibitor of angiotensin I converting enzyme able to differentiate between its two active sites. *Proc. Natl. Acad. Sci. U. S. A.* **96**, 4330-4335.

Dive, V., Georgiadis, D., Matziari, M., Makaritis, A., Beau, F., Cuniasse, P., and Yiotakis, A. (2004) Phosphinic peptides as zinc metalloproteinase inhibitors. *Cell Mol. Life Sci.* **61**, 2010-2019.

Dixon, M. (1953) The determination of enzyme inhibitor constants. *Biochem. J.* **55**, 170-171.

Drag, M. and Salvesen, G.S. (2010) Emerging principles in protease-based drug discovery. *Nat. Rev. Drug Discov.* **9**, 690-701.

du Bois, R.M. (2010) Strategies for treating idiopathic pulmonary fibrosis. *Nat. Rev. Drug Discov.* **9**, 129-140.

Ehlers, M.R. (2006) Safety issues associated with the use of angiotensin-converting enzyme inhibitors. *Expert. Opin. Drug Saf.* **5**, 739-740.

Ehlers, M.R., Schwager, S.L., Scholle, R.R., Manji, G.A., Brandt, W.F., and Riordan, J.F. (1996) Proteolytic release of membrane-bound angiotensin-converting enzyme: role of the juxtamembrane stalk sequence. *Biochemistry* **35**, 9549-9559.

Ehlers, M.R.W., Fox, E.A., Strydom, D.J., and Riordan, J.F. (1989) Molecular cloning of human testicular angiotensin-converting enzyme: The testis isozyme is identical to the C-terminal half of endothelial angiotensin-converting enzyme. *Proc. Natl. Acad. Sci. U. S. A.* **86**, 7741-7745.

Ehlers, M.R.W. and Riordan, J.F. (1991) Angiotensin-converting enzyme: zinc and inhibitor-binding stoichiometries of the somatic and testis isozymes. *Biochemistry* **30**, 7118-7126.

Ehlers, M.R.W. and Riordan, J.F. (1989) Angiotensin-Converting Enzyme: New Concepts Concepts Concerning Its Biological Role. *Biochemistry* **28**, 5311-5318.

Eisenthal, R. and Cornish-Bowden, A. (1974) The direct linear plot. A new graphical procedure for estimating enzyme kinetic parameters. *Biochem. J.* **139**, 715-720.

El Dorry, H.A., Bull, H.G., Iwata, K., Thornberry, N.A., Cordes, E.H., and Soffer, R.L. (1982) Molecular and catalytic properties of rabbit testicular dipeptidyl carboxypeptidase. *J. Biol. Chem.* **257**, 14128-14133.

Emanueli, C., Grady, E.F., Madeddu, P., Figini, M., Bunnett, N.W., Parisi, D., Regoli, D., and Geppetti, P. (1998) Acute ACE inhibition causes plasma extravasation in mice that is mediated by bradykinin and substance P. *Hypertension* **31**, 1299-1304.

Erdos, E.G., Tan, F., and Skidgel, R.A. (2010) Angiotensin I-converting enzyme inhibitors are allosteric enhancers of kinin B1 and B2 receptor function. *Hypertension* **55**, 214-220.

Esther, C.R., Howard, T.E., Marino, E.M., Goddard, J.M., Capecchi, M.R., and Bernstein, K.E. (1996) Mice lacking angiotensin-converting enzyme have low blood pressure, renal pathology, and reduced male fertility. *Lab Invest.* **74**, 953-965.

Fernandez, M., Liu, X., Wouters, M.A., Heyberger, S., and Husain, A. (2001) Angiotensin I-converting enzyme transition state stabilisation by his1089. *J. Biol. Chem.* **276**, 4998-5004.

Friedland, J. and Silverstein, E. (1976) A Sensitive Fluorimetric Assay for Serum Angiotensin-converting Enzyme. *Am. J. Clin. Path.* **66**, 416-424.

Fuchs, S., Frenzel, K., Hubert, C., Lyng, R., Muller, L., Michaud, A., Xiao, H.D., Adams, J.W., Capecchi, M.R., Corvol, P., Shur, B.D., and Bernstein, K.E. (2005) Male fertility is dependent on dipeptidase activity of testis ACE. *Nat. Med.* **11**, 1140-1142.

Fuchs, S., Xiao, H.D., Cole, J.M., Adams, J.W., Frenzel, K., Michaud, A., Zhao, H., Keshelava, G., Capecchi, M.R., Corvol, P., and Bernstein, K.E. (2004) Role of the N-terminal catalytic domain of angiotensin-converting enzyme investigated by targeted inactivation in mice. *J. Biol. Chem.* **279**, 15946-15953.

Fuchs, S., Xiao, H.D., Hubert, C., Michaud, A., Campbell, D.J., Adams, J.W., Capecchi, M.R., Corvol, P., and Bernstein, K.E. (2008) Angiotensin-converting enzyme C-terminal catalytic domain is the main site of angiotensin I cleavage in vivo. *Hypertension* **51**, 267-274.

Fyhrquist, F. and Saijonmaa, O. (2008) Renin-angiotensin system revisited. *J. Intern. Med.* **264**, 224-236.

Gasteiger, E., Gattiker, A., Hoogland, C., Ivanyi, I., Appel, R.D., and Bairoch, A. (2003) ExPASy: The proteomics server for in-depth protein knowledge and analysis. *Nucleic Acids Res.* **31**, 3784-3788.

Georgiadis, D., Beau, F., Czarny, B., Cotton, J., Yiotakis, A., and Dive, V. (2003) Roles of the two active sites of somatic angiotensin-converting enzyme in the cleavage of angiotensin I and bradykinin: insights from selective inhibitors. *Circ. Res.* **93**, 148-154.

Georgiadis, D., Cuniasse, P., Cotton, J., Yiotakis, A., and Dive, V. (2004) Structural determinants of RXPA380, a potent and highly selective inhibitor of the angiotensin-converting enzyme C-domain. *Biochemistry* **43**, 8048-8054.

Gordon, K., Redelinghuys, P., Schwager, S.L., Ehlers, M.R., Papageorgiou, A.C., Natesh, R., Acharya, K.R., and Sturrock, E.D. (2003) Deglycosylation, processing and crystallization of human testis angiotensin-converting enzyme. *Biochem. J.* **371**, 437-442.

Grillon, C., Rieger, K., Bakala, J., Schott, D., Morgat, J.L., Hannappel, E., Voelter, W., and Lenfant, M. (1990) Involvement of thymosin beta 4 and endoproteinase Asp-N in the biosynthesis of the tetrapeptide AcSerAspLysPro a regulator of the hematopoietic system. *FEBS Lett.* **274**, 30-34.

Hagaman, J.R., Moyer, J.S., Bachman, E.S., Sibony, M., Magyar, P.L., Welch, J.E., Smithies, O., Krege, J.H., and O' Brien, D.A. (1998) Angiotensin-converting enzyme and male fertility. *Proc. Natl. Acad. Sci. U. S. A.* **95**, 2552-2557.

Harris, R.B., Ohlsson, J.T., and Wilson, I.B. (1981) Inhibition and affinity chromatography of human serum angiotensin converting enzyme with cysteinyl-proline derivatives. *Arch. Biochem. Biophys.* **206**, 105-112.

Hemming, M.L. and Selkoe, D.J. (2005) Amyloid beta-protein is degraded by cellular angiotensin-converting enzyme (ACE) and elevated by an ACE inhibitor. *J. Biol. Chem.* **280**, 37644-37650.

Hemming, M.L., Selkoe, D.J., and Farris, W. (2007) Effects of prolonged angiotensin-converting enzyme inhibitor treatment on amyloid beta-protein metabolism in mouse models of Alzheimer disease. *Neurobiol. Dis.* **26**, 273-281.

Henriksen, E.J. and Jacob, S. (2003) Modulation of metabolic control by angiotensin converting enzyme (ACE) inhibition. *J. Cell Physiol* **196**, 171-179.

Higaki, J., Aoki, M., Morishita, R., Kida, I., Taniyama, Y., Tomita, N., Yamamoto, K., Moriguchi, A., Kaneda, Y., and Ogihara, T. (2000) In vivo evidence of the importance of cardiac angiotensin-converting enzyme in the pathogenesis of cardiac hypertrophy. *Arterioscler. Thromb. Vasc. Biol.* **20**, 428-434.

Howard, T.E., Shai, S.-Y., Langford, K.G., Martin, B.M., and Bernstein, K.E. (1990) Transcription of testicular angiotensin-converting enzyme (ACE) is initiated within the 12th intron of the somatic ACE gene. *Mol. Cell Biol.* **10**, 4294-4302.

Hu, J., Igarashi, A., Kamata, M., and Nakagawa, H. (2001) Angiotensin-converting enzyme degrades Alzheimer amyloid beta-peptide (A beta); retards A beta aggregation, deposition, fibril formation; and inhibits cytotoxicity. *J. Biol. Chem.* **276**, 47863-47868.

Hubert, C., Houot, A.-M., Corvol, P., and Soubrier, F. (1991) Structure of the Angiotensin I-converting Enzyme Gene. Two alternate promoters correspond to evolutionary steps of a duplicated gene. *J. Biol. Chem.* **266**, 15377-15383.

Jaspard, E., Wei, L., and Alhenc-Gelas, F. (1993) Differences in the properties and enzymatic specificities of the two active sites of angiotensin I-converting enzyme (kininase II). *J. Biol. Chem.* **268**, 9496-9503.

Jullien, N.D., Cuniasse, P., Georgiadis, D., Yiotakis, A., and Dive, V. (2006) Combined use of selective inhibitors and fluorogenic substrates to study the specificity of somatic wild-type angiotensin-converting enzyme. *FEBS J.* **273**, 1772-1781.

Junot, C., Gonzales, M.F., Ezan, E., Cotton, J., Vazeux, G., Michaud, A., Azizi, M., Vassiliou, S., Yiotakis, A., Corvol, P., and Dive, V. (2001) RXP 407, a selective inhibitor of the N-domain of angiotensin I-converting enzyme, blocks in vivo the degradation of hemoregulatory peptide acetyl-Ser-Asp-Lys-Pro with no effect on angiotensin I hydrolysis. *J. Pharmacol. Exp. Ther.* **297**, 606-611.

Kakoki, M. and Smithies, O. (2009) The kallikrein-kinin system in health and in diseases of the kidney. *Kidney Int.* **75**, 1019-1030.

Kang, T., Park, H.I., Suh, Y., Zhao, Y.G., Tschesche, H., and Sang, Q.X. (2002) Autolytic processing at Glu586-Ser587 within the cysteine-rich domain of human adamalysin 19/disintegrin-metalloproteinase 19 is necessary for its proteolytic activity. *J. Biol. Chem.* **277**, 48514-48522.

Kehoe, P.G. (2009) Angiotensins and Alzheimer's disease: a bench to bedside overview. *Alzheimers. Res. Ther.* **1**, 3-10.

Knight, C.G. (1995) Active-site titration of peptidases. *Methods Enzymol.* **248**, 85-101.

Koo, K.D., Kim, M.J., Kim, S., Kim, K.H., Hong, S.Y., Hur, G.C., Yim, H.J., Kim, G.T., Han, H.O., Kwon, O.H., Kwon, T.S., Koh, J.S., and Lee, C.S. (2007) Synthesis, SAR, and X-ray structure of novel potent DPPIV inhibitors: oxadiazolyl ketones. *Bioorg. Med. Chem. Lett.* **17**, 4167-4172.

Kost, O.A., Balyasnikova, I.V., Chemodanova, E.E., Nikolskaya, I.I., Albrecht, R.F., and Danilov, S.M. (2003) Epitope-dependent blocking of the angiotensin-converting enzyme

dimerization by monoclonal antibodies to the N-terminal domain of ACE: possible link of ACE dimerization and shedding from the cell surface. *Biochemistry* **42**, 6965-6976.

Krege, J.H., John, S.W., Langenbach, L.L., Hodgin, J.B., Hagaman, J.R., Bachman, E.S., Jennette, J.C., O'Brien, D.A., and Smithies, O. (1995) Male-female differences in fertility and blood pressure in ACE-deficient mice. *Nature* **375**, 146-148.

Kroger, W.L., Douglas, R.G., O'Neill, H.G., Dive, V., and Sturrock, E.D. (2009) Investigating the domain specificity of phosphinic inhibitors RXPA380 and RXP407 in angiotensin-converting enzyme. *Biochemistry* **48**, 8405-8412.

Lanzillo, J.J., Polsky-Cynkin, R., and Fanburg, B.L. (1980) Large-scale purification of angiotensin I-converting enzyme from human plasma utilizing an immunoadsorbent affinity gel. *Anal. Biochem.* **103**, 400-407.

Lazartigues, E., Feng, Y., and Lavoie, J.L. (2007) The two fACEs of the tissue renin-angiotensin systems: implication in cardiovascular diseases. *Curr. Pharm. Des.* **13**, 1231-1245.

Lehmann, D.J., Cortina-Borja, M., Warden, D.R., Smith, A.D., Sleegers, K., Prince, J.A., van Duijn, C.M., and Kehoe, P.G. (2005) Large meta-analysis establishes the ACE insertion-deletion polymorphism as a marker of Alzheimer's disease. *Am. J. Epidemiol.* **162**, 305-317.

Lenfant, M., Wdzieczak-Bakala, J., Guittet, E., Prome, J.C., Sotty, D., and Frindel, E. (1989) Inhibitor of hematopoietic pluripotent stem cell proliferation: purification and determination of its structure. *Proc. Natl. Acad. Sci. U. S. A.* **86**, 779-782.

Li, P., Xiao, H.D., Xu, J., Ong, F.S., Kwon, M., Roman, J., Gal, A., Bernstein, K.E., and Fuchs, S. (2010) Angiotensin-converting enzyme N-terminal inactivation alleviates bleomycin-induced lung injury. *Am. J. Pathol.* **177**, 1113-1121.

Liao, T.D., Yang, X.P., D'Ambrosio, M., Zhang, Y., Rhaleb, N.E., and Carretero, O.A. (2010) N-acetyl-seryl-aspartyl-lysyl-proline attenuates renal injury and dysfunction in hypertensive rats with reduced renal mass: council for high blood pressure research. *Hypertension* **55**, 459-467.

Lieberman, J. and Sastre, A. (1980) Serum angiotensin-converting enzyme: elevations in diabetes mellitus. *Ann. Intern. Med.* **93**, 825-826.

Lin, C.X., Rhaleb, N.E., Yang, X.P., Liao, T.D., D'Ambrosio, M.A., and Carretero, O.A. (2008) Prevention of aortic fibrosis by N-acetyl-seryl-aspartyl-lysyl-proline in angiotensin II-induced hypertension. *Am. J. Physiol Heart Circ. Physiol.* **295**, H1253-H1261.

Liu, Y., Kati, W., Chen, C.M., Tripathi, R., Molla, A., and Kohlbrenner, W. (1999) Use of a fluorescence plate reader for measuring kinetic parameters with inner filter effect correction. *Anal. Biochem.* **267**, 331-335.

Liu, Y.H., D'Ambrosio, M., Liao, T.D., Peng, H., Rhaleb, N.E., Sharma, U., Andre, S., Gabius, H.J., and Carretero, O.A. (2009) N-acetyl-seryl-aspartyl-lysyl-proline prevents cardiac remodeling and dysfunction induced by galectin-3, a mammalian adhesion/growth-regulatory lectin. *Am. J. Physiol Heart Circ. Physiol.* **296**, H404-H412.

Lombard, M.N., Sotty, D., Wdzieczak-Bakala, J., and Lenfant, M. (1990) In vivo effect of the tetrapeptide, N-acetyl-Ser-Asp-Lys-Pro, on the G1-S transition of rat hepatocytes. *Cell Tissue Kinet.* **23**, 99-103.

Marques, G.D., Quinto, B.M., Plavinik, F.L., Krieger, J.E., Marson, O., and Casarini, D.E. (2003) N-domain angiotensin I-converting enzyme with 80 kDa as a possible genetic marker of hypertension. *Hypertension* **42**, 693-701.

Masse, A., Ramirez, L.H., Bindoula, G., Grillon, C., Wdzieczak-Bakala, J., Raddassi, K., Deschamps, d.P., Mencia-Huerta, J.M., Koscielny, S., Potier, P., Sainteny, F., and Carde, P. (1998) The tetrapeptide acetyl-N-Ser-Asp-Lys-Pro (Goralatide) protects from doxorubicin-induced toxicity: improvement in mice survival and protection of bone marrow stem cells and progenitors. *Blood* **91**, 441-449.

Matthews, B.W. (1988) Structural basis of the action of thermolysin and related zinc peptidases. *Acc. Chem. Res.* **21**, 333-340.

McPherson, M.J. (1990) Directed mutagenesis: a practical approach. *IRL Press.*

Michaud, A., Chauvet, M.T., and Corvol, P. (1999) N-domain selectivity of angiotensin I-converting enzyme as assessed by structure-function studies of its highly selective substrate, N-acetyl-seryl-aspartyl-lysyl-proline. *Biochem. Pharmacol.* **57**, 611-618.

Michaud, A., Williams, T.A., Chauvet, M.T., and Corvol, P. (1997) Substrate dependence of angiotensin I-converting enzyme inhibition: captopril displays a partial selectivity for inhibition of N-acetyl-seryl-aspartyl-lysyl-proline hydrolysis compared with that of angiotensin I. *Mol. Pharmacol.* **51**, 1070-1076.

Millar, R.P., Lu, Z.L., Pawson, A.J., Flanagan, C.A., Morgan, K., and Maudsley, S.R. (2004) Gonadotropin-releasing hormone receptors. *Endocr. Rev.* **25**, 235-275.

Morimoto, T., Gandhi, T.K., Fiskio, J.M., Seger, A.C., So, J.W., Cook, E.F., Fukui, T., and Bates, D.W. (2004) An evaluation of risk factors for adverse drug events associated with angiotensin-converting enzyme inhibitors. *J. Eval. Clin. Pract.* **10**, 499-509.

Mus-Veteau, I. (2002) Heterologous expression and purification systems for structural proteomics of mammalian membrane proteins. *Comp. Funct. Genomics* **3**, 511-517.

Natesh, R., Schwager, S.L., Evans, H.R., Sturrock, E.D., and Acharya, K.R. (2004) Structural details on the binding of antihypertensive drugs captopril and enalaprilat to human testicular angiotensin I-converting enzyme. *Biochemistry* **43**, 8718-8724.

Natesh, R., Schwager, S.L., Sturrock, E.D., and Acharya, K.R. (2003) Crystal structure of the human angiotensin-converting enzyme-lisinopril complex. *Nature* **421**, 551-554.

Nchinda, A.T., Chibale, K., Redelinghuys, P., and Sturrock, E.D. (2006a) Synthesis and molecular modeling of a lisinopril-tryptophan analogue inhibitor of angiotensin I-converting enzyme. *Bioorg. Med. Chem. Lett.* **16**, 4616-4619.

Nchinda, A.T., Chibale, K., Redelinghuys, P., and Sturrock, E.D. (2006b) Synthesis of novel keto-ACE analogues as domain-selective angiotensin I-converting enzyme inhibitors. *Bioorg. Med. Chem. Lett.* **16**, 4612-4615.

Ntai, I. and Bachmann, B.O. (2008) Identification of ACE pharmacophore in the phosphonopeptide metabolite K-26. *Bioorg. Med. Chem. Lett.* **18**, 3068-3071.

Nussberger, J., Cugno, M., Amstutz, C., Cicardi, M., Pellacani, A., and Agostoni, A. (1998) Plasma bradykinin in angio-oedema. *Lancet* **351**, 1693-1697.

O'Neill, H.G., Redelinghuys, P., Schwager, S.L., and Sturrock, E.D. (2008) The role of glycosylation and domain interactions in the thermal stability of human angiotensin-converting enzyme. *Biol. Chem.* **389**, 1153-1161.

Oba, R., Igarashi, A., Kamata, M., Nagata, K., Takano, S., and Nakagawa, H. (2005) The N-terminal active centre of human angiotensin-converting enzyme degrades Alzheimer amyloid beta-peptide. *Eur. J. Neurosci.* **21**, 733-740.

Ondetti, M.A., Rubin, B., and Cushman, D.W. (1977) Design of specific inhibitors of angiotensin-converting enzyme: new class of orally active antihypertensive agents. *Science* **196**, 441-444.

Pantoliano, M.W., Holmquist, B., and Riordan, J.F. (1984) Affinity chromatographic purification of angiotensin converting enzyme. *Biochemistry* **23**, 1037-1042.

Papworth, C., Braman, J., and Wright, D.A. (1996) Site-directed mutagenesis in One Day with 80% efficiency. *Strategies* **9**, 3-4.

Patchett, A.A., Harris, E., Tristram, E.W., Wyvratt, M.J., Wu, M.T., Taub, D., Peterson, E.R., Ikeler, T.J., ten Broeke, J., Payne, L.G., Ondeyka, D.L., Thorsett, E.D., Greenlee, W.J., Lohr, N.S., Hoffsommer, R.D., Joshua, H., Ruyle, W.V., Rothrock, J.W., Aster, S.D., Maycock, A.L., Robinson, F.M., Hirschmann, R., Sweet, C.S., Ulm, E.H., Gross, D.M., Vassil, T.C., and Stone, C.A. (1980) A new class of angiotensin-converting enzyme inhibitors. *Nature* **288**, 280-283.

Peng, H., Carretero, O.A., Brigstock, D.R., Oja-Tebbe, N., and Rhaleb, N.E. (2003) Ac-SDKP reverses cardiac fibrosis in rats with renovascular hypertension. *Hypertension* **42**, 1164-1170.

Peng, H., Carretero, O.A., Liao, T.D., Peterson, E.L., and Rhaleb, N.E. (2007) Role of N-acetyl-seryl-aspartyl-lysyl-proline in the antifibrotic and anti-inflammatory effects of the angiotensin-converting enzyme inhibitor captopril in hypertension. *Hypertension* **49**, 695-703.

Peng, H., Carretero, O.A., Peterson, E.L., and Rhaleb, N.E. (2010) Ac-SDKP inhibits transforming growth factor-beta1-induced differentiation of human cardiac fibroblasts into myofibroblasts. *Am. J. Physiol Heart Circ. Physiol.* **298**, H1357-H1364.

Peng, H., Carretero, O.A., Raij, L., Yang, F., Kapke, A., and Rhaleb, N.E. (2001) Antifibrotic effects of N-acetyl-seryl-aspartyl-Lysyl-proline on the heart and kidney in aldosterone-salt hypertensive rats. *Hypertension* **37**, 794-800.

Peng, H., Carretero, O.A., Vuljaj, N., Liao, T.D., Motivala, A., Peterson, E.L., and Rhaleb, N.E. (2005) Angiotensin-converting enzyme inhibitors: a new mechanism of action. *Circulation* **112**, 2436-2445.

Pradelles, P., Frobert, Y., Creminon, C., Ivonine, H., and Frindel, E. (1991) Distribution of a negative regulator of haematopoietic stem cell proliferation (AcSDKP) and thymosin beta 4 in mouse tissues. *FEBS Lett.* **289**, 171-175.

Probstfield, J.L. and O'Brien, K.D. (2010) Progression of cardiovascular damage: the role of renin-angiotensin system blockade. *Am. J. Cardiol.* **105**, 10A-20A.

Ramaraj, P., Kessler, S.P., Colmenares, C., and Sen, G.C. (1998) Selective restoration of male fertility in mice lacking angiotensin-converting enzymes by sperm-specific expression of the testicular isozyme. *J. Clin. Invest.* **102**, 371-378.

Rasoul, S., Carretero, O.A., Peng, H., Cavasin, M.A., Zhuo, J., Sanchez-Mendoza, A., Brigstock, D.R., and Rhaleb, N.E. (2004) Antifibrotic effect of Ac-SDKP and angiotensin-converting enzyme inhibition in hypertension. *J. Hypertens.* **22**, 593-603.

Rawlings, N.D., Barrett, A.J., and Bateman, A. (2010) MEROPS: the peptidase database. *Nucleic Acids Res.* **38**, D227-D233.

Redelinghuys, P., Nchinda, A.T., and Sturrock, E.D. (2005) Development of domain-selective angiotensin I-converting enzyme inhibitors. *Ann. N. Y. Acad. Sci.* **1056**, 160-175.

Rhaleb, N.E., Peng, H., Harding, P., Tayeh, M., LaPointe, M.C., and Carretero, O.A. (2001) Effect of N-acetyl-seryl-aspartyl-lysyl-proline on DNA and collagen synthesis in rat cardiac fibroblasts. *Hypertension* **37**, 827-832.

Rice, G.I., Thomas, D.A., Grant, P.J., Turner, A.J., and Hooper, N.M. (2004) Evaluation of angiotensin-converting enzyme (ACE), its homologue ACE2 and neprilysin in angiotensin peptide metabolism. *Biochem. J.* **383**, 45-51.

Rieder, M.J., Taylor, S.L., Clark, A.G., and Nickerson, D.A. (1999) Sequence variation in the human angiotensin converting enzyme. *Nat. Genet.* **22**, 59-62.

Rieger, K.J., Saez-Servent, N., Papet, M.P., Wdzieczak-Bakala, J., Morgat, J.L., Thierry, J., Voelter, W., and Lenfant, M. (1993) Involvement of human plasma angiotensin I-converting enzyme in the degradation of the haemoregulatory peptide N-acetyl-seryl-aspartyl-lysyl-proline. *Biochem. J.* **296 (Pt 2)**, 373-378.

Rigat, B., Hubert, C., Alhenc-Gelas, F., Cambien, F., Corvol, P., and Soubrier, F. (1990) An insertion/deletion polymorphism in the angiotensin I-converting enzyme gene accounting for half the variance of serum enzyme levels. *J. Clin. Invest.* **86**, 1343-1346.

Ripka, J.E., Ryan, J.W., Valido, F.A., Chung, A.Y., Peterson, C.M., and Urry, R.L. (1993) N-glycosylation of forms of angiotensin converting enzyme from four mammalian species. *Biochem. Biophys. Res. Commun.* **196**, 503-508.

Roks, A.J., van Geel, P.P., Pinto, Y.M., Buikema, H., Henning, R.H., de Zeeuw, D., and van Gilst, W.H. (1999) Angiotensin-(1-7) is a modulator of the human renin-angiotensin system. *Hypertension* **34**, 296-301.

Ronchi, F.A., Andrade, M.C., Carmona, A.K., Krieger, J.E., and Casarini, D.E. (2005) N-domain angiotensin-converting enzyme isoform expression in tissues of Wistar and spontaneously hypertensive rats. *J. Hypertens.* **23**, 1869-1878.

Rousseau, A., Michaud, A., Chauvet, M.-T., Lenfant, M., and Corvol, P. (1995) The hemoregulatory peptide N-acetyl-Ser-Asp-Lys-Pro is a natural and specific substrate of the N-terminal active site of human angiotensin-converting enzyme. *J. Biol. Chem.* **270**, 3656-3661.

Rushworth, C.A., Guy, J.L., and Turner, A.J. (2008) Residues affecting the chloride regulation and substrate selectivity of the angiotensin-converting enzymes (ACE and ACE2) identified by site-directed mutagenesis. *FEBS J.* **275**, 6033-6042.

Sadhukhan, R. and Sen, I. (1996) Different glycosylation requirements for the synthesis of enzymatically active angiotensin-converting enzyme in mammalian cells and yeast. *J. Biol. Chem.* **271**, 6429-6434.

Sambrook, J., Fritsch, E.F., and Maniatis, T. (1989) Molecular Cloning: A Laboratory Manual (2nd ed.). *Cold Spring Harbour Laboratory Press* 1.29-1.84.

Santos, R.A., Simoes e Silva AC, Maric, C., Silva, D.M., Machado, R.P., de, B., I, Heringer-Walther, S., Pinheiro, S.V., Lopes, M.T., Bader, M., Mendes, E.P., Lemos, V.S., Campagnole-Santos, M.J., Schultheiss, H.P., Speth, R., and Walther, T. (2003) Angiotensin-(1-7) is an endogenous ligand for the G protein-coupled receptor Mas. *Proc. Natl. Acad. Sci. U. S. A.* **100**, 8258-8263.

Schartl, M., Bocksch, W.G., Dreysse, S., Beckmann, S., Franke, O., and Hunten, U. (1994) Remodeling of myocardium and arteries by chronic angiotensin converting enzyme inhibition in hypertensive patients. *J. Hypertens. Suppl* **12**, S37-S42.

Schechter, I. and Berger, A. (1967) On the size of the active site in proteases. I. Papain. *Biochem. Biophys. Res. Commun.* **27**, 157-162.

Schwager, S.L., Carmona, A.K., and Sturrock, E.D. (2006) A high-throughput fluorimetric assay for angiotensin I-converting enzyme. *Nat. Protoc.* **1**, 1961-1964.

Shapiro, R. and Riordan, J.F. (1983) Critical lysine residue at the chloride binding site of angiotensin converting enzyme. *Biochemistry* **22**, 5315-5321.

Sharma, U., Rhaleb, N.E., Pokharel, S., Harding, P., Rasoul, S., Peng, H., and Carretero, O.A. (2008) Novel anti-inflammatory mechanisms of N-Acetyl-Ser-Asp-Lys-Pro in hypertension-induced target organ damage. *Am. J. Physiol Heart Circ. Physiol.* **294**, H1226-H1232.

Silverstein, E., Pertschuk, L.P., and Friedland, J. (1979) Immunofluorescent localization of angiotensin converting enzyme in epithelioid and giant cells of sarcoidosis granulomas. *Proc. Natl. Acad. Sci. U. S. A* **76**, 6646-6648.

Skeggs, L.T., Kahn, J.R., and Shumway, N.P. (1956) The preparation and function of the hypertensin-converting enzyme. *J. Exp. Med.* **103**, 295-299.

Skeggs, L.T., Marsh, W.H., Kahn, J.R., and Shumway, N.P. (1954) The purification of hypertensin I. *J. Exp. Med.* **100**, 363-370.

Skidgel, R.A., Engelbrecht, S., Johnson, A.R., and Erdos, E.G. (1984) Hydrolysis of substance p and neurotensin by converting enzyme and neutral endopeptidase. *Peptides* **5**, 769-776.

Skidgel, R.A. and Erdos, E.G. (1985) Novel activity of human angiotensin I converting enzyme: release of the NH2- and COOH-terminal tripeptides from the luteinizing hormone-releasing hormone. *Proc. Natl. Acad. Sci. U. S. A.* **82**, 1025-1029.

Skirgello, O.E., Binevski, P.V., Pozdnev, V.F., and Kost, O.A. (2005) Kinetic probes for inter-domain co-operation in human somatic angiotensin-converting enzyme. *Biochem. J.* **391**, 641-647.

Soubrier, F., Alhenc-Gelas, F., Hubert, C., Allegrini, J., John, M., Tregear, G., and Corvol, P. (1988) Two putative active centers in human angiotensin I - converting enzyme revealed by molecular cloning. *Proc. Natl. Acad. Sci. U. S. A.* **85**, 9386-9390.

Speirs, C., Wagniart, F., and Poggi, L. (1998) Perindopril postmarketing surveillance: a 12 month study in 47,351 hypertensive patients. *Br. J. Clin. Pharmacol.* **46**, 63-70.

Stewart, T.A., Weare, J.A., and Erdos, E.G. (1981) Human peptidyl dipeptidase (converting enzyme, kininase II). *Methods Enzymol.* **80 Pt C**, 450-460.

Sturrock, E.D., Danilov, S.M., and Riordan, J.F. (1997) Limited Proteolysis of Human Kidney Angiotensin-Converting Enzyme and Generation of Catalytically Active N- and C-Terminal Domains. *Biochem. Biophys. Res. Commun.* **236**, 16-19.

Sturrock, E.D., Natesh, R., van Rooyen, J.M., and Acharya, K.R. (2004) Structure of angiotensin I-converting enzyme. *Cell Mol. Life Sci.* **61**, 2677-2686.

Sun, X., Becker, M., Pankow, K., Krause, E., Ringling, M., Beyermann, M., Maul, B., Walther, T., and Siems, W.E. (2008) Catabolic attacks of membrane-bound angiotensin-converting enzyme on the N-terminal part of species-specific amyloid-beta peptides. *Eur. J. Pharmacol.* **588**, 18-25.

Thunnissen, M.M., Andersson, B., Samuelsson, B., Wong, C.H., and Haeggstrom, J.Z. (2002) Crystal structures of leukotriene A4 hydrolase in complex with captopril and two competitive tight-binding inhibitors. *FASEB J.* **16**, 1648-1650.

Toropygin, I.Y., Kugaevskaya, E.V., Mirgorodskaya, O.A., Elisseeva, Y.E., Kozmin, Y.P., Popov, I.A., Nikolaev, E.N., Makarov, A.A., and Kozin, S.A. (2008) The N-domain of angiotensin-converting enzyme specifically hydrolyzes the Arg-5-His-6 bond of Alzheimer's Abeta-(1-16) peptide and its isoAsp-7 analogue with different efficiency as evidenced by quantitative matrix-assisted laser desorption/ionization time-of-flight mass spectrometry. *Rapid Commun. Mass Spectrom.* **22**, 231-239.

Turner, A.J. and Hooper, N.M. (2002) The angiotensin-converting enzyme gene family: genomics and pharmacology. *Trends Pharmacol. Sci.* **23**, 177-183.

Tzakos, A.G., Galanis, A.S., Spyroulias, G.A., Cordopatis, P., Manessi-Zoupa, E., and Gerothanassis, I.P. (2003) Structure-function discrimination of the N- and C-catalytic domains of human angiotensin-converting enzyme: implications for Cl- activation and peptide hydrolysis mechanisms. *Protein Engineering* **16**, 993-1003.

Tzakos, A.G. and Gerothanassis, I.P. (2005) Domain-Selective Ligand-Binding Modes and Atomic Level Pharmacophore Refinement in Angiotensin I Converting Enzyme (ACE) Inhibitors. *Chembiochem.* **6**, 1089-1103.

Udenfriend, S., Stein, S., Bohlen, P., Dairman, W., Leimgruber, W., and Weigele, M. (1972) Fluorescamine: a reagent for assay of amino acids, peptides, proteins, and primary amines in the picomole range. *Science* **178**, 871-872.

Vickers, C., Hales, P., Kaushik, V., Dick, L., Gavin, J., Tang, J., Godbout, K., Parsons, T., Baronas, E., Hsieh, F., Acton, S., Patane, M., Nichols, A., and Tummino, P. (2002) Hydrolysis of biological peptides by human angiotensin-converting enzyme-related carboxypeptidase. *J. Biol. Chem.* **277**, 14838-14843.

Walters, W.P., Ajay, and Murcko, M.A. (1999) Recognizing molecules with drug-like properties. *Curr. Opin. Chem. Biol.* **3**, 384-387.

Wang, G.T., Chung, C.C., Holzman, T.F., and Krafft, G.A. (1993) A continuous fluorescence assay of renin activity. *Anal. Biochem.* **210**, 351-359.

Wang, M., Liu, R., Jia, X., Mu, S., and Xie, R. (2010) N-acetyl-seryl-aspartyl-lysyl-proline attenuates renal inflammation and tubulointerstitial fibrosis in rats. *Int. J. Mol. Med.* **26**, 795-801.

Wang, W., Maniar, M., Jain, R., Jacobs, J., Trias, J., and Yuan, Z. (2001) A fluorescence-based homogeneous assay for measuring activity of UDP-3-O-(R-3-hydroxymyristoyl)-N-acetylglucosamine deacetylase. *Anal. Biochem.* **290**, 338-346.

Watermeyer, J.M., Kroger, W.L., O'Neill, H.G., Sewell, B.T., and Sturrock, E.D. (2008) Probing the basis of domain-dependent inhibition using novel ketone inhibitors of Angiotensin-converting enzyme. *Biochemistry* **47**, 5942-5950.

Watermeyer, J.M., Kroger, W.L., O'Neill, H.G., Sewell, B.T., and Sturrock, E.D. (2010) Characterization of domain-selective inhibitor binding in angiotensin-converting enzyme using a novel derivative of lisinopril. *Biochem. J.* **428**, 67-74.

Wdzieczak-Bakala, J., Fache, M.P., Lenfant, M., Frindel, E., and Sainteny, F. (1990) AcSDKP, an inhibitor of CFU-S proliferation, is synthesized in mice under steady-state conditions and secreted by bone marrow in long-term culture. *Leukemia* **4**, 235-237.

Wei, L., Alhenc-Gelas, F., Corvol, P., and Clauser, E. (1991) The two homologous domains of human angiotensin I - converting enzyme are both catalytically active. *J. Biol. Chem.* **266**, 9002-9008.

Wei, L., Clauser, E., Alhenc-Gelas, F., and Corvol, P. (1992) The two homologous domains of human angiotensin I-converting enzyme interact differently with competitive inhibitors. *J. Biol. Chem.* **267**, 13398-13405.

Williams, T.A., Danilov, S., Alhenc-Gelas, F., and Soubrier, F. (1996) A study of chimeras constructed with the two domains of angiotensinI-converting enzyme. *Biochem. Pharmacol.* **51**, 11-14.

Williams, T.A., Gouttaya, M., Tougard, C., Michaud, A., Chauvet, M.T., and Corvol, P. (1997) Cleavage-secretion of angiotensin I-converting enzyme in yeast. *Mol. Cell Endocrinol.* **128**, 39-45.

Woodman, Z.L., Oppong, S.Y., Cook, S., Hooper, N.M., Schwager, S.L.U., Brandt, W.F., Ehlers, M.R.W., and Sturrock, E.D. (2000) Shedding of somatic angiotensin-converting enzyme (ACE) is inefficient compared with testis ACE despite cleavage at identical stalk sites. *Biochem. J.* **347**, 711-718.

Woodman, Z.L., Schwager, S.L., Redelinghuys, P., Carmona, A.K., Ehlers, M.R., and Sturrock, E.D. (2005) The N domain of somatic angiotensin-converting enzyme negatively regulates ectodomain shedding and catalytic activity. *Biochem. J.* **389**, 739-744.

Wu, G., Robertson, D.H., Brooks, C.L., III, and Vieth, M. (2003) Detailed analysis of grid-based molecular docking: A case study of CDOCKER-A CHARMm-based MD docking algorithm. *J. Comput. Chem.* **24**, 1549-1562.

Xiao, H.D., Fuchs, S., Frenzel, K., Teng, L., Li, P., Shen, X.Z., Adams, J., Zhao, H., Keshelava, G.T., Bernstein, K.E., and Cole, J.M. (2004) The use of knockout mouse technology to achieve tissue selective expression of angiotensin converting enzyme. *J. Mol. Cell Cardiol.* **36**, 781-789.

Yamamoto, D., Takai, S., Hirahara, I., and Kusano, E. (2010) Captopril directly inhibits matrix metalloproteinase-2 activity in continuous ambulatory peritoneal dialysis therapy. *Clin. Chim. Acta* **411**, 762-764.

Yang, F., Yang, X.P., Liu, Y.H., Xu, J., Cingolani, O., Rhaleb, N.E., and Carretero, O.A. (2004) Ac-SDKP reverses inflammation and fibrosis in rats with heart failure after myocardial infarction. *Hypertension* **43**, 229-236.

Yin, J., Li, G., Ren, X., and Herrler, G. (2007) Select what you need: a comparative evaluation of the advantages and limitations of frequently used expression systems for foreign genes. *J. Biotechnol.* **127**, 335-347.

Yokosawa, H., Endo, S., Ogura, Y., and Ishii, S. (1983) A new feature of angiotensin-converting enzyme in the brain: hydrolysis of substance P. *Biochem. Biophys. Res. Commun.* **116**, 735-742.

Yu, X.C., Sturrock, E.D., Wu, Z., Biemann, K., Ehlers, M.R., and Riordan, J.F. (1997) Identification of N-linked glycosylation sites in human testis angiotensin-converting enzyme and expression of an active deglycosylated form. *J. Biol. Chem.* **272**, 3511-3519.

Zhuo, J.L., Carretero, O.A., Peng, H., Li, X.C., Regoli, D., Neugebauer, W., and Rhaleb, N.E. (2007) Characterization and localization of Ac-SDKP receptor binding sites using 125I-labeled Hpp-Aca-SDKP in rat cardiac fibroblasts. *Am. J. Physiol Heart Circ. Physiol.* **292**, H984-H993.

Zou, K., Yamaguchi, H., Akatsu, H., Sakamoto, T., Ko, M., Mizoguchi, K., Gong, J.S., Yu, W., Yamamoto, T., Kosaka, K., Yanagisawa, K., and Michikawa, M. (2007) Angiotensin-converting enzyme converts amyloid beta-protein 1-42 (Abeta(1-42)) to Abeta(1-40), and its inhibition enhances brain Abeta deposition. *J. Neurosci.* **27**, 8628-8635.